International Journal of Biomaterials

Advanced Surface Modifications for Blood-Contacting Surfaces of Medical Devices

Guest Editors: Zhongjun J. Wu, Narayana Garimella, Rolf Larsson, and Eduard Brynda

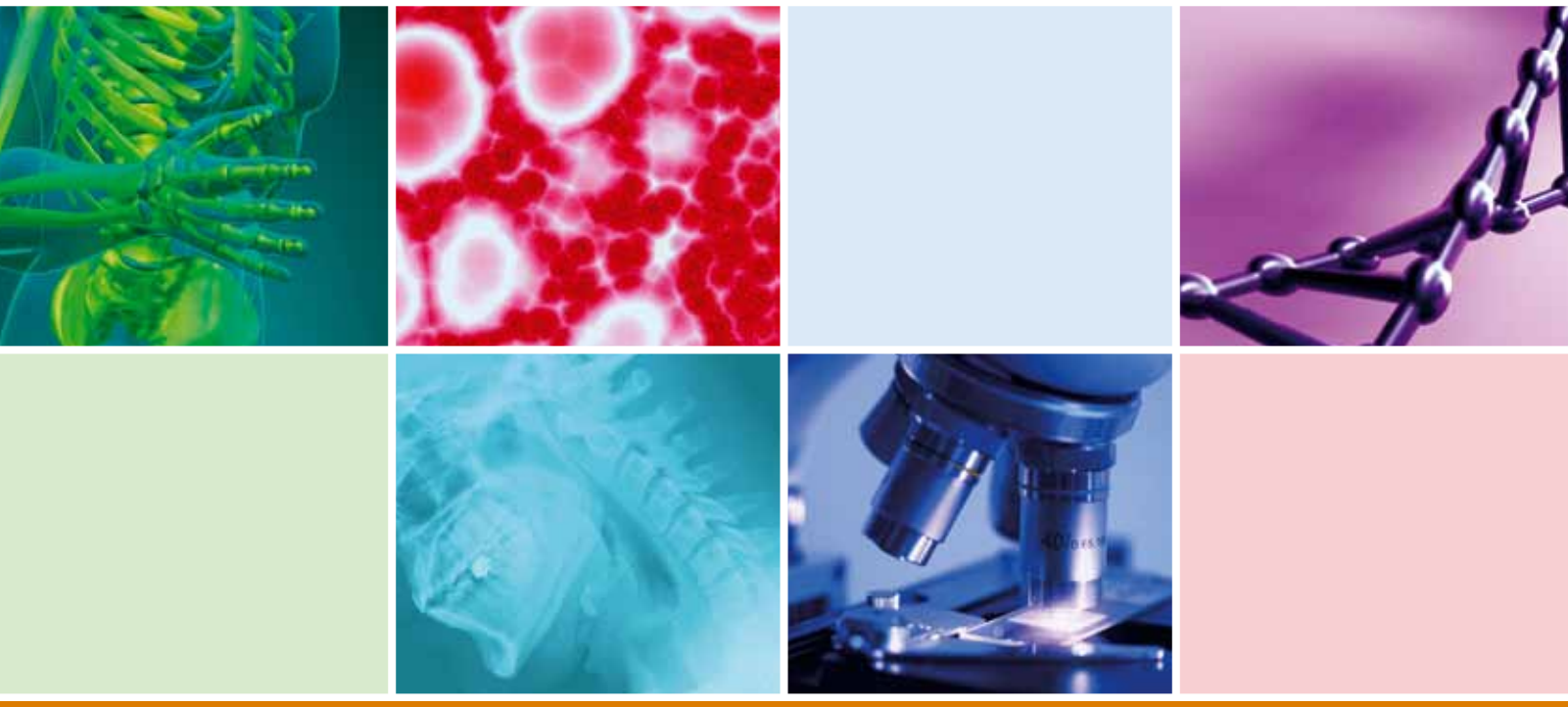

Advanced Surface Modifications for Blood-Contacting Surfaces of Medical Devices

International Journal of Biomaterials

Advanced Surface Modifications for Blood-Contacting Surfaces of Medical Devices

Guest Editors: Zhongjun J. Wu, Narayana Garimella, Rolf Larsson, and Eduard Brynda

Editorial Board

Contents

Hindawi Publishing Corporation
International Journal of Biomaterials
Volume 2012, Article ID 291735, 2 pages
doi:10.1155/2012/291735

Editorial

Advanced Surface Modifications for Blood-Contacting Surfaces of Medical Devices

Zhongjun J. Wu,[1] Narayana Garimella,[1] Rolf Larsson,[2] and Eduard Brynda[3]

[1] *Artificial Organs Laboratory, Department of Surgery, University of Maryland, Baltimore, MD 21201, USA*
[2] *Department of Immunology, Genetics and Pathology, Uppsala University, 75185 Uppsala, Sweden*
[3] *Department of Polymer Membranes, Institute of Macromolecular Chemistry, Academy of Sciences of the Czech Republic, 16206 Prague, Czech Republic*

Correspondence should be addressed to Zhongjun J. Wu, zwu@smail.umaryland.edu

Received 11 March 2012; Accepted 11 March 2012

Surface modification of biomaterial interfaces remains an active field of research with a clear aim to enhance and retain blood compatibility of blood-contacting medical devices. Issues such as activation of coagulation pathways, altered hemostasis, inflammatory responses, and thrombosis are potential clinical complications during blood interaction with artificial surfaces that needs to be addressed when a new device is developed or there is a modification of a device or implant in the form of material, surface characteristics, shape, or function.

Large surface areas in certain devices, such as blood oxygenator membranes, hemodialysis membranes, or nano-sized particles, present unique surface-related challenges. Minimizing pro-coagulant protein adsorption, platelet activation and deposition on the biomaterial interface are key factors that ultimately decide the performance and long-term reliability of a device. Among various types of biomedical devices, polymeric ones have a lion's share and accordingly substantial attention is being paid to surface-modification of polymeric surfaces. Several challenges in attaining modification of the surfaces include, but are not limited to, device specifics, application specifics and underlying thermodynamic and kinetic specific parameters.

International Journal of Biomaterials has launched this special issue with emphasis on analyzing numerous strategies in light of the ongoing advancements in design and development of blood-contacting medical devices. Peer-reviewed, original research, and review papers in the area of blood-compatible surface advancements are included. The topics comprise new methods and combination of principles, novel evaluation techniques, and current and future directions. The papers in this issue address several aspects of blood-contacting surfaces including modulation of interfacial bioactivities, evaluation methods and improvements in surface modification techniques.

Altogether, five research papers and one review paper of this special issue are concerned with materials, devices, parameters, and mechanisms in relation to blood compatibility. P. A. Patston et al. describe modulation of specific blood contact activation parameter (kallikrein) by C1-inhibitor in the presence of type IV collagen. They not only demonstrate the tight binding of C1-inhibitor with type IV collagen but also show collagen's influence in reducing the rate of inhibition. This paper provides an additional insight into collagen containing biomaterial surfaces. B. Dhandayuthapani and coworkers report on critical evaluation of nanocomposite scaffolds comprising single wall carbon nanotubes and Zein fibers. This paper covers structural, physicochemical, and hemocompatibility assessments that bring into focus the applicability of these unique composite scaffolds. M. Faria et al. contribute with another detailed evaluation in particular of surfaces composed of poly(ester urethane urea) oxygenation membranes. This paper incorporates cross-sectional studies of membranes and analyses to assess physicochemical and hemocompatibility features of their surfaces. Oligonucleotide and Parylene surface coating for a specific hemocompatible surface modification is described by M. Schleicher et al. in a separate paper. This is an interesting contribution in the direction of biofunctionalization of vascular implant surfaces. W. Van

Oeveren and coworkers present a comparative study between different blood circulation models. They estimate functional as well as mechanical blood damage features under specific conditions. The review article of this special issue focuses on physicochemical and biological methods of surface modifications related to surfaces of cardiovascular implants. It is contributed by A. de Mel et al. The paper highlights the role of nanotechnology in connection with surface modification.

We are confident that this special issue provides a comprehensive review as well as new insights related to surface modification and evaluation technologies for blood contacting applications.

Zhongjun J. Wu
Narayana Garimella
Rolf Larsson
Eduard Brynda

Hindawi Publishing Corporation
International Journal of Biomaterials
Volume 2012, Article ID 707863, 8 pages
doi:10.1155/2012/707863

Review Article

Surface Modification of Biomaterials: A Quest for Blood Compatibility

Achala de Mel,[1] Brian G. Cousins,[1] and Alexander M. Seifalian[1,2]

[1] *UCL Centre for Nanotechnology & Regenerative Medicine, University College London, Pond Street, London NW3 2QG, UK*
[2] *Royal Free Hampstead NHS Trust Hospital, Pond Street, London NW3 2QG, UK*

Correspondence should be addressed to Alexander M. Seifalian, a.seifalian@ucl.ac.uk

Received 16 September 2011; Accepted 22 February 2012

Academic Editor: Narayana Garimella

Cardiovascular implants must resist thrombosis and intimal hyperplasia to maintain patency. These implants when in contact with blood face a challenge to oppose the natural coagulation process that becomes activated. Surface protein adsorption and their relevant 3D confirmation greatly determine the degree of blood compatibility. A great deal of research efforts are attributed towards realising such a surface, which comprise of a range of methods on surface modification. Surface modification methods can be broadly categorized as physicochemical modifications and biological modifications. These modifications aim to modulate platelet responses directly through modulation of thrombogenic proteins or by inducing antithrombogenic biomolecules that can be biofunctionalised onto surfaces or through inducing an active endothelium. Nanotechnology is recognising a great role in such surface modification of cardiovascular implants through biofunctionalisation of polymers and peptides in nanocomposites and through nanofabrication of polymers which will pave the way for finding a closer blood match through haemostasis when developing cardiovascular implants with a greater degree of patency.

1. Introduction

Cardiovascular disease accounts for a significant percentage of mortality and morbidity in the ageing population and has an estimated increase in the coming years [1]. There is an urgent clinical need for improved cardiovascular devices, which mainly include vascular bypass grafts, vascular stents, and heart valves, which will promote desirable blood-biomaterial interactions with a high patency. Vascular occlusive disease holds the greatest risk factor most emphasised in the coronary arteries where cardiac ischemia may lead to complete heart failure. Main reperfusion-based surgical intervention options for these diseases involve angioplasty, stenting, endarterectomy, and bypass graft surgery depending on the degree of occlusion. Cases with greater than 70% occluded arteries are required to be treated with bypass grafts. For small diameter bypass grafts, autologous bypass conduits are preferred for primary revascularisation [2]. However, 3–30% patients are presented with no autologous vessels due to previous disease conditions and thus there is a need for vascular grafts which could perform closely to autologous vessels [3]. Graft thrombogenicity due to material surface incompatibility and altered flow dynamics at the site of anastomosis or distal outflow are recognised as primary reasons for blood contacting device failure [4]. There is a great interest in research strategies that focus upon surface techniques by modifying the physicochemical properties at the implant surface [5] and by combining a biomimetic approach through functionalisation which presents an exciting challenge to improve patency rates clinically (Figure 1). This paper aims to review some of the significant approaches in modifying a material surface to create optimal interactions with blood.

2. Blood-Implant Surface Interactions: Thrombogenicity

The initial events leading to thrombosis surrounding the tissue-implant interface are mediated by surface interactions with adsorbed proteins (intrinsic pathway) or through the release of tissue factor (TF) from damaged cells at the site of

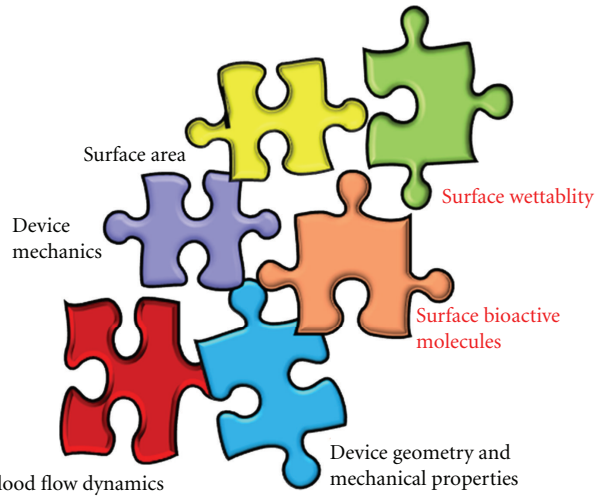

Figure 1: Haemocompatibility-determining factors in a cardiovascular device; marked in red are areas of interest in this paper.

injury (extrinsic pathway) [6] (Figure 2). The intrinsic pathway is independent of injury. Adsorbed surface proteins form a complex composed of collagen, high molecular weight kininogen (HMWK), prekallikrein, and factor XII. Inactive precursors (clotting factors) change conformation and are converted into active enzymes via a biochemical cascade resulting in platelet activation (with the aid of additional cofactors). Cleavage of prothrombin via the prothrombinase complex bound to cellular membranes generates thrombin, and by converting fibrinogen to fibrin, forms a stable insoluble gel (red thrombus or clot).

Vascular injury and damage to the endothelium releases TF, collagen, and von Willebrand factor (vWF) to initiate the extrinsic pathway. Clotting factors interact with platelet surface receptors and play a fundamental role in the interaction of collagen to initiate thrombosis, release growth factors and cytokines to enhance the coagulation cascade and strengthen the haemostatic plug. The platelets change morphology and agglomerate forming a thrombus layer. It is important to note that both pathways converge during the formation of the prothrombinase complex leading to thrombin generation referred to as the common pathway.

Vascular procedures such as arteriovenous graft placement and angioplasty damage the adventitial and medial tissues of the arterial wall with injury to the endothelium lining the intima [4]. For example, angioplasty is a controlled traumatic event, which is aimed at causing plaque rupture by widening a narrowed or obstructed vessel. These processes can expose otherwise intact subendothelial matrix removing the protective endothelium and expose medial smooth muscle cells (SMC) directly to blood flow, and other procoagulants and proinflammatory blood constituents. Tissue trauma rapidly initiates the recruitment of inflammatory cells that release potent cytokines and promote SMC migration and proliferation. The anticoagulant and vascular protective functions of intact endothelium from prostacyclin (PGI_2) and nitric oxide (NO) required for the regulation of blood flow soon diminish [7]. Both molecules are necessary to inhibit platelet adhesion, aggregation and activation to the endothelium and SMC, which are considered early events in the development of intimal hyperplasia (IH). Furthermore, NO inhibits SMC proliferation and migration. In addition, the adventitial layer is partially removed for creating the anastomosis during surgery depriving the vessel wall of oxygen and vital nutrients [8].

Almost all materials are considered to be thrombogenic with the exception of the endothelial cell (EC) layer, which lines the vasculature. Large diameter vascular grafts were originally thought to be antithrombogenic in nature. For example, expanded polytetrafluoroethylene (ePTFE) bypass grafts appear nonthrombogenic due to the high flow rates of blood past the luminal surface, but in reality, all are thrombogenic to a certain degree.

In healthy individuals the flow of blood is laminar but when compared with diseased or occluded arteries may often be transitional or even turbulent in behaviour. At the blood-biomaterial interface, haemodynamic forces of shear stress at the wall surface play a critical role in blood contacting devices and influence protein adsorption [9], platelet and leukocyte adhesion. Leukocytes recognise specific proteins and adhere under flowing conditions to initiate further cell signalling and recruitment events. A study evaluating leukocyte adhesion on polyurethanes materials has shown that cell density decreased with increasing shear stress. Certain shear stress models have been studied (particular when applied to seeded vascular grafts) to promote EC retention and found to correlate with changes in the EC phenotype [10]. Various strategies exist to inhibit these processes and prolong graft patency, including modification of grafts with various anticoagulants (heparin), antiplatelet factors (glycoprotein IIb/IIIa inhibitors), and antiproliferating agents (rapamycin). In the following sections we consider different surface modification techniques that are designed to minimise complications that arise at the blood-biomaterial interface.

3. Role of Proteins in Optimal Blood-Biomaterial Interactions

Cardiovascular implants, in the body, are subjected to the "Vroman effect" [11] which highlights the dynamic interactions with water and proteins to synthetic material. This event is rapid (<1 sec), leading to the formation of a thin protein film in the order of nanometers in thickness [12]. The adsorption of proteins (composed of polar, nonpolar, and charged side groups) contributes to the surface activity. Once present at the surface, protein molecules interact with water, electrolytes, and the underlying surface chemistry (and energy) of the material through hydrogen bonding, van der Waals, pi-pi (π-π) stacking, and electrostatic interactions. Exactly which force governs the interaction of proteins on surfaces depends upon the particular protein and other factors including size, charge, conformation, and unfolding rate described by Vroman [13]. Chemical and physical properties of the materials, for example, surface chemistry, energy (charge) and topography, influence the interfacial

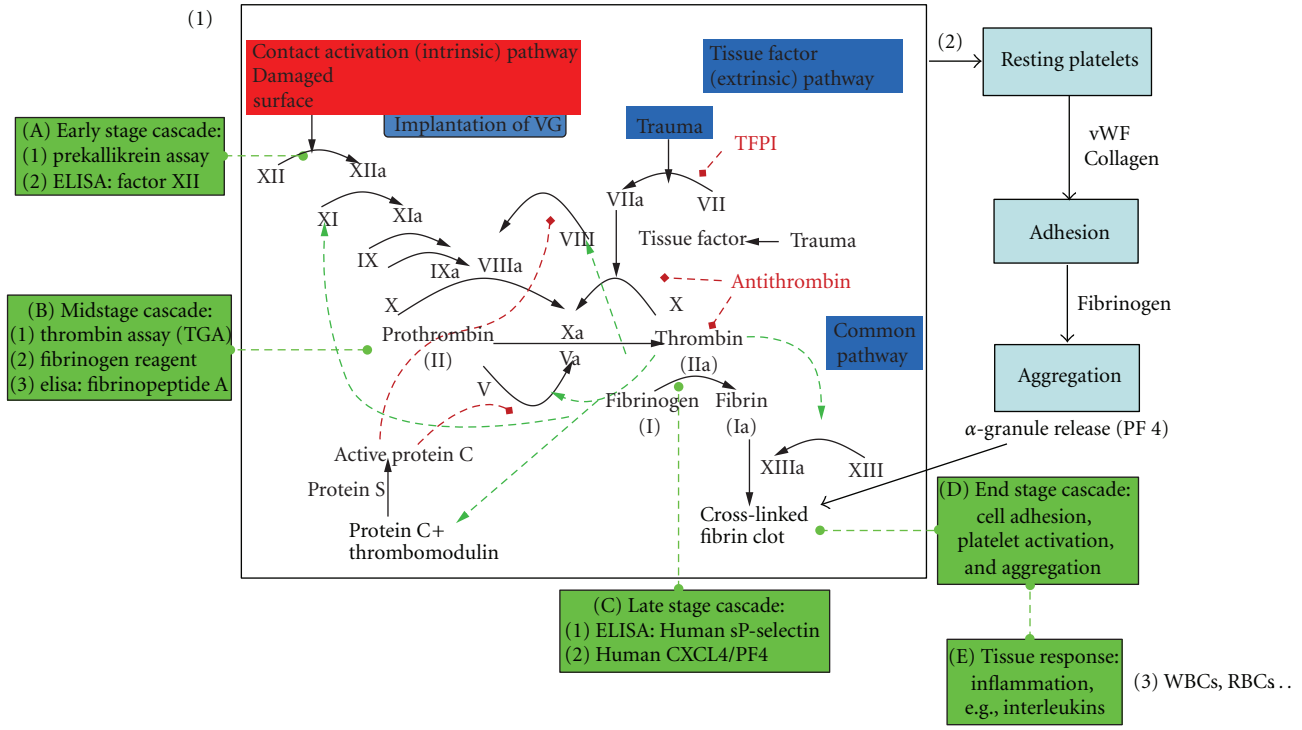

FIGURE 2: Intrinsic pathway of blood coagulation: highlighted are the main factors which are involved in blood coagulation. Numbered events distinguish as (1) biochemical, (2) platelets, and (3) whole blood (red and white blood cells). Image is adapted from http://en.wikipedia.org/wiki/File:Coagulation_full.svg.

behaviour adjacent to the biomaterial. The interfacial region at the blood-biomaterial surface continually alters and redistributes the protein/electrolyte/water layer, and the host cells and tissues react to changes in this layer. Material surfaces with zero interfacial energy and reduced enthalpic and entropic effects do not strongly support cell/thrombin adhesion [14]. Surface wettability of a biomaterial is highly significant and, in addition to differential protein adsorption, platelets respond differently to hydrophobic or hydrophilic monomers [15].

Adsorption of plasma and extracellular matrix (ECM) proteins (fibrinogen, albumin, and γ-globulin), and to a lesser degree fibronectin, collagen, vWF, coagulation factors XI and XII, and HMWK play a crucial role in balancing thrombosis and haemostasis [16]. Such proteins direct and aid the adhesion of red blood cells, platelets (the first cellular components to adsorb to the protein film), followed by leukocytes, and EC. The cellular components interact with the protein layer to guide migration, initiate blood coagulation, and stimulate cell proliferation and differentiation, as specific proteins present binding sites for macromolecules and receptors guiding the recruitment of further cells interacting within the vasculature.

Protein adsorption and subsequent cell attachment and behaviour in response to an implanted foreign material is determined by a variety of material properties including surface chemistry, topography, dissolution rate, and the micro-/macromechanical elasticity. Material surface properties can therefore be modified by physicochemical modification and/or biofunctionalisation to promote desirable protein and cellular interactions. Figure 3 summarizes the main mechanisms, which influence blood compatibility.

4. Surface Modification of Blood Contacting Materials

Much effort has focused on surface modification to optimise antithrombogenic surface properties and two approaches exist in the development of cardiovascular grafts. The first approach involves the design of a permanent vascular replacement, which has a nonadhesive, inert, nonbiofouling surface. Physicochemical methods have been applied to achieve this aim using electrochemical polishing, surface roughening, ordered patterning, plasma treatment [17], chemical etching, and passive or covalent surface coatings. The second approach aims to functionalise the grafts in such a way that it facilitates (or activates) a cascade of biological events which eventually regenerates or replaces functioning tissue. Biofunctionalisation of surfaces is a popular research theme, which relies on the tools of biology to create biomimetic surfaces to incorporate biologically active (or inactive) molecules to generate specific response(s) [18–22].

Figure 4, Table 1 present a summary of the principle methods in applied surface modification techniques. In this way, surface modification can be directed towards optimising the following: (1) protein adsorption (2), the generation of thrombin (and its formation leading to blood coagulation),

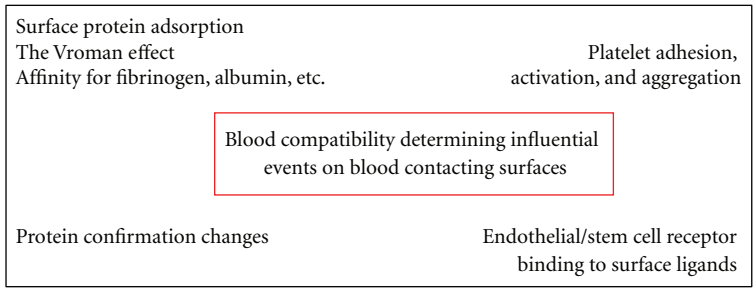

Figure 3: Main mechanisms influencing blood compatibility.

(3) platelet adhesion (followed by aggregation and activation), and (4) cellular behaviour at the surface of the prosthesis. All strategies are designed to optimise patency-limiting thrombogenic events at the blood-biomaterial interface. For example, vascular graft endothelialisation has been highlighted as the ultimate solution to address thrombogenicity, and its associated complications.

4.1. Physicochemical Modification. A range of physical techniques has been applied to modify the surface topography of vascular graft materials. Topography on the micron and nanometre scale is an important physical property, which influences protein adsorption, platelet adhesion, thrombogenicity, and cell behaviour [23]. The inclusion of pores, pits, and groves become unavoidable at this scale during the manufacturing process of blood contacting devices. For example, a recent study revealed that the surface roughness of ePTFE graft luminal surfaces was significantly higher (147.0 nm) when compared with external surfaces (1.74 nm). Plasma proteins such as fibrinogen have been shown to adhere to nanostructures and bind to platelet receptors more efficiently than flat structures [24]. Albumin, fibrinogen, and fibronectin all interact with a dialysis membrane's surface topography, which plays a crucial role in the adsorption process. Such surfaces have been shown to promote fibronectin and vitronectin adsorption and direct a cascade of interactions from the blood and surrounding tissues. Surface porosity is a crucial factor when considering the topography of vascular graft materials [25]. A recent study looked at the effect of porosity (ranging from 5 to 90 μm in diameter) on EC growth. It was found that EC cell growth was enhanced by smaller pores (5–20 μm in diameter) and at a lower interpore distances.

Changing the surface topography on the micron and nanometre scale also lead to localised changes in surface chemistry as both physicochemical cues are intrinsically linked. The primary aim of topographical and chemical surface modification is to encourage desirable protein, cellular, and tissue interactions at the blood-biomaterial interface, thus improving patency and performance of the material, since all are known contributory factors that influence thrombogenicity. Nanocomposite materials are recognised to offer favourable solutions as biomaterials for cardiovascular implants. Nanocomposite polymers in general have found to be amphiphilic, thermodynamically stable and, when used in vascular bypass graft development, they have shown to exert novel advantageous properties such as favourable blood response [27], biostability [28], and enhanced mechanical properties compared to grafts with conventional material. While being viscoelastic, polyhedral-oligomeric-silsesquioxane-poly(carbonate-urea)urethane (POSS-PCU) has been shown to have strength similar to natural arteries. POSS-nanocomposite polymer, used for cardiovascular implants, which include vascular bypass grafts, stents, and heart valves has been proved to have antithrombogenic properties [29].

Nonfouling surfaces have been used to prevent protein adsorption and platelet adhesion. Much effort has focused upon the passivation of materials using polymers to achieve a nonadhesive, nonbiofouling surfaces such as PEG (polyethylene glycol), hydrogels (containing dextran), and PEO (polyethylene oxide). For example, ePTFE grafts have been coated with polypropylene sulphide (PPS)-PEG and evaluated in arteriovenous models. This study included heparinised and nonheparinised graft perfusion and evaluated cell adhesion and thrombus formation. No difference was observed in cell adhesion when compared with controls; however, the surface coating significantly decreased thrombus formation when used in conjunction with heparin. Dextrans (hydrophilic polysaccharides) show a similar effect to PEG with regard to protein adsorption. Dextrans, PEG, and PEO can be further chemically modified along the polymer backbone with cell-selective peptides to promote specific cell adhesion. Spin coating of the luminal surface of ePTFE was recently achieved using a biodegradable elastomer poly(1,8-octanediol citrate) (POC). The POC coatings had no effect on graft compliance and delayed thrombosis *in vitro* when compared with controls. This study highlighted that POC-ePTFE grafts maintained EC adhesion and proliferation of porcine cells similar to that of the native tissues, and within 10 days the EC was confluent, while only random patches were evident on ePTFE controls.

4.2. Biofunctionalisation

4.2.1. Endothelialisation. The endothelium is in intimate contact with the blood flow and consists of a single layer of EC, which functions as a dynamic organ and covers the entire surface of the circulating system from the heart to the smallest capillary. Endothelialisation of cardiovascular

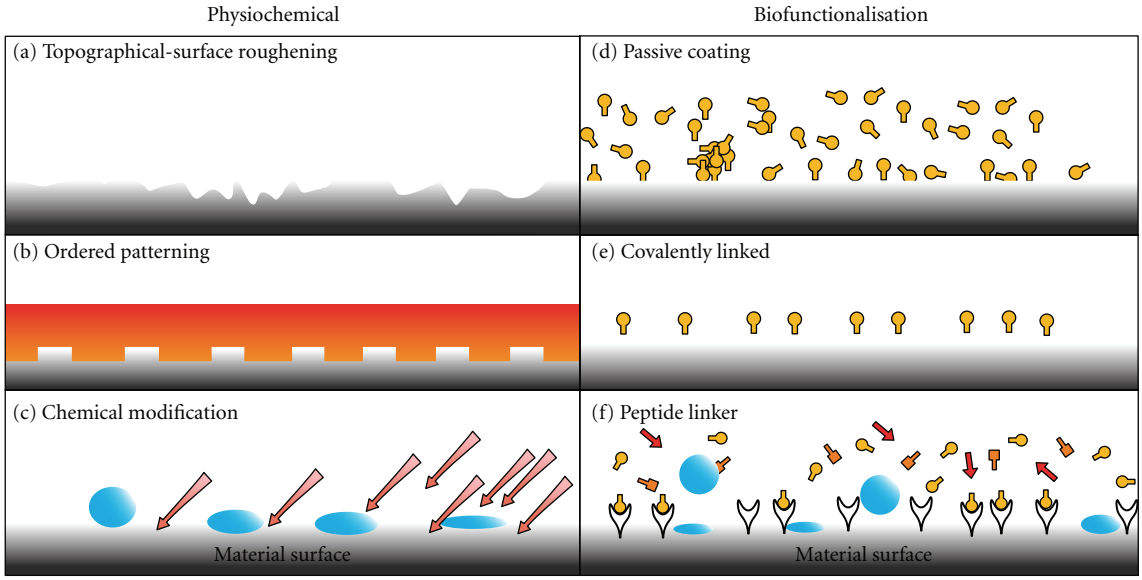

Figure 4: Examples of various physical, chemical, and biofunctionalisation techniques to enhance haemocompatibility. Biofunctionalised surfaces interact with cell surface receptors, that is integrins. Whereas physiochemical modification can influence cell-material interactions through charge, topography, and attractive/repulsive forces due to hydrophobic and hydrophilic interactions [26].

Table 1: Summary of the various modification techniques currently employed for optimising blood-material interactions [26].

Modification	Description
Physical immobilisation	Polymer gelling (growth factor mixed with the material in the liquid state and change temp, pH or ion concentration to obtain a gel with nanopores) Emulsion techniques (factors which are insoluble in aqueous solutions) High pressure gas foaming (incorporate GF into porous scaffolds, without the use of solvents)
Covalent modification	Surface distribution of ligands Distribution of ligands through the bulk of the material
Surface adsorption	Passive adsorption driven by secondary interactions between the molecule and the protein Self-assembled monolayers (SAMs) adsorption of the peptide (which is designed with hydrophobic tail and a spacer) from solution Microcontact printing of alkanethiol SAMs, photolithography (on hard materials), soft lithography (on elastomeric materials) Direct protein patterning: drop dispensing, microfluidic patterning
Crosslinking	Photo/chemical crosslinking
Altering surface wettability	Ion bombardment UV irradiation Exposure to plasma discharge
Altering surface roughness	Deposition of polymer films/islands, nanoparticles, metallographic paper or diamond paste polishing, sand blasting, photolithography, and e-beam etching

implants is considered most favourable as this would protect the vessels by producing natural biochemicals, for example, NO for vasoprotection. There is a great deal of research involved in inducing endothelialisation of cardiovascular implants and *insitu* endothelialisation is considered to be most favourable. This need for *insitu* endothelialisation has led to a considerable interest in stem cells which have the potential to induce endothelialisation. This interest in endothelial progenitor stem cells inturn has given rise to an exciting area of research on "stem cell technology" for vascular grafts.

Stem cells/EPC are on the threshold of realising their great potential in cardiovascular therapy and stem cell interactions with various biomaterials which have been extensively studied [30–34]. Cells are inherently sensitive to physical, biochemical, and chemical stimuli from their surroundings. Cells are in intimate contact with the ECM, which is formed from a complex connection of proteins, glycoproteins, and proteoglycans. The ECM provides not only structural support but also contains a reservoir of cell signalling motifs (ligands) and growth factors that guide cellular anchorage and behaviour. The local cell environment

or "niche" provides defined environmental cues that determine cell-specific behaviour, including selective recruitment, proliferation, differentiation, and the production of the numerous proteins needed for hierarchical tissue organisation. The plethora of ECM compositions contain insoluble macromolecules fibrillar proteins (e.g., collagen) and glycoproteins (e.g., elastin, fibronectin, laminin) which interact with proteins on cell surfaces and soluble macromolecules such as growth factors. The organisation, density, spatial geometry, and biochemistry of these ECM components determine mechanical strength, cell response, and ultimately hierarchical tissue organization.

Features of the ECM such as nanoscale topography, optimised mechanical properties, and presentation of bioresponsive motifs have inspired multiple examples of biomaterials design for tissue engineering scaffolds. One strategy in vascular research is to present endothelium-derived macromolecules or their cell interacting domains onto vascular grafts to mimic these features of the ECM and to assist specific cell adhesion. Bioresponsive vascular grafts can target several biological processes to promote *insitu* endothelialisation including: (1) promoting the mobilisation of EPC from the bone marrow, (2) encouraging cell-specific (circulating EC, EPC, and/or stem cells) homing to the vascular graft site, (3) providing cell-specific adhesion motifs (peptides) on the vascular grafts (of a predetermined spatial concentration), and (4) directing the behaviour of the cells after adhesion to rapidly form a mature, fully functioning endothelium capable of self-repair.

Optimal cell attachment, migration, proliferation, and differentiation on a biomaterial require a surface which mimics the natural ECM. Natural ECM proteins range in diameter from 50–500 nm. The significance of mimicking the ECM, which facilitates the interactions with the cell receptors such as integrins, has been discussed. This also recognises the effect of peptides such as RGD [35], which are derived from functional domains of ECM components and their effects on enhancing accelerated endothelialisation. Nevertheless, nonreceptor-mediated interaction of ECM such as porosity, 3D spatial arrangement also has a great influence in cell interaction.

The microtopography of scaffold materials is not entirely ideal for vascular cells, particularly EC as they are naturally placed in a nanometre scale environment. Nanotopography surfaces created by surface roughening of a range of materials including polymers have shown enhanced cellular adhesion [36–40]. Recent reviews have discussed various nanotechniques which could potentially be applied to vascular graft engineering. Nanostructures has been shown to facilitate protein interactions which then promote cell adhesion [9, 41, 42]. Some of these proteins are selective such as vitronectin and fibronectin where they mediate enhanced vascular cell interactions with the polymer [37, 38]. Three main nanotechnology approaches, electrospinning [43, 44], self-assembly, and phase separation, help to create nanofibres and to create a nanoarchitecture bypass graft surface for optimal cell interactions [45].

In addition to mimicking an ECM, research has looked into antibody-mediated stem cell recruitment as a rather impressive approach in stem cell technology for applications in vascular graft endothelialisation. EC and EPC have been found to express CD34+, and therefore CD34+ antibodies can be attached onto bypass graft surfaces to facilitate interaction between graft and progenitor cells. Antihuman CD34 monoclonal antibodies (IgG2a, epitope class III) were immobilised to the ePTFE graft material (Orbus Medical Technologies) with a proprietary multistep process.

In additional, further studies have shown that superparamagnetic nanoparticles labelled endothelial cells can be used to obtain an endothelial cell lining, for instance, as on the luminal surface PTFE tubular grafts, coated with fibronectin with the aid of a customized electromagnet [46].

4.2.2. Antithrombogenic Surfaces Independent of an Endothelium. The cardiovascular protective role of the endothelium is recognized to be attributed to NO. Therefore, there is a great interest in inducing NO from cardiovascular implants and this has recently been reviewed in depth [47]. Recent reviews have also detailed numerous anticoagulant and antiplatelet agents that include, heparin, warfarin, hirudin, dipyridamole clopidogrel, aspirin, cilostazol, and glycoprotein IIb/IIIa inhibitors (abciximab, eptifibatide, tirofiban), which are clinically used in addition to their applications in engineered vascular graft surfaces [4, 48].

5. Summary and Future Perspective

Blood contacting materials, which are used to fabricate cardiovascular implants, are expected to preferably promote endothelial adhesion but resist other blood cell adhesion that can give rise to thrombosis and intimal hyperplasia. A greater understanding of the interactions of blood proteins with material surfaces will enable better designing of surfaces for blood contact. Surface modifications of materials will be highly influenced by nanotechnology as this enables to impart favourable properties without influencing the structural and mechanical properties of the base material, which forms the structure of a device of interest. It is also of significance that a particular surface modification should be always tailored to the implant of interest and should be tested for its efficacy in physiological haemodynamic conditions. We believe that a reasonable progress has been made in the search for optimal blood contacting materials, but research into NO eluting polymers, endothelialisation, and nanotechnology associated with surface modification of such materials may promise more sophisticated solutions in the quest for optimal blood compatibility.

References

[1] S. Allender and M. Rayner, "Coronary heart disease statistics; British Heart Foundation," Heart Statistics, 2007, http://www.bhf.org.uk/heart-health/statistics.aspx.

[2] M. Desai, A. M. Seifalian, and G. Hamilton, "Role of prosthetic conduits in coronary artery bypass grafting," *European Journal of Cardio-Thoracic Surgery*, vol. 40, no. 2, pp. 394–398, 2011.

[3] M. S. Baguneid, A. M. Seifalian, H. J. Salacinski, D. Murray, G. Hamilton, and M. G. Walker, "Tissue engineering of blood

vessels," *British Journal of Surgery*, vol. 93, no. 3, pp. 282–290, 2006.

[4] S. Sarkar, K. M. Sales, G. Hamilton, and A. M. Seifalian, "Addressing thrombogenicity in vascular graft construction," *Journal of Biomedical Materials Research*, vol. 82, no. 1, pp. 100–108, 2007.

[5] M. D. Mager, V. Lapointe, and M. M. Stevens, "Exploring and exploiting chemistry at the cell surface," *Nature Chemistry*, vol. 3, no. 8, pp. 582–589, 2011.

[6] M. B. Gorbet and M. V. Sefton, "Biomaterial-associated thrombosis: roles of coagulation factors, complement, platelets and leukocytes," *Biomaterials*, vol. 25, no. 26, pp. 5681–5703, 2004.

[7] B. Tesfamariam, "Platelet function in intravascular device implant-induced intimal injury," *Cardiovascular Revascularization Medicine*, vol. 9, no. 2, pp. 78–87, 2008.

[8] L. Li, C. M. Terry, Y. T. E. Shiu, and A. K. Cheung, "Neointimal hyperplasia associated with synthetic hemodialysis grafts," *Kidney International*, vol. 74, no. 10, pp. 1247–1261, 2008.

[9] V. Mironov, V. Kasyanov, and R. R. Markwald, "Nanotechnology in vascular tissue engineering: from nanoscaffolding towards rapid vessel biofabrication," *Trends in Biotechnology*, vol. 26, no. 6, pp. 338–344, 2008.

[10] J. Hoffmann, J. Groll, J. Heuts et al., "Blood cell and plasma protein repellent properties of star-peg-modified surfaces," *Journal of Biomaterials Science, Polymer Edition*, vol. 17, no. 9, pp. 985–996, 2006.

[11] H. Noh and E. A. Vogler, "Volumetric interpretation of protein adsorption: competition from mixtures and the vroman effect," *Biomaterials*, vol. 28, no. 3, pp. 405–422, 2007.

[12] T. A. Horbett, "Proteins: structure, properties and adsorption to surfaces," in *Biomaterials Science: An Introduction to Materials in Medicine*, B. D. Ratner, A. S. Hoffman, F. J. Schoen, and J. E. Lemons, Eds., pp. 133–141, Academia Press, 1996.

[13] L. Vroman, "Effect of adsorbed proteins on the wettability of hydrophilic and hydrophobic solids," *Nature*, vol. 196, no. 4853, pp. 476–477, 1962.

[14] J. D. Andrade and V. Hlady, "Protein adsorption and materials biocompatibility: a tutorial review and suggested hypotheses," *Advances in Polymer Science*, pp. 1–63, 1987.

[15] K. L. Menzies and L. Jones, "The impact of contact angle on the biocompatibility of biomaterials," *Optometry and Vision Science*, vol. 87, no. 6, pp. 387–399, 2010.

[16] S. P. Watson, "Platelet activation by extracellular matrix proteins in haemostasis and thrombosis," *Current Pharmaceutical Design*, vol. 15, no. 12, pp. 1358–1372, 2009.

[17] A. Solouk, B. G. Cousins, H. Mirzadeh, M. Solati-Hashtjin, S. Najarian, and A. M. Seifalian, "Surface modification of poss-nanocomposite biomaterials using reactive oxygen plasma treatment for cardiovascular surgical implant applications," *Biotechnology and Applied Biochemistry*, vol. 58, no. 3, pp. 147–161, 2011.

[18] C. M. Nickson, P. J. Doherty, and R. L. Williams, "Novel polymeric coatings with the potential to control in-stent restenosis—an in vitro study," *Journal of Biomaterials Applications*, vol. 24, no. 5, pp. 437–452, 2010.

[19] A. de Mel, G. Punshon, B. Ramesh et al., "In situ endothelialization potential of a biofunctionalised nanocomposite biomaterial-based small diameter bypass graft," *Bio-Medical Materials and Engineering*, vol. 19, no. 4-5, pp. 317–331, 2009.

[20] P. W. Kämmerer, M. Heller, J. Brieger, M. O. Klein, B. Al-Nawas, and M. Gabriel, "Immobilisation of linear and cyclic rgd-peptides on titanium surfaces and their impact on endothelial cell adhesion and proliferation," *European Cells & Materials*, vol. 21, pp. 364–372, 2011.

[21] M. M. Reynolds and G. M. Annich, "The artificial endothelium," *Organogenesis*, vol. 7, no. 1, pp. 42–49, 2011.

[22] K. Kanie, R. Kato, Y. Zhao, Y. Narita, M. Okochi, and H. Honda, "Amino acid sequence preferences to control cell-specific organization of endothelial cells, smooth muscle cells, and fibroblasts," *Journal of Peptide Science*, vol. 17, no. 6, pp. 479–486, 2011.

[23] M. S. Lord, B. Cheng, S. J. McCarthy, M. Jung, and J. M. Whitelock, "The modulation of platelet adhesion and activation by chitosan through plasma and extracellular matrix proteins," *Biomaterials*, vol. 32, no. 28, pp. 6655–6662, 2011.

[24] M. Yaseen, X. Zhao, A. Freund, A. M. Seifalian, and J. R. Lu, "Surface structural conformations of fibrinogen polypeptides for improved biocompatibility," *Biomaterials*, vol. 31, no. 14, pp. 3781–3792, 2010.

[25] M. Ahmed, H. Ghanbari, B. G. Cousins, G. Hamilton, and A. M. Seifalian, "Small calibre polyhedral oligomeric silsesquioxane nanocomposite cardiovascular grafts: influence of porosity on the structure, haemocompatibility and mechanical properties," *Acta Biomaterialia*, vol. 7, no. 11, pp. 3857–3867, 2011.

[26] A. de Mel, G. Jell, M. M. Stevens, and A. M. Seifalian, "Biofunctionalization of biomaterials for accelerated in situ endothelialization: a review," *Biomacromolecules*, vol. 9, no. 11, pp. 2969–2979, 2008.

[27] R. Y. Kanna, H. J. Salacinski, J. De Groot et al., "The antithrombogenic potential of a polyhedral oligomeric silsesquioxane (POSS) nanocomposite," *Biomacromolecules*, vol. 7, no. 1, pp. 215–223, 2006.

[28] R. Y. Kannan, H. J. Salacinski, M. Odlyha, P. E. Butler, and A. M. Seifalian, "The degradative resistance of polyhedral oligomeric silsesquioxane nanocore integrated polyurethanes: an in vitro study," *Biomaterials*, vol. 27, no. 9, pp. 1971–1979, 2006.

[29] H. Ghanbari, A. de Mel, and A. M. Seifalian, "Cardiovascular application of polyhedral oligomeric silsesquioxane nanomaterials: a glimpse into prospective horizons," *International Journal of Nanomedicine*, vol. 6, pp. 775–786, 2011.

[30] A. Wilson, P. E. Butler, and A. M. Seifalian, "Adipose-derived stem cells for clinical applications: a review," *Cell Proliferation*, vol. 44, no. 1, pp. 86–98, 2011.

[31] K. Saha, J. F. Pollock, D. V. Schaffer, and K. E. Healy, "Designing synthetic materials to control stem cell phenotype," *Current Opinion in Chemical Biology*, vol. 11, no. 4, pp. 381–387, 2007.

[32] N. S. Hwang, S. Varghese, and J. Elisseeff, "Controlled differentiation of stem cells," *Advanced Drug Delivery Reviews*, vol. 60, no. 2, pp. 199–214, 2008.

[33] E. Dawson, G. Mapili, K. Erickson, S. Taqvi, and K. Roy, "Biomaterials for stem cell differentiation," *Advanced Drug Delivery Reviews*, vol. 60, no. 2, pp. 215–228, 2008.

[34] C. Chai and K. W. Leong, "Biomaterials approach to expand and direct differentiation of stem cells," *Molecular Therapy*, vol. 15, no. 3, pp. 467–480, 2007.

[35] N. Alobaid, H. J. Salacinski, K. M. Sales et al., "Nanocomposite containing bioactive peptides promote endothelialisation by circulating progenitor cells: an in vitro evaluation," *European Journal of Vascular and Endovascular Surgery*, vol. 32, no. 1, pp. 76–83, 2006.

[36] D. C. Miller, T. J. Webster, and K. M. Haberstroh, "Technological advances in nanoscale biomaterials: the future of synthetic

vascular graft design," *Expert Review of Medical Devices*, vol. 1, no. 2, pp. 259–268, 2004.

[37] D. C. Miller, K. M. Haberstroh, and T. J. Webster, "Mechanism(s) of increased vascular cell adhesion on nanostructured poly(lactic-co-glycolic acid) films," *Journal of Biomedical Materials Research*, vol. 73, no. 4, pp. 476–484, 2005.

[38] D. C. Miller, K. M. Haberstroh, and T. J. Webster, "PLGA nanometer surface features manipulate fibronectin interactions for improved vascular cell adhesion," *Journal of Biomedical Materials Research*, vol. 81, no. 3, pp. 678–684, 2007.

[39] R. J. McMurray, N. Gadegaard, P. M. Tsimbouri et al., "Nanoscale surfaces for the long-term maintenance of mesenchymal stem cell phenotype and multipotency," *Nature Materials*, vol. 10, no. 8, pp. 637–644, 2011.

[40] L. E. McNamara, R. J. McMurray, M. J. Biggs, F. Kantawong, R. O. Oreffo, and M. J. Dalby, "Nanotopographical control of stem cell differentiation," *Journal of Tissue Engineering*, vol. 2010, article 120623, 2010.

[41] A. de Mel, C. Bolvin, M. Edirisinghe, G. Hamilton, and A. M. Seifalian, "Development of cardiovascular bypass grafts: endothelialization and applications of nanotechnology," *Expert Review of Cardiovascular Therapy*, vol. 6, no. 9, pp. 1259–1277, 2008.

[42] M. Loizidou and A. M. Seifalian, "Nanotechnology and its applications in surgery," *British Journal of Surgery*, vol. 97, no. 4, pp. 463–465, 2010.

[43] Q. P. Pham, U. Sharma, and A. G. Mikos, "Electrospinning of polymeric nanofibers for tissue engineering applications: a review," *Tissue Engineering*, vol. 12, no. 5, pp. 1197–1211, 2006.

[44] R. Murugan and S. Ramakrishna, "Nano-featured scaffolds for tissue engineering: a review of spinning methodologies," *Tissue Engineering*, vol. 12, no. 3, pp. 435–447, 2006.

[45] J. J. Norman and T. A. Desai, "Methods for fabrication of nanoscale topography for tissue engineering scaffolds," *Annals of Biomedical Engineering*, vol. 34, no. 1, pp. 89–101, 2006.

[46] H. Perea, J. Aigner, J. T. Heverhagen, U. Hopfner, and E. Wintermantel, "Vascular tissue engineering with magnetic nanoparticles: seeing deeper," *Journal of Tissue Engineering and Regenerative Medicine*, vol. 1, no. 4, pp. 318–321, 2007.

[47] A. De Mel, F. Murad, and A. M. Seifalian, "Nitric oxide: a guardian for vascular grafts?" *Chemical Reviews*, vol. 111, no. 9, pp. 5742–5767, 2011.

[48] A. G. Kidane, H. Salacinski, A. Tiwari, K. R. Bruckdorfer, and A. M. Seifalian, "Anticoagulant and antiplatelet agents: their clinical and device application(s) together with usages to engineer surfaces," *Biomacromolecules*, vol. 5, no. 3, pp. 798–813, 2004.

Hindawi Publishing Corporation
International Journal of Biomaterials
Volume 2012, Article ID 673163, 7 pages
doi:10.1155/2012/673163

Research Article

Comparison of Modified Chandler, Roller Pump, and Ball Valve Circulation Models for *In Vitro* Testing in High Blood Flow Conditions: Application in Thrombogenicity Testing of Different Materials for Vascular Applications

Wim van Oeveren,[1] Ignace F. Tielliu,[2] and Jurgen de Hart[3]

[1] *Haemoscan and Department of Cardiothoracic Surgery, UMCG, Haemoscan, Stavangerweg 23-23, 9723 JC, Groningen, The Netherlands*
[2] *University Medical Center Groningen (UMCG), P.O. Box 9700 RB Groningen, The Netherlands*
[3] *Hemolab, Den Dolech 2, 5612 AZ Eindhoven, The Netherlands*

Correspondence should be addressed to Wim van Oeveren, w.vanoeveren@haemoscan.com

Received 14 October 2011; Accepted 22 February 2012

Academic Editor: Narayana Garimella

Three different models, a modified Chandler loop, roller pump, and a new ball valve model (Hemobile), were compared with regard to intrinsic damage of blood components and activation of platelets. The Hemobile was used for testing of polymer tubes. High flow was not possible with the Chandler loop. The roller pump and the Hemobile could be adjusted to high flow, but he pump induced hemolysis. Platelet numbers were reduced in the roller pump and Chandler loop ($P < 0.05$), but remained high in the Hemobile. Platelet aggregation was reduced in all models. The Hemobile was applied for testing vascular graft materials, and allowed different circuits circulated simultaneously at 37°C. ePTFE, Dyneema Purity UHMWPE fiber and PET fiber based tubes, all showed hemolysis below 0.2% and reduced platelet count and function. Binding of fibrin and platelets was higer on PET, inflammatory markers were lowest on Dyneema Purity UHMWPE. We concluded that the Hemobile minimally affects blood and could be adjusted to high blood flows, simulating arterial shear stress. The Hemobile was used to measure hemocompatibility of graft material and showed Dyneema Purity UHMWPE fiber in many ways more hemocompatible than ePTFE and PET.

1. Introduction

The use of medical devices for temporary use or implantation in the blood circulation has resulted in an increased demand for evaluation of complications brought about by these devices. This resulted also in-better defined ISO requirements for testing [1] One important and relevant aspect of testing of medical devices is the condition of blood exposed to the device. Anticoagulation and flow conditions must be as similar as possible as in the clinical setting in order to achieve relevant test results. For some devices, including grafts, stents, and catheters, this implies similar anticoagulation treatment as used in clinical situations, but also high flow through or around the device to obtain relevant shear stress conditions [2, 3]. However, in some reports, blood was treated with other anticoagulants than in clinical situations. In addition, test devices were incubated under static conditions [4–7].

Flow models for testing may consist of animal models or *in vitro* test systems. Animal models should be avoided if equally quality results may be obtained in other ways. In addition, animal blood has essential differences compared with human blood, particularly with regard to clotting and platelet function. Two types of *in vitro* flow models (often with human blood) have been used extensively: the modified Chandler loop and the roller pump closed-loop system. The

modified Chandler loop [8] consists of closed tubing partly filled with air. On rotation, devices in the tubing repetitively circulate through the air-liquid interface. Use of this system may induce artefacts due to major forces applied to blood elements and protein denaturation at the air-liquid interface [9–11]. Another flow model is the roller pump closed-loop system. This model appeared effective for short circulation times [12–14], but intrinsic blood damage reduces sensitivity and does not allow prolonged exposure to blood [15]. To overcome the disadvantages of these models, the Hemobile was constructed. It consists of a simple mechanical device which generates a semicircular movement. In addition, the tubing contains no air, and there is no mechanical device compressing the tubing. In this way it was attempted to reduce damage and activation and to simulate pulsatile flow in a frequency similar to the arterial circulation. The Hemobile model was compared with the Chandler loop and roller pump model for intrinsic damage to blood components and activation of platelets. The Hemobile was further used in testing tubular structures made of various polymers to show its effectiveness in determination of hemocompatibility by means of *in vitro* circulation of human blood.

2. Materials and Methods

2.1. Blood Collection. Fresh human blood was obtained by vena puncture with a 19 Gauge needle under low pressure from five healthy adult volunteers and anticoagulated with a clinical dose of heparin (1.5 IU/mL) (Leo Pharmaceutical Products BV, Weesp, The Netherlands).

2.2. Before Incubation. Before starting the experiment, cell count (cell counter Medonic CA 530, Medonic, Sweden) and platelet function analysis (Platelet Function Analyzer-100) were performed and platelet aggregation was determined by adding 50 mMol ADP to a mixture of 500 μL of blood and 500 μL of saline and with the use of a whole blood aggregometer (Chrono Log Corp. aggregometer, Kordia Life Sciences, Leiden, The Netherlands) to confirm proper blood quality relevant for this study and to provide baseline characteristics.

2.3. Flow Models. Three circulation models were compared; the modified Chandler loop, roller pump, and Hemobile model (Figure 1). The principle of the modified Chandler model is based on a chamber of air that remains on top of a vertical rotating circular loop (De Spatel BV, Roden, the Netherlands). The roller pump is a nonocclusive pump for clinical use in extracorporeal circuits (Stöckert, Munich, Germany). The Hemobile (Haemoscan BV, Groningen, the Netherlands) consists of a cylinder, which is forced in a semirotating movement. On this cylinder the circular loop circuits can be positioned. Due to the semirotating movement and the slowness of blood, a pulsating movement of blood through the circuits is generated which mimics pulsatile flow. A ball valve ensures a directed flow of up to 40 mL/min through 3 mm tubing at 60 beats/min, thus creating shear stresses of 12 dynes/cm^2. Also, the flow wave form generated by the model is more physiological compared to the roller pump and Chandler model.

2.4. Study Design Model Validation. A comparative study was performed to assess intrinsic blood damage for three different closed-loop circulation models, without any test device in the circuit. Each set of experiments (three different circuits in triplicate) was performed five times with fresh venous blood from a different donor for each set. Due to restrictions of the Chandler loop model, the flow through 3 mm tubing was limited to 25 mL/min (6 dynes/cm^2) in all experiments. The first set of experiments was performed under circumstances of similar flow (25 mL/min) in all three test systems.

The following sets of experiments ($n = 4$) were performed with the roller pump and Hemobile at an exceeded blood flow of 40 mL/min (12 dynes/cm^2), which resembles shear stresses in the coronary blood circulation.

After these validation experiments, the Hemobile was used to test the hemocompatibility of woven tubular structures from polyester (PET) fiber and Dyneema Purity UHMWPE fiber, in comparison with expanded polytetrafluoroethylene (ePTFE) tubes. Platelet function, thrombosis, and hematology were tested according ISO10993/4.

2.5. Incubation. All experiments were performed with closed PVC tubing circuits (Raumedic) with a length of 45 cm and an internal diameter of 3 mm. The Chandler loop and roller pump circuits contained Luer-lock connectors. The Hemobile circuits were fitted with a ball valve connector (Halkey-Roberts, Street Petersburg, FL, USA). The roller pump circuit was partially immersed in water, whereas the Chandler loop and Hemobile were completely placed in an oven (Figure 1). The temperature in all three circuits was permanently kept at 37°C. The circuits of the roller pump and Hemobile were filled with 4.5 mL of blood and the circuits rotating on the Chandler loop system with 4.0 mL of blood and 0.5 mL of air.

2.6. After Incubation. After one hour of circulation, the circuits were emptied. Cell count, platelet function analysis, and platelet aggregation measurements were performed on the circulated blood, as described above. The rest of the blood was mixed with 0.2 M EDTA and centrifuged at 11,000 ×g for one minute. Plasma was used for analysis of thromboxane B2 (TXB2), Thrombin-Antithrombin III (TAT) complexes, elastase, and hemoglobin concentrations.

Activation of the arachidonic acid pathway in platelets results in the release of the potent platelet aggregating agent thromboxane A2, which is rapidly converted to the inactive product TXB2. TXB2 was measured by means of an enzyme immunoassay (Biotrak, Amersham, UK), based on competition of labelled TXB2 with sample TXB2. In this test the label is a peroxidase, which converts the substrate tetramethylbenzidine, yielding a yellow colour which is measured at 450 nm by a spectrophotometer (Powerwave 200, Biotek Instruments, Winooski, VT, USA).

TAT was measured as an indication of coagulation activity. Thrombin formation during the *in vitro* experiments was

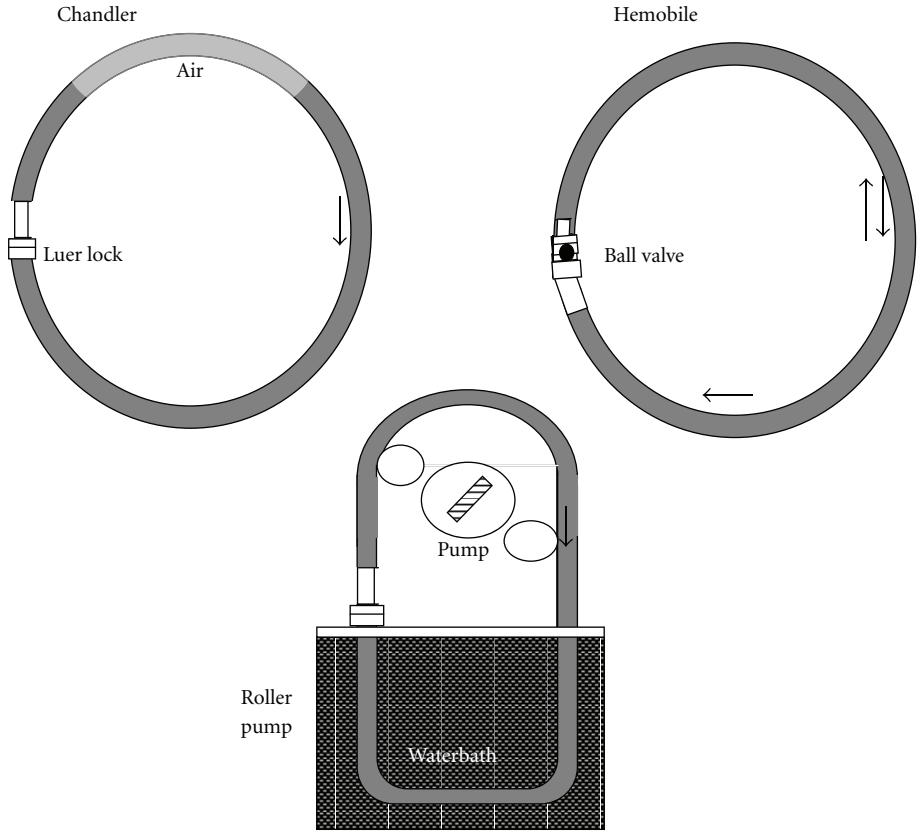

Figure 1: Schematic presentation of *in vitro* modified Chandler loop, Hemobile, and roller pump circulation model. All models could contain a chamber in the circulation loop, containing a biomaterial or product for testing.

determined by means of TAT complexes in EDTA plasma. A TAT ELISA was performed with capture and detection of antibodies from Cederlane Laboratories (Hornby, Canada).

Release of polymorphonuclear (PMN) elastase *in vivo* is a specific marker for inflammation reactions. Free in plasma, elastase is rapidly neutralised by α1-antitrypsin inhibitor to form a stable complex. Elastase was determined by ELISA by means of capture antibody against human elastase and labelled detection antibody against alpha1 antitrypsin (Affinity Biologicals, Ontario, Canada).

Complement activation was determined by ELISA based on a mouse anti human C5-9 antibody (DAKO, Glostrup, Denmark) and goat anti-C5 detection antibody (Quidel, San Diego, CA, USA).

Free hemoglobin as an index for erythrocyte damage was measured as described by Harboe [16] and using a spectrophotometer (Power Wave 200). The emptied PVC circuits and the incubated graft material were washed with Tris-buffered saline (pH 7.4). Platelet adhesion onto the surface of the circuits was measured by means of a colorimetric assay, based on the presence of acid phosphatase in platelets [17]. Platelet binding was measured based on the release of platelet acid phosphatase in Citrate buffer (pH 5.4), containing p-nitrophenyl phosphatase and Triton X100. Substrate conversion is proportional to the amount of platelets, which was determined by a standard curve and platelet counting.

Scanning electron microscopy (SEM) was achieved on material fixated in 2% glutaraldehyde in cacodylate buffer, treated with osmium tetraoxide in cacodylate buffer and gold sputtered critical point dried samples. These were visualized at 2 kV (Jeol 6301 F, Jeol Ltd., Tokyo, Japan).

2.7. Statistical Analysis. Normally distributed variables were reported as mean with standard deviation (SD). ANOVA was performed for all blood parameters to assess any difference in blood cell damage or activation between the circuits. Posthoc evaluation was performed by *t*-test.

3. Results

3.1. Whole Blood Assays at 25 mL/min Flow. Platelet-count was significantly reduced by the roller pump and by the modified Chandler loop, but not by the Hemobile (Figure 2). Platelet function was partially decreased in all systems, in particular in the roller pump system. Platelet adhesion to the PVC tubing was lowest in the Chandler loop (Table 1).

3.2. Plasma Assays. TXB2 and free hemoglobin were significantly higher after roller pump circulation than after

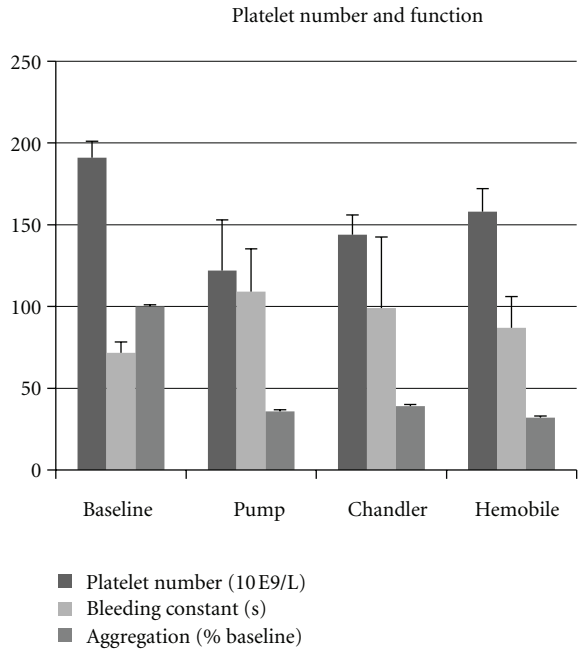

Figure 2: Effects of three circulation models on platelets. Platelet number declined in all models, while bleeding time increased and aggregation reduced.

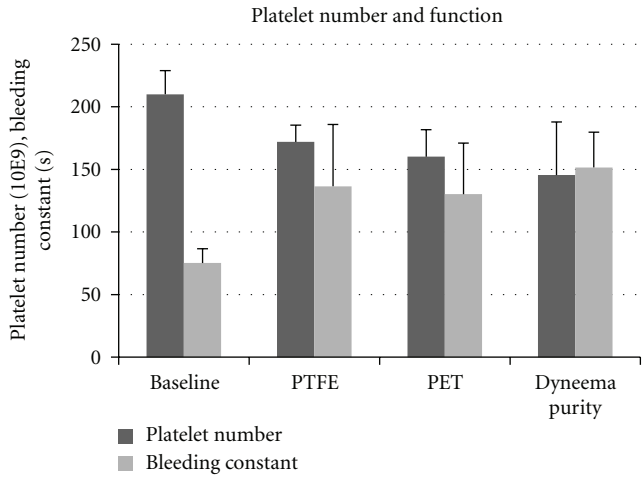

Figure 3: Effect of three types of graft on platelet function. Platelet number and functions were similar after contact with vascular graft materials made of ePTFE, PET or Dyneema Purity UHMWPE fiber.

Chandler loop and Hemobile circulation (Table 1). TAT was similarly increased in all systems.

3.3. Results at 40 mL/min Flow. Pump and Hemobile could be applied at a flow of 40 mL/min, which was not possible with the Chandler model. Platelet number remained higher, and hemolysis was lower in the Hemobile circuits (Table 2).

3.4. Application of the Hemobile in Thrombogenicity Testing. Platelet count was reduced in the circuits containing a test chamber with ePTFE, PET, or Dyneema Purity UHMWPE fiber by approximately 30% following circulation compared to baseline. Platelet function was reduced in all circuits to a similar extent (Figure 3). Platelet binding based on the adhesion of antibody against the platelet GpIIb receptor showed increased values on PET, whereas Dyneema Purity UHMWPE fiber had lowest GpIIb receptors (Figure 4). In the ePTFE circuits, release of TXB2 and TAT was lowest, whereas elastase, complement activation, and hemolysis were lowest in Dyneema Purity UHMWPE fiber circuits (Table 3).

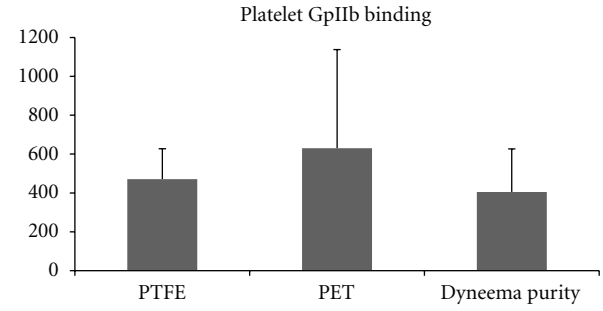

Figure 4: Effect of three types of graft on platelet binding (receptor GpIIb). Platelet adhesion was lowest in the vascular grafts made of Dyneema Purity UHMWPE fiber, as compared to ePTFE and PET.

3.5. Scanning Electron Microscopy. SEM photos were made of all types of vascular graft materials. More detailed pictures showed platelets and fibrin usually separate and not as a dense thrombus on the surface. Differences between the 3 types of graft materials were not clear from these pictures, although ePTFE seemed to remain more devoid of deposition than PET and Dyneema Purity UHMWPE fiber (Figure 5).

4. Discussion

Initial experimental blood circulation models with a roller pump, already refined in previous studies [13, 14, 18], appeared efficient, reliable, and cost-effective to assess the haemocompatibility of grafts before their clinical use. However, blood damage induced by the pump caused a limitation of the exposure of the test object to circulating blood. The modified Chandler loop model is currently most frequently used for these purposes [19, 20]. It induces less blood damage than the roller pump but has two major disadvantages. First, the continuous blood-air contact induces leukocyte and platelet aggregation, protein denaturation [9–11], and shear forces on particulate material, which can result in detachment [21, 22]. In our experiments, indeed less platelets were observed on tubing exposed to blood-air contact in the Chandler loop than in the roller pump or Hemobile circuit. The second disadvantage of the Chandler loop is the limitation of blood circulation due to the requirement to keep the air on top of the circuit. Air tends to circulate with the tubing at higher circulation speed. Thus, our 3 mm tubing did not allow a blood flow over 25 mL/min, which is half of the arterial flow in the coronary system. At a flow of

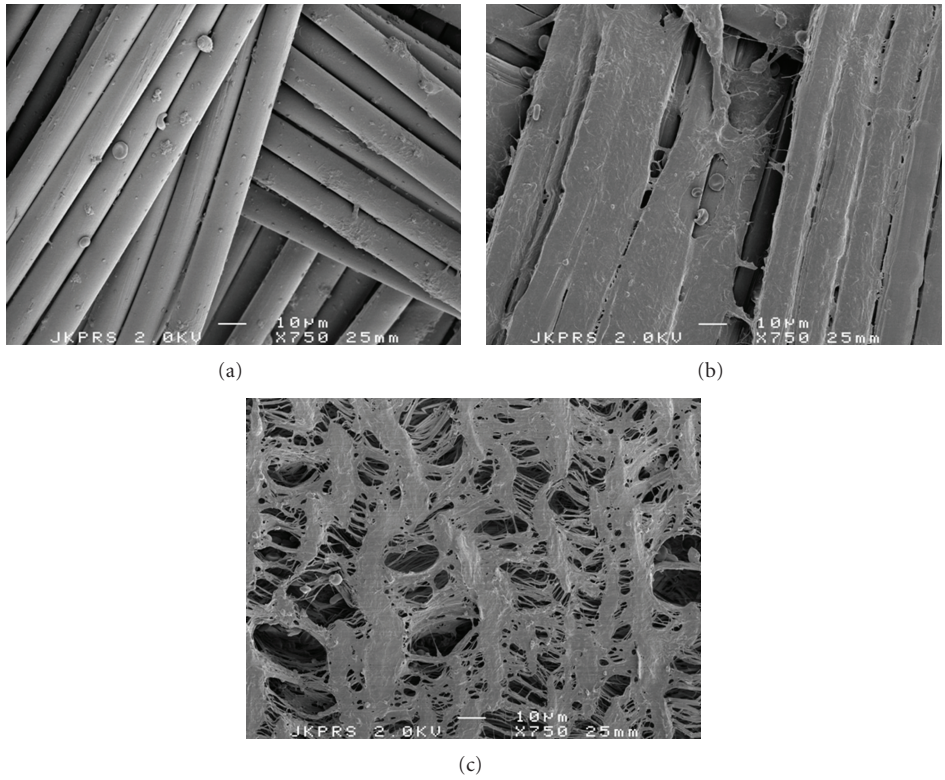

(a) (b)

(c)

Figure 5: Scanning Electron Microscopy. (a) PET fiber: platelets clusters and erythrocytes were observed attached to the fibers. (b) Dyneema Purity UHMWPE fiber weave: separate platelets some erythrocytes and a protein layer were observed on the fibers. (c) Expanded PTFE: small clusters of platelet were observed.

Table 1: Activation markers in plasma after Chandler loop, roller pump and Hemobile blood circulation at 25 mL/min.

	Baseline	Chandler	Roller pump	Hemobile
TxB2 (pg/mL)	34 ± 12	712 ± 296	1222 * ±166	879 ± 167
TAT (μg/mL)	3.2 ± 1.7	66.7 ± 21.5	65.4 ± 24.4	64.3 ± 20.6
Hemolysis (gHb/L)	0.07 ± 0.06	0.21 ± 0.19	0.85** ± 0.14	0.21 ± 0.06
Platelet adhesion	—	0.46$^{\#}$ ± 0.41	0.72 ± 0.42	0.89 ± 0.53

$^{*}P < 0.05$, $^{**}P < 0.01$ compared to Chandler loop and Hemobile; $^{\#}P < 0.05$ compared to roller pump and Hemobile
TXB2: tromboxane B2; TAT: thrombin-antithrombin III.

25 and 40 mL/min, the Hemobile could be used and was less traumatic for blood than the roller pump model.

It is well known that any type of foreign body material can be thrombogenic by promoting the formation of thrombin and platelet activation, which facilitates platelets to adhere and to express surface receptors (Gp IIbIIIa) of activated phase [23]. Platelet binding becomes then irreversible and can promote more thrombus formation. Therefore, proper testing of the characteristics of graft material is an important issue in modulating blood interaction. The small tubular system used in the present models allows multiple tests with fresh human blood. The modified Chandler loop and Hemobile can be easily loaded with a number of circuits at a time. Fast screening of thrombogenicity of vascular grafts and other small medical devices is possible. The adjustable flow and shear and the pulsatility in the Hemobile renders it in a model that allows standardised testing of these devices at the cost of low intrinsic blood damage, while closely mimicking the *in vivo* conditions. Our results indicated that the changes in circulating blood are most of all dependent on the material used in the test loop. Moreover a direct comparison of material surfaces was possible by using blood of the same donor for different circuits.

The feasibility of the Hemobile has been demonstrated by applying the model in hemocompatibility studies of different vascular graft materials.

Woven tubes made of PET fiber and Dyneema Purity UHMWPE fiber have been compared to commercially available ePTFE vascular graft. Our results showed that Dyneema Purity UHMWPE fiber has in many ways better properties than ePTFE by lower activation of the inflammatory response and lower hemolysis.

Table 2: Roller pump and Hemobile performed at 40 mL/min blood circulation.

	Baseline	Roller pump	Hemobile
Platelet number (10E9/L)	115 ± 36	70 ± 28	117 ± 32*
Bleeding constant (sec)	72 ± 7	108 ± 20	99 ± 21
Aggregation (slope)	18.7 ± 7.1	6.9 ± 3	8.7 ± 4.7
Adhesion (10E6/cm^2)	—	0.75 ± 0.73	0.53 ± 0.45
Hemolysis (gHb/L)	0.07 ± 0.06	0.95 ± 0.51	0.18 ± 0.11**

*$P < 0.05$; **$P < 0.01$ compared to roller pump.

Table 3: Activation markers in plasma after Hemobile circulation at 40 mL/min in the presence of different grafts (average ± SD).

	Baseline	ePTFE	PET	Dyneema Purity
TxB2 (pg/mL)	21 ± 14	779 ± 642	964 ± 428	948 ± 246
TAT (μg/mL)	0.7 ± 0.7	73.7 ± 118	147.6 ± 53	90.0 ± 131
elastase (μg/mL)	0.32 ± 0.35	4.36 ± 5.27	3.00 ± 3.01	2.85 ± 2.97
C5b-9 (U/mL)	1.55 ± 2.17	3.31 ± 3.01	3.41 ± 2.82	2.60 ± 2.63
hemolysis (gHb/L)	0, 02 ± 0.01	0, 14 ± 0.1	0, 15 ± 0.11	0, 08 ± 0.002

TXB2: thromboxane B2; TAT: thrombin-antithrombin III.

A limitation of *in vitro* models is mainly represented by the absence of an endothelial layer in the circulating system. Throughout the release of cytokines, the endothelium has a major role in mediating the interplay between the injured vessel wall and circulating blood cells [24–26]. This is effectuated by the release of cytokines and (anti)thrombotic components as well as the expression of adhesion molecules. The lacking of this character can somehow alter the likelihood of our experimental representation. Prior to use in patients an animal model should prove the validity of the *in vitro* data. Nevertheless, all the other elements depicting the blood-graft phase boundary scene are present, while the use of human blood from one donor in test and control circuits is a major advantage for comparison of the materials.

Acknowledgments

The study was partly sponsored by DSM Biomedical, Urmond, The Netherlands. The correspondence author declares that none of the authors of the paper, have a direct financial relation with the commercial identity mentioned in this paper that might lead to a conflict of interest.

References

[1] TC 194/WG9. ISO 10993-4:2002 Biological evaluation of medical devices—Part 4: selection of tests for interactions with blood.

[2] K. Kawakami, Y. Harada, M. Sakasita, H. Nagai, M. Handa, and Y. Ikeda, "A new method for continuous measurement of platelet adhesion under flow conditions," *Asaio Journal*, vol. 39, no. 3, pp. M558–M560, 1993.

[3] V. Balasubramanian, E. Grabowski, A. Bini, and Y. Nemerson, "Platelets, circulating tissue factor, and fibrin colocalize in ex vivo thrombi: real-time fluorescence images of thrombus formation and propagation under defined flow conditions," *Blood*, vol. 100, no. 8, pp. 2787–2792, 2002.

[4] V. I. Sevastianov and V. M. Parfeev, "Fatigue and hemocompatibility of polymer materials," *Artificial Organs*, vol. 11, no. 1, pp. 20–25, 1987.

[5] M. Dadsetan, H. Mirzadeh, N. Sharifi-Sanjani, and P. Salehian, "In vitro studies of platelet adhesion on laser-treated polyethylene terephthalate surface," *Journal of Biomedical Materials Research*, vol. 54, no. 4, pp. 540–546, 2001.

[6] S. F. Mohammad and D. B. Olsen, "Immobilized albumin-immunoglobulin g for improved hemocompatibility of biopolymers," *Asaio Transactions*, vol. 35, no. 3, pp. 384–387, 1989.

[7] C. Beythien, W. Terres, and C. W. Hamm, "In vitro model to test the thrombogenicity of coronary stents," *Thrombosis Research*, vol. 75, no. 6, pp. 581–590, 1994.

[8] A. B. Chandler, "In vitro thrombotic coagulation of blood: a method for producing a thrombus," *Laboratory Investigation*, vol. 7, pp. 110–116, 1958.

[9] T. Thorsen, H. Klausen, R. T. Lie, and H. Holmsen, "Bubble-induced aggregation of platelets: effects of gas species, proteins, and decompression," *Undersea & Hyperbaric Medicine*, vol. 20, no. 2, pp. 101–119, 1993.

[10] S. Ritz-Timme, N. Eckelt, E. Schmidtke, and H. Thomsen, "Genesis and diagnostic value of leukocyte and platelet accumulations around "air bubbles" in blood after venous air embolism," *International Journal of Legal Medicine*, vol. 111, no. 1, pp. 22–26, 1998.

[11] R. Miller, V. B. Fainerman, R. Wüstneck, J. Krägel, and D. V. Trukhin, "Characterisation of the initial period of protein adsorption by dynamic surface tension measurements using different drop techniques," *Colloids and Surfaces A*, vol. 131, no. 1–3, pp. 225–230, 1998.

[12] D. A. Wang, J. Ji, C. Y. Gao, G. H. Yu, and L. X. Feng, "Surface coating of stearyl poly(ethylene oxide) coupling-polymer on polyurethane guiding catheters with poly(ether urethane) film-building additive for biomedical applications," *Biomaterials*, vol. 22, no. 12, pp. 1549–1562, 2001.

[13] S. H. J. Monnink, A. J. Van Boven, H. O. J. Peels et al., "Silicon-carbide coated coronary stents have low platelet and leukocyte adhesion during platelet activation," *Journal of Investigative Medicine*, vol. 47, no. 6, pp. 304–310, 1999.

[14] G. Amoroso, A. J. Van Boven, C. Volkers, H. J. G. M. Crijns, and W. Van Oeveren, "Multilink stent promotes less platelet and leukocyte adhesion than a traditional stainless steel stent: an in vitro experimental study," *Journal of Investigative Medicine*, vol. 49, no. 3, pp. 265–272, 2001.

[15] K. Münch, M. F. Wolf, P. Gruffaz et al., "Use of simple and complex in vitro models for multiparameter characterization of human blood-material/device interactions," *Journal of Biomaterials Science, Polymer Edition*, vol. 11, no. 11, pp. 1147–1163, 2000.

[16] M. Harboe, "A method for determination of hemoglobin in plasma by near-ultraviolet spectrophotometry," *Scandinavian Journal of Clinical and Laboratory Investigation*, vol. 11, no. 1, pp. 66–70, 1959.

[17] P. Bellavite, G. Andrioli, P. Guzzo et al., "A colorimetric method for the measurement of platelet adhesion in microtiter plates," *Analytical Biochemistry*, vol. 216, no. 2, pp. 444–450, 1994.

[18] J. Mulvihill, T. Crost, J. L. Renaux, and J. P. Cazenave, "Evaluation of haemodialysis membrane biocompatibility by parallel assessment in an ex vivo model in healthy volunteers," *Nephrology Dialysis Transplantation*, vol. 12, no. 9, pp. 1968–1973, 1997.

[19] K. Christensen, R. Larsson, H. Emanuelsson, G. Elgue, and A. Larsson, "Effects on blood compatibility *in vitro* by combining a direct $P2Y_{12}$ receptor inhibitor and heparin coating of stents," *Platelets*, vol. 17, no. 5, pp. 318–327, 2006.

[20] S. Sinn, T. Scheuermann, S. Deichelbohrer, G. Ziemer, and H. P. Wendel, "A novel in vitro model for preclinical testing of the hemocompatibility of intravascular stents according to iso 10993-4," *Journal of Materials Science*, vol. 22, pp. 1521–1528, 2011.

[21] W. C. Culp, T. R. Porter, T. C. McCowan et al., "Microbubble-augmented ultrasound declotting of thrombosed arteriovenous dialysis grafts in dogs," *Journal of Vascular and Interventional Radiology*, vol. 14, no. 3, pp. 343–347, 2003.

[22] C. Gómez-Suárez, H. J. Busscher, and H. C. Van Der Mei, "Analysis of bacterial detachment from substratum surfaces by the passage of air-liquid interfaces," *Applied and Environmental Microbiology*, vol. 67, no. 6, pp. 2531–2537, 2001.

[23] M. H. Jeong, W. G. Owen, M. E. Staab et al., "Porcine model of stent thrombosis: platelets are the primary component of acute stent closure," *Catheterization and Cardiovascular Diagnosis*, vol. 38, no. 1, pp. 38–43, 1996.

[24] R. Komatsu, M. Ueda, T. Naruko, A. Kojima, and A. E. Becker, "Neointimal tissue response at sites of coronary stenting in humans: macroscopic, histological, and immunohistochemical analyses," *Circulation*, vol. 98, no. 3, pp. 224–233, 1998.

[25] H. M. M. Van Beusekom, D. M. Whelan, S. H. Hofma et al., "Long-term endothelial dysfunction is more pronounced after stenting than after balloon angioplasty in porcine coronary arteries," *Journal of the American College of Cardiology*, vol. 32, no. 4, pp. 1109–1117, 1998.

[26] P. K. Shah, "Plaque disruption and coronary thrombosis: new insight into pathogenesis and prevention," *Clinical Cardiology*, vol. 20, no. 12, pp. II38–II44, 1997.

Hindawi Publishing Corporation
International Journal of Biomaterials
Volume 2012, Article ID 397813, 14 pages
doi:10.1155/2012/397813

Research Article

Oligonucleotide and Parylene Surface Coating of Polystyrene and ePTFE for Improved Endothelial Cell Attachment and Hemocompatibility

Martina Schleicher,[1] Jan Hansmann,[2] Bentsian Elkin,[2] Petra J. Kluger,[2] Simone Liebscher,[1] Agnes J. T. Huber,[1] Olaf Fritze,[1] Christine Schille,[3] Michaela Müller,[2] Katja Schenke-Layland,[2,4] Martina Seifert,[5,6] Heike Walles,[2] Hans-Peter Wendel,[1] and Ulrich A. Stock[1]

[1] *Department of Thoracic, Cardiac and Vascular Surgery, University Hospital, Hoppe-Seyler-Strasse 3, 72076 Tuebingen, Germany*
[2] *Fraunhofer Institute for Interfacial Engineering and Biotechnology, Nobelstrasse 12, 70569 Stuttgart, Germany*
[3] *Department of Prosthodontics, Section of Medical Materials and Technology, University Hospital, Osianderstrasse 2-8, 72076 Tübingen, Germany*
[4] *Inter-University Centre for Medical Technology (IZST), Eberhard Karls University, Silcherstrasse 7, 72076 Tuebingen, Germany*
[5] *Institute of Medical Immunology, Charité Universitätsmedizin Berlin, Föhrer Straße 15, 13353 Berlin, Germany*
[6] *Berlin-Brandenburg Center for Regenerative Therapies (BCRT), Charité Universitätsmedizin Berlin, Föhrer Straße 15, 13353 Berlin, Germany*

Correspondence should be addressed to Ulrich A. Stock, ulrich.stock@med.uni-tuebingen.de

Received 15 July 2011; Revised 10 November 2011; Accepted 14 November 2011

Academic Editor: Rolf Larsson

In vivo self-endothelialization by endothelial cell adhesion on cardiovascular implants is highly desirable. DNA-oligonucleotides are an intriguing coating material with nonimmunogenic characteristics and the feasibility of easy and rapid chemical fabrication. The objective of this study was the creation of cell adhesive DNA-oligonucleotide coatings on vascular implant surfaces. DNA-oligonucleotides immobilized by adsorption on parylene (poly(monoaminomethyl-para-xylene)) coated polystyrene and ePTFE were resistant to high shear stress (9.5 N/m^2) and human blood serum for up to 96 h. Adhesion of murine endothelial progenitor cells, HUVECs and endothelial cells from human adult saphenous veins as well as viability over a period of 14 days of HUVECs on oligonucleotide coated samples under dynamic culture conditions was significantly enhanced ($P < 0.05$). Oligonucleotide-coated surfaces revealed low thrombogenicity and excellent hemocompatibility after incubation with human blood. These properties suggest the suitability of immobilization of DNA-oligonucleotides for biofunctionalization of blood vessel substitutes for improved *in vivo* endothelialization.

1. Introduction

Current blood vessel replacement concepts, which use either prosthetic or biological grafts, achieve excellent mid-term results. The clinical application, however, is accompanied by a variety of limitations. Biological conduits (e.g., autologous greater saphenous vein) have better hemodynamic characteristics and avoid long-term anticoagulation but are limited in availability. On the long term, however, they fail due to intimal hyperplasia and fibrosis. Allograft transplants such as superficial femoral arteries have optimal hemodynamic properties, avoid any anticoagulation, and are resistant to infections to a certain extent. However, due to tissue scarcity, their availability is limited. In general, 5–30% of patients have no suitable autologous grafts available due to previous use or concomitant disease. In these cases, expanded polytetrafluoroethylene (ePTFE) grafts are used. However, despite their prevalence, these grafts have a lower patency rate due to

noncompliance, thrombogenic surface, and the tendency to form intimal hyperplasia in particular in anastomotic areas [1]. None of the currently available blood vessel substitutes possess any regenerative or growth potential. This shortcoming is crucial especially for the treatment of pediatric patients and grafts with repeated injury (e.g., hemodialysis shunts).

The multidisciplinary approach of tissue engineering might offer an attractive pathway to overcome these shortcomings and develop blood vessel substitutes identical or similar to native human arteries. In vascular grafts, an *in vitro* established autologous endothelial cell layer on the implant surface prior to implantation provides an excellent barrier between the synthetic material and the blood flow and has been reported to reduce thrombosis and intimal hyperplasia [2–4]. Overcoming these limitations will result in a distinct improvement of graft performance and patency [2–5]. Indeed, clinical studies have demonstrated that such grafts can function as well as autologous vein grafts [6]. However, this concept imposes a variety of demands for successful transfer from the preclinical large animal setups to the clinical arena. Due to the high risk of bacterial and fungal infection throughout the entire *in vitro* culture (which takes up to 6 weeks from cell harvest to implantation of the engineered product), the process requires a cost-intensive infrastructure.

Accordingly, ongoing research focuses on the development of facilitated spontaneous *in vivo* endothelialization of vascular implants [7–11]. Several pathways are conceivable to achieve endothelialization *in vivo*. One is the capture, immobilization and adhesion of circulating endothelial (EC) or endothelial progenitor cells (EPC) from the blood stream. An alternative is promotion of transanastomotic ingrowth of endothelial cells from the native vessel on and into the graft. Both require a suitable graft surface for cell adhesion and proliferation. However, it is reported that EC do not adhere to currently available vascular graft materials like ePTFE and polyethylene terephtalate (Dacron) [12, 13]. Furthermore, transanastomotic ingrowth of EC in currently used vascular grafts does not exceed 1-2 cm even after years of clinical implantation [14]. Hence, materials that promote *in situ* endothelialization of cardiovascular implants (without intimal hyperplasia or thrombus formation during endothelium development) would be highly desirable. Different approaches exist, mostly using extracellular-matrix- (ECM-) derived proteins or peptides with functional domains of ECM proteins [7].

Another intriguing coating material for implant surfaces is deoxyribonucleic acid (DNA). DNA is a naturally occurring material with a homogenous molecular structure in all vertebrate species [15, 16]. DNA is nontoxic with little or no immunogenicity in contrast to other biological antigens like proteins and sugars [15, 17, 18]. Another advantage of DNA molecules are their easy and rapid chemically synthetization. Use of DNA as coating material has already been suggested for dental applications [19], and a DNA-chitosan complex was used as scaffold material for tissue engineering [20]. Van Den Beucken et al. fabricated multilayered DNA coatings consisting of poly-D-lysine (PDL) or poly(allylamine hydrochloride) (PAH) and DNA and demonstrated increased proliferation of primary rat dermal fibroblasts (RDFs) and cyto- as well as histocompatibility of the multilayered DNA coatings [21]. Challenges in application of DNA for surface functionalization are the easy nucleolytic degradation of the substance and its solubility in aqueous solutions [19]. Furthermore, DNA is an optimal material for immobilization of additional growth or adhesion factors, as DNA offers accessible functional groups for chemical coupling reactions and the possibility to incorporate molecules via groove binding and intercalation [22, 23].

Apart from controlled cell adhesion, the coating matrix needs to possess excellent mechanical properties in terms of flexibility and long-lasting *in vivo* adherence to the implant surface. These properties are known to be supplied by poly (p-xylylene) (PPX) and its derivates, known by their commercial trade name as parylenes [24, 25]. Parylenes can be conformally coated onto irregular substrates by a vapor deposition process and are chemically inert and nonbiodegradable. The FDA has already recognized some parylenes, such as Parylene C and Parylene N, as Class VI polymers for coating implanted medical devices due to their biocompatibility [26, 27].

Here, we report a concept of a stable DNA coating and EC and EPC adhesion on DNA coatings using continuous shear stress application.

2. Materials and Methods

2.1. Oligonucleotides. Oligonucleotides were synthesized by TIB Molbiol (Berlin, Germany). As single-sequence 5′-GGG-AGCTCAGAATAAACGCTCAACAACCCGTCAACGAAC-CGGAGTGTGGCAGGTTCGACATGAGGCCCGGATC-3′ was used. The DNA oligonucleotide library contained a 40-base central random sequence: 5′- GAATTCAGTCGGAC-AGCG-N_{40}-GATGGACGAATATCGTCTCCC-3′. For detection, oligonucleotides were 5′-labeled with 6-carboxyfluorescein (6FAM). For immobilization, a 5′-C12-NH_2 modification was used.

2.2. Cells and Culture. Murine embryonic EPC (eEPC) line T17b cells [28] were cultured in flasks precoated with 0.1% gelatin. The culture medium consisted of DMEM (4.5 g/L glucose, Lonza, Köln, Germany) supplemented with 20% FCS, 0.1 mmol/L β-mercaptoethanol (Serva, Heidelberg, Germany), 1 mmol/L nonessential amino acids (Gibco, Paisley, UK), 100 U/mL penicillin, 100 μg/mL streptomycin (Gibco, Paisley, UK), and 2 mmol/L L-glutamine (Lonza, Köln, Germany).

Human umbilical vein endothelial cells (HUVECs) were cultured in VascuLife VEGF Culture Medium containing 2% FCS (Lifeline Cell Technology, Walkersville, USA).

Human ECs were harvested from human saphenous veins. 4 to 5 cm long remnants of saphenous veins from patients undergoing aortocoronary bypass procedures were used as a cell source. Tissue procurement and use were approved by our local ethics committee and informed consent was obtained. The veins were cannulated, flushed with DMEM (4.5 g/L glucose, Lonza, Köln, Germany), and filled with 0.2% collagenase A (Roche, Mannheim, Germany).

Cells were harvested after 20 min of collagenase incubation at 37°C, 5% CO_2. The culture medium consisted of DMEM (4.5 g/L glucose, Lonza, Köln, Germany) supplemented with recombinant basic fibroblast growth factor (bFGF, 10 ng/mL; Boehringer, Ingelheim, Germany), 100 U/mL penicillin, 100 μg/mL streptomycin (Gibco, Paisley, UK), and 10% FCS.

2.3. Parylene Deposition Process. Standard ePTFE vascular prostheses were obtained from Jotec GmbH, Hechingen, Germany (FlowLine Bipore and FlowLine Bipore Heparin), and ePTFE patch material from W.L. Gore & Associates, Inc., Flagstaff, Arizona, USA (Gore-Tex Cardiovascular Patch). ePTFE was activated using microwave plasma (400 W, hydrogen and nitrogen in equal parts, 30 s) prior to coating with parylenes. Poly (monochloro-para-xylene) ("Galxyl C"-parylene C, from Galentis S.P.A., Marcon, Italy) and poly (monoaminomethyl-para-xylene) (diX AM-aminoparylene, from Kisco Conformal Coating Ltd., Düsseldorf, Germany) were coated on polystyrene dishes, polypropylene sheets, and activated ePTFE using a chemical vapour deposition (CVD) process in a PDS 2010 coater (SCS Specialty Coating Systems, Indiana, USA). A general description of parylene CVD processes is given by Lahann [29]. This technique enables thin homogeneous and conformal deposition on a variety of substrates. Deposition is performed under vacuum at room temperature. A thin (ca. 0.1 μm) diX AM coating was deposited onto a thicker (ca. 2 μm) intermediate layer of inert Parylene C according to recommendations from the diX AM manufacturer. After deposition, the samples were stored in the dark using argon atmosphere to avoid amine's oxidation.

2.4. Surface Characterization

2.4.1. Parylene Thickness Determination. The thickness of the intermediate Parylene C layer was determined by both gravimetry and ellipsometry on reference samples. In the first case, the mass increase of an aluminum foil which was parylene coated in the same deposition run was determined. For ellipsometry, single crystalline Si substrates were used. The thickness of diX AM parylene top coatings was determined by ellipsometry only. The ellipsometric measurements were performed on a SE 801 spectroscopic ellipsometer (Sentech Instruments GmbH, Berlin, Germany).

2.4.2. XPS Measurements. The samples were stored in dark under argon and transferred into the XPS apparatus within 24 h of deposition. The surface elemental composition was verified by X-ray photoelectron spectroscopy (XPS) analysis using an Axis Nova system (Kratos Analytical, Manchester, UK) with monochromatic Al Kα X-Ray source. For all samples, overview spectra and detailed spectra of all elements found in the overview were recorded.

2.4.3. ESR Measurements. For determination of the number of chemically available amino groups on the diX AM surface electron spin resonance spectroscopy (ESR) in combination with chemical derivatization was applied (similar technique was used by Samal et al. [30] for qualitative detection of surface functionalization). First, functionalized stable free radicals (4-carboxy-TEMPO, Sigma-Aldrich) were bound to surface amino groups via an EDC-mediated reaction. Subsequently, the number of radicals in the sample was measured using ESR. Polypropylene film samples (45 × 90 mm) coated on both sides with diX AM were incubated for 24 hours with 0.65 mml/L 4-carboxy-TEMPO, 1.55 mg/mL EDC in 0.1 M MES buffer (pH 5.0) at room temperature. After a thorough washing, the films were dried, tightly rolled, and then put into the sample holder tube of the ESR device (MS200, Magnettech GmbH). To obtain the absolute number of spins in the sample, the double integral of the measured signal was related to that of a Cr(III) standard. The number of spins measured should then equal the number of amino groups having reacted with the carboxy moiety of the 4-carboxy-TEMPO.

2.4.4. Contact Angle Measurements. Contact angle measurements were performed to determine the changes in wettability of the prepared surfaces. The captive bubble technique was chosen for analyses because the surfaces were constantly in contact with fluid media. The coated samples were completely immersed in PBS with the coated side face down. The captive bubble contact angle measurements were taken at 22°C using a video capture system (OCA 40, DataPhysics Instruments GmbH, Filderstadt, Germany). An air bubble was brought in contact with the solid sample from below. After a few seconds, the static contact angle near the three-phase line was measured. For each sample, at least six contact angles were measured.

2.5. Oligonucelotide Immobilization on diX AM-Coated Surfaces. If not stated differently, 1.7 μM DNA-oligonucleotides were applied to the diX AM-coated surface in HEPES buffer (20 mM, pH 7.0) at room temperature. After 2 h, Tris-HCl was added to a concentration of 50 mM and incubated for 15 min. For experiments with cell incubation, the surfaces were washed with 0.2% BSA. Then, a triple washing step with PBS followed. For cell experiments, an incubation with a PBS-antibiotic solution (10 mL PBS with 0.5 mL antibiotic-solution: 0.3 mg amikacin, 0.75 mg flucytosine, 0.3 mg vancomycin, 0.075 mg ciprofloxacin, 0.3 mg metronidazole) for 24 h at 4°C was performed.

2.6. Shear Stress Resistance Test. DiX AM-coated polypropylene sheets with applied oligonucleotides (0.5 μM) were exposed to flow-induced shear stress for 1 h at 37°C in a closed circular system. The system consisted of silicon tubing, a fluid reservoir, a peristaltic pump, and a following vessel to attenuate pump-induced pressure variability. The test fluid consisted of 1000 ppm xanthan gum. Wall shear stress for 1000 ppm Xanthan gum, a non-Newtonian power-law fluid [31], was calculated as follows. For a non-Newtonian power-law fluid applies

$$\tau_{zr} = k\gamma^n, \tag{1}$$

where τ_{zr} is the shear stress in a tube at length z and radius r and γ the shear rate [32]. Shear-rate-dependent shear stress

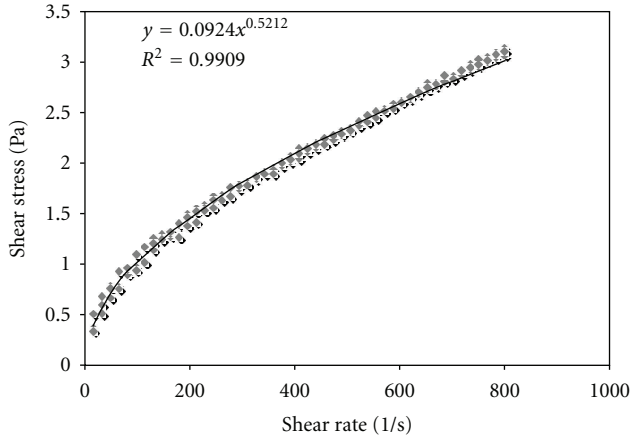

Figure 1: Shear stress dependency on shear rate of 1000 ppm Xanthan gum measured by rotational rheometry.

of the xanthan gum solution was determined by rotational rheometry (UDS 200, Physica, Ostflidern) using the following settings: shear rate 0.01–800 1/s, 50 measurement points, measurement duration per point 10 s, three individual 1000 ppm Xanthan gum solutions. From the measurement, the following values were gained: $k = 0.0924\,\text{Pa} * s^n$ and $n = 0.5212$ (Figure 1). To achieve a wall shear stress of $\tau_{\text{wall}} = 9.5\ \text{N/m}^2$ in a tube with a radius of $R = 0.135\,\text{cm}$, the required flow rate Q was calculated as follows [32]:

$$Q = \frac{\pi R^3}{1/n+3}\left(\frac{\tau_{\text{wall}}}{k}\right)^{1/n} = 11.4\,\text{cm}^3/\text{s}. \quad (2)$$

2.7. Serum Stability. DiX AM coated with oligonucleotides (0.5 μM) was incubated with serum derived from fresh human blood for 15 min, 24 h, 48 h, 72 h, and 96 hours at 37°C. Serum was changed every 24 hours. Amount of oligonucleotide remaining on diX AM surface was determined.

2.8. Oligonucleotide Detection. Oligonucleotides were modified with 6FAM and could be detected by a fluorescence microplate reader (Mithras LB 940, BertholdTech, Bad Wildbad, Germany). For confirmation of the results and better quantification, an ELISA system was developed, using an antifluorescein antibody (Molecular Probes, Cat# A-889, Eugene, USA) and an alkaline-phosphatase-conjugated secondary antibody (ZYMED Laboratories, Invitrogen, Cat# 65-6122, Carlsbad, USA). Incubation time was 2 h at room temperature each. As substrate Alkaline Phosphatase Yellow (pNPP) Liquid Substrate System for ELISA (Sigma) was used.

2.9. Dynamic Cell Adhesion Test. Oligonucleotides were applied to marked areas or the whole surface of diX AM coated Petri-dishes or diX AM-coated 12-well plates. Petri-dishes were incubated with $0.05 * 10^6$ cells for 1–2.5 h at 37°C, 5% CO_2 in cell-corresponding or experiment-dependent medium or buffer on a rocking orbital shaker (The Belly Button, Stovall Life Science Inc. Greensboro, USA). Following medium exchange to remove nonadherent cells, Petri-dishes were inspected by phase-contrast microscopy (Zeiss Axio Observer Z1, Germany). Cells in images with the same area were counted. An alamarBlue assay (AbD Serotec, Oxford, UK) was performed after 22 h to determine the relative number of metabolically active adherent cells. 150 μL alamarBlue reagent were added to the samples in 1.5 mL medium and incubated for four hours at 37°C and 5% CO_2. Two times 100 μL of each sample were pipetted into a clear flat bottom microplate and measured at 530 nm extinction and 600 nm emission wavelength (Mithras LB 940, BertholdTech, Bad Wildbad, Germany).

2.10. Staining of Adhesion Markers. Oligonucleotides were applied to marked areas of diX AM coated Petri-dishes. Oligonucleotide-coated and diX AM-coated Petri-dishes and tissue-culture Petri-dishes were incubated with $0.05 * 10^6$ HUVECs at 37°C, 5% CO_2 in medium containing FCS on a rocking orbital shaker (The Belly Button, Stovall Life Science Inc, Greensboro, USA). After one hour medium including non-adherent cells was removed. Adherent cells were fixed with 4% paraformaldehyde (Sigma) for 10 min at room temperature. After a washing step with PBS (Lonza), PBS containing 2% FCS and 0.1% Triton (Sigma) was applied for 15 min. Samples were incubated over night at 4°C with the primary antibodies (anti-vinculin or CD49e (Integrin alpha 5), abcam, Cambridge, UK) in PBS containing 2% FCS and 0.1% Triton. After a washing step, the secondary antibody (Goat polyclonal Secondary Antibody to Mouse IgG-H&L (Chromeo 488), abcam, Cambridge, UK) was applied for 1 h at 37°C. Cells were stained with phalloidin (Alexa Fluor 568 phalloidin, Invitrogen, Carlsbad, USA) for 20 min at room temperature following a further washing step with PBS. As a last staining step, cells were incubated with DAPI (Sigma) for 2 min. Following staining of adherent cells, Petri-dishes were inspected by fluorescence microscopy at a magnification of 200x (Zeiss Axio Observer Z1, Germany).

2.11. Viability Test over a Period of 14 Days. For viablity tests, standard ePTFE vascular prostheses either uncoated or coated with heparin (FlowLine Bipore and FlowLine Bipore Heparin, Jotec GmbH, Hechingen, Germany) or ePTFE (FlowLine Bipore) coated with Parylene C, diX AM, and oligonucleotieds as described above were used. The three differently coated materials were cut into samples and glued with silicone paste into 48-well suspension culture plates. $3 * 10^4$ HUVECs were seeded into each well. After 2.5 h, incubation using continuous agitation (The Belly Button, Stovall Life Science Inc, Greensboro, USA) medium was exchanged and nonadherent cells removed. Cell viability was measured with the alamarBlue assay after 1, 2, 5, 8, 12, and 14 days.

2.12. Hemocompatibility Testing. 12-well Polystyrene plates and ePTFE patches (Gore-Tex Cardiovascular Patch, W.L. Gore & Associates, Inc., Flagstaff, Arizona, USA) were coated with diX AM and oligonucleotides as described above. ePTFE was cut into 12-well-sized samples and glued into 12-well suspension culture plates using silicone paste. Human blood

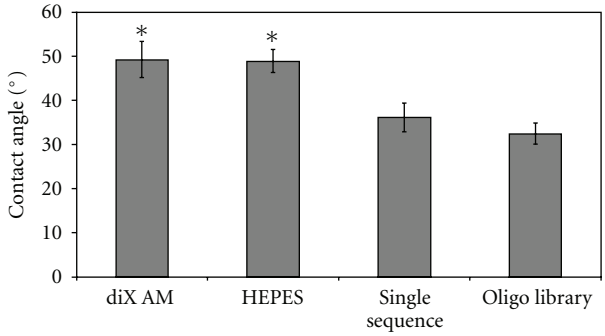

Figure 2: Contact angle measurements by the captive bubble method using PBS. Contact angle was significantly lower for oligonucleotide coated samples compared to diX AM or HEPES treated samples (*, $P < 0.05$, $n = 6$).

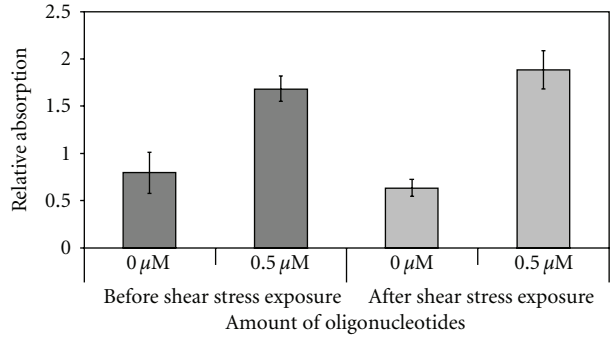

Figure 3: Oligonucleotide coating stability. Polypropylene sheets were coated with diX AM and oligonucleotides were applied to the coated surface. Oligonucleotides were detected by an ELISA system. Samples were exposed to a constant fluid flow inducing at least 9, 5 N/m^2 shear stress on the surface for 1 h ($n = 6$).

samples were obtained from six healthy volunteers following giving informed consent (approved by the ethical committee of University Hospital Tuebingen). Whole blood from each volunteer was collected in heparin precoated monovettes (1,5 IU Liquemin, Roche, Grenzach-Whylen, Germany per mL blood). Two 12-wells in each group were incubated with 3 mL donor blood each. After 1 h incubation at 37°C with continuous shaking, the two blood samples of each group were pooled and further processed using the following protocols. 2.4 mL blood from each group was added to an EDTA-monovette. Blood cell count, including platelet count, was performed using a Cobas Micros 60 S/N (Axon Lab, Reichenbach, Germany). 2.8 mL blood from each group was collected in a Citrate-monovette. Monovettes were centrifuged at 2000 g for 15 min at room temperature. 600 μL supernatant was used for thrombin-antithrombin complex (Enzygnost TAT micro, Dade Behring Marburg, Germany) and PMN-Elastase determination (Milenia PMN-Elastase, Milenia Biotec, Germany). 5.4 mL blood from each group was added to 0.3 mL of CTAD anticoagulant monovettes (Becton Dickinson, USA). Tubes were placed on ice for 15 min. Following centrifugation at 2500 g for 20 min at 4°C 1.4 mL, plasma from the middle fraction was aspirated and transferred to a new neutral monovette. After repeated centrifugation, 200 μl plasma was used for determination of β-Thromboglobulin (ASSERACHROM β-TG Kit, Diagnostica Stago, France).

2.13. Statistics. All quantitative results were expressed as mean standard deviation. The differences among groups were analyzed with one-way ANOVA, and independent samples t-test was performed between each of two groups in case of a significant statistical difference existed. P values < 0.05 were considered statistically significant.

3. Results

3.1. DiX AM and Oligonucleotide Coating Surface Characterization. Substrates were coated with parylene C as an intermediate layer and with diX AM as top coating. Coating thicknesses measured by ellipsometry on a simultaneously coated Si wafer were 550–2200 nm for parylene C and 40–120 nm for diX AM, depending on charge deposition parameters. The elemental composition in percent of total number of atoms excluding hydrogen of the surface measured by XPS was as follows: N-6.2 at.% (theoretically expected for diX AM-5.9 at.%), C-90.7 at.%, Cl-1.9 at.%, and O-1.2 at.%. Chlorine is not contained in diX AM but makes up 14.2 at.% of Parylene C, which was the intermediate layer under diX AM. Thus, we presume the Cl signal measured by XPS to originate from Parylene C. As the diX AM coating was thicker than the XPS sampling depth of 5 to 10 nm, we interpret the Cl signal as an indication that the diX AM coating was not completely closed. Concerning Oxygen content, amines are generally known to be prone to oxidation. St-Georges-Robillard [33] have recently investigated oxidation of diX AM on air and found simultaneous depletion of amino groups and increase of Oxygen content on a time scale of several days. The number of chemically available amino groups on the diX AM surface as determined by ESR Spectroscopy was 0.94 ± 0.33 1/nm^2.

To examine if changed surface wettability has an impact on cell adhesion, samples were analyzed by the captive bubble method. Samples coated by a single oligonucleotide sequence or by the oligonucleotide library had significantly lower contact angles resulting in increased hydrophilic surface characteristics compared to diX AM ($P < 0.001$; Figure 2). This was independent of the used buffer (HEPES) as the contact angle for HEPES-treated samples did not differ from the angle of the diX AM surface.

3.2. Immobilization of Oligonucleotides and Shear Stress Resistance of Adhered Oligonucleotides. On diX AM-coated surfaces, immobilized oligonucleotides were detected via fluorescence labeling of the oligonucleotides and an ELISA-System targeting the fluorescence label. After application of oligonucleotides, four washing steps were applied. Fluorescence and absorbance, respectively, were significantly higher, when oligonucleotides were applied to the diX AM surface (Figure 3, prior to shear stress exposure, data of fluorescence

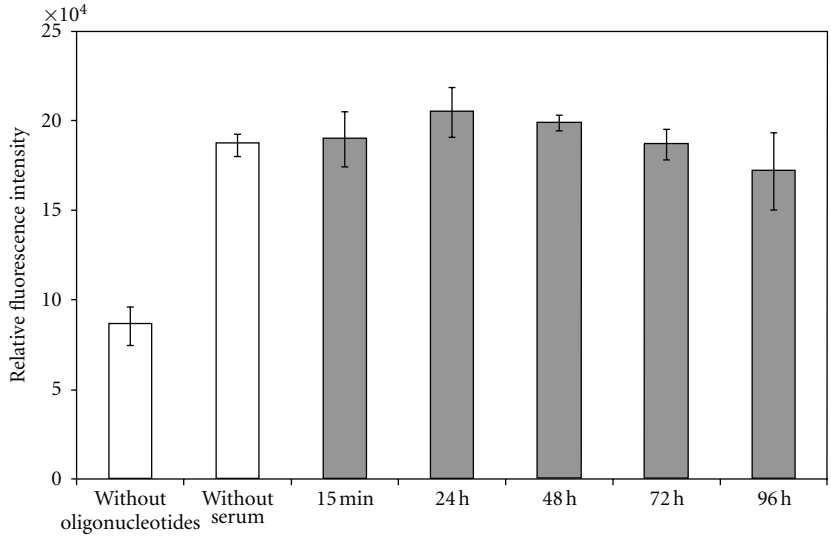

Figure 4: Stability against degradation by human blood serum of on diX AM-immobilized oligonucleotides. No significant degradation of oligonucleotides could be detected after 96 h incubation in comparison to the samples without serum incubation ($P = 0.079$, $n = 9$).

detection not shown). Immobilization by sole adhesion of the oligonucleotides on the diX AM-coated surface is possible.

Oligonucleotides were exposed to physiologic shear stress to test if the adhesion is stable enough to withstand occurring shear stresses *in vivo*. For the assay, a mean wall shear stress of 9.5 N/m^2 was chosen, as shear stress on native *in vivo* heart valve and artery surfaces are estimated to approximate 8 N/m^{2}and 1.5 N/m^2 [34, 35]. Accordingly, the chosen setup exceeded the maximum physiologic levels. The used fluid, Xanthan gum, simulated shear thinning viscosity behavior and particle characteristics of blood [36, 37]. No significant decrease of oligonucleotide amount on the sheared diX AM surface could be detected compared to the oligonucleotide control ($P = 0.076$; Figure 3).

3.3. Serum Stability of Adhered Oligonucleotides. To exclude degradation of the applied oligonucelotides by human blood serum, samples were incubated between 15 min and 96 h with human blood serum. The mean values of each time point differed by ±9.6% from the mean of the sample without serum incubation (Figure 4). No significant degradation of oligonucleotides could be detected after 96 h incubation in comparison to the samples without serum incubation ($P = 0.079$).

3.4. Cell Adhesion and Viability on Oligonucleotide-Coated diX AM. Cell adhesion experiments were conducted with different cell types in FCS supplied medium (10% for eEPC and human EC, 2% for HUVEC). DiX AM samples where ol-igonucleotides with the same sequence, an oligonucleotide library, HEPES, or nothing of all was applied were used. Cells of a murine embryonic EPC cell line (eEPCs) adhered predominantly to areas coated with either the single oligonucleotide sequence or the oligonucleotide library (Figure 5(a)). HUVECs and human EC derived from human saphenous veins showed the same behavior. In Figure 5(b), the mean number of cells per mm^2 on each coating and cell type is shown. Cell number on oligonucleotide-coated surfaces was significantly higher than on uncoated diX AM or the HEPES control ($P < 0.05$). Thus, oligonucleotides enhanced the adhesion of all cell types compared to cell adhesion on diX AM or buffer-treated diX AM. Experiments ($n = 9$) containing controls on tissue culture (TC) surface were conducted with HUVECs. Cell adhesion on oligonucleotide-coated areas was significantly higher than on TC surfaces ($P < 0.05$), see Figure 6.

To examine the effect of the oligonucleotide coating on cell adhesion without previous protein deposition from FCS, eEPC cells were applied to the samples in serum-free medium or buffers. For cells applied to the samples in PBS without Ca^{2+}/Mg^{2+}, PBS with Ca^{2+}/Mg^{2+}/Glucose or serum-free eEPC medium no significantly enhanced adhesion to oligonucleotide-coated areas could be detected (Figure 7(a)). Cells adhered to all samples equally. To further investigate the effects of FCS diX AM and oligonucleotide-coated Petri-dishes were preincubated for two hours with FCS supplemented eEPC medium. Medium was removed and 5×10^4 mouse EPC cells in serum-free medium applied for 2.5 h at 37°C, 5% CO_2 on a three-dimensional orbital shaker. On Petri-dishes preincubated with FCS-containing medium and cells applied in serum-free medium, the same behavior of cell adhesion like in Petri-dishes where cells were applied in FCS containing medium was observed. Adhesion of cells was significantly higher on oligonucleotide-coated areas then on control areas ($P < 0.05$, Figure 7(b)).

In a further experiment, it was investigated if the amount of oligonucleotide used for coating the diX AM surface plays a role in efficiency of cell adhesion. Different concentrations of the single oligonucleotide sequence and the oligonucleotide library were applied to a diX AM-coated 12-well plate. 5×10^4 mouse EPC cells were applied to each well in FCS supplied medium and incubated at 37°C,

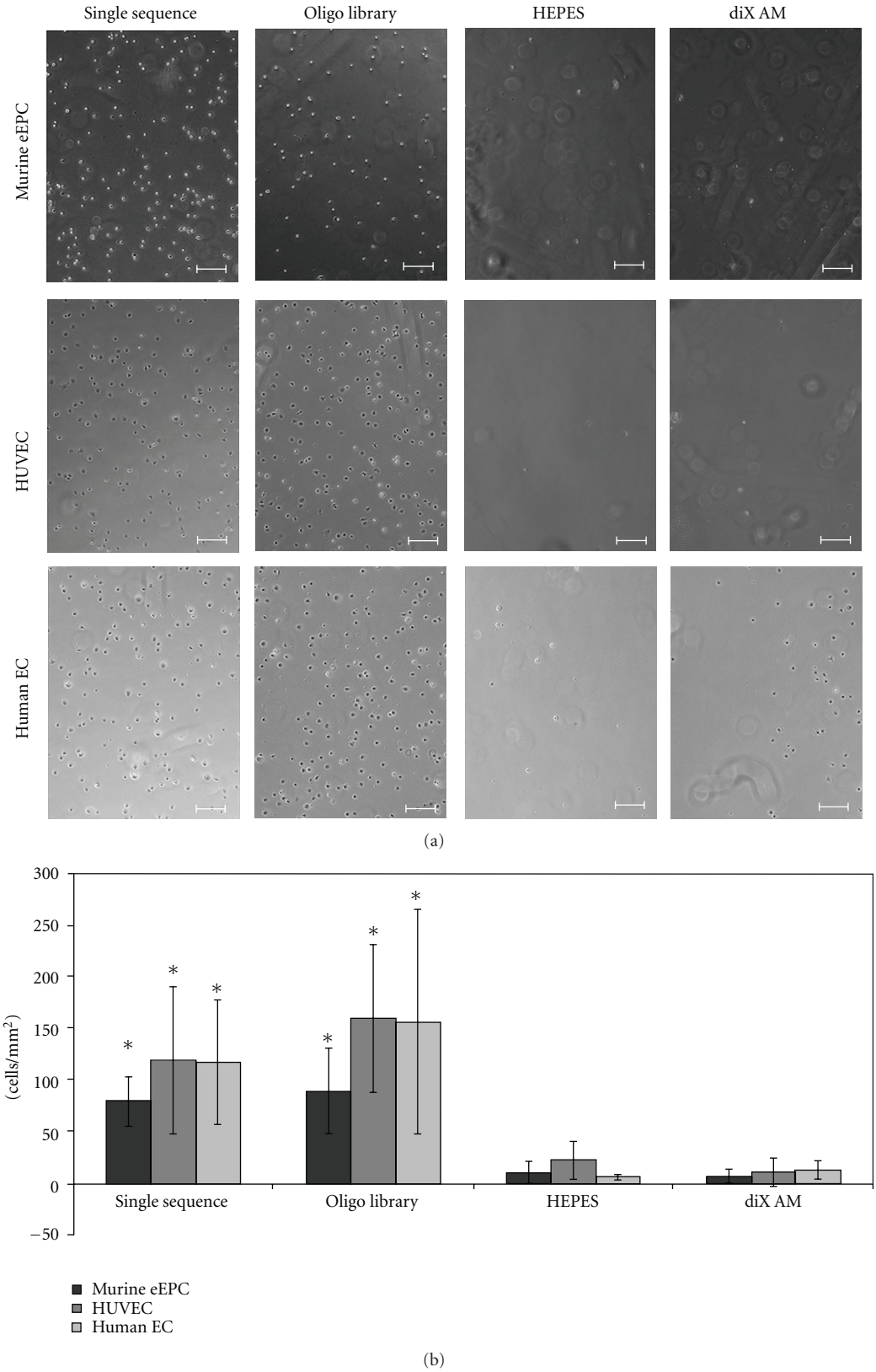

Figure 5: Cell adhesion to oligonucleotide-coated diX AM surfaces in FCS containing medium under dynamic conditions. Samples were incubated with 0,05 $*$ 10^6 cells for 1 h in corresponding medium containing FCS. (a): Scale bar equals 200 μm. (b): Number of adhered cells per mm^2 was counted in microscopy images ($n = 6$). Groups marked with $*$ are significantly different to HEPES and diX AM samples ($P < 0.05$).

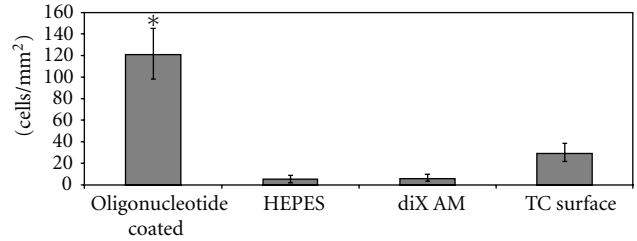

Figure 6: Adhesion of HUVECs to oligonucleotide-coated diX AM surfaces in FCS containing-medium under dynamic conditions compared to tissue culture (TC) surfaces. Samples were incubated with 0,05 $*$ 10^6 cells for 1 h in medium containing FCS. Number of adhered cells per mm^2 was counted in microscopy images ($n = 9$). Group marked with $*$ is significantly different to HEPES, diX AM, and TC surface samples ($P < 0.05$).

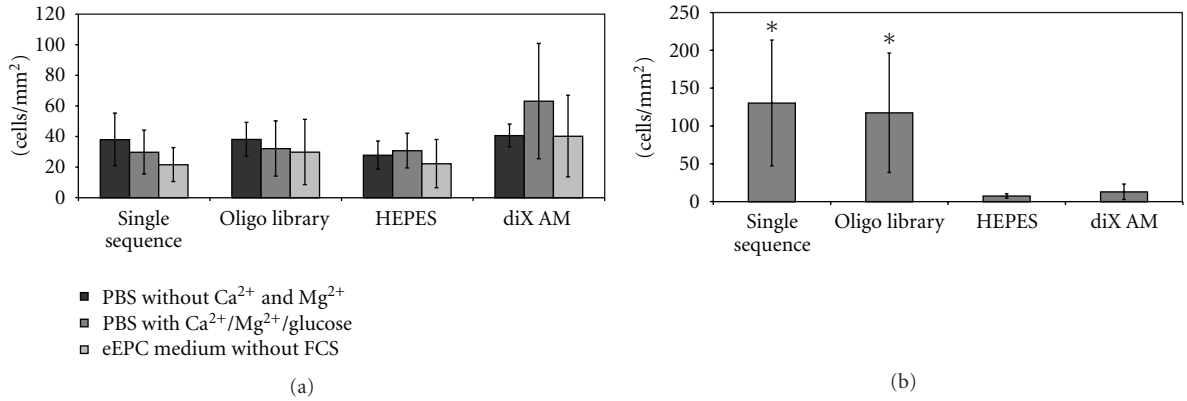

Figure 7: Influence of FCS on cell adhesion on oligonucleotide coated diX AM surfaces. (a) Samples were incubated with 0,05 $*$ 10^6 eEPC cells for 2,5 h under dynamic conditions in medium or buffer without FCS. Cell number was counted in microscopy images ($n = 6$). ANOVA tests revealed no significant difference between the groups. (b) Samples were preincubated with eEPC Medium containing FCS for 2 h. Afterwards 0,05 $*$ 10^6 eEPC cells were applied for 2,5 h under dynamic conditions in medium without FCS. Cell number was counted in microscopy images ($n = 6$). Groups marked with $*$ are significantly different to HEPES and diX AM samples ($P < 0.05$).

5%·CO_2. After 1 h, all the nonadherent cells were washed off and the adherent cells incubated for a further 22 hours. After 22 hours, cell number was determined via the alamarBlue Assay. There was no significant difference between the samples with different oligonucleotide concentrations visible (Figure 8). Also, the utilization of a single sequence or of a library did not make any significant difference; but a significant difference in number of adhered cells was observed between oligonucleotide-coated samples and samples coated with diX AM only or on diX AM samples treated with buffer (HEPES) only ($P < 0.05$).

To further characterize cell adhesion, samples were incubated with HUVECs for 1 h and adherent cells were stained for Vinculin, CD49e (Integrin alpha 2 subunit) and F-Actin. Cells on oligonucleotide-coated surfaces showed a flat morphology and covered a bigger area than cells on diX AM control surfaces which showed a spherical morphology (Figure 9). Cell morphology on oligonucleotide-coated surfaces was similar to cell morphology on TC (tissue culture) surfaces. Cell density was higher on oligonucleotide-coated surfaces and on TC surfaces as on these surfaces more cells adhered than on diX AM control surfaces.

Viability of HUVECs over a period of 14 days was compared between two standard vascular prosthetic materials, ePTFE and ePTFE coated with heparin, and the newly developed coating, diX AM and oligonucleotides on ePTFE. Cell viability was significantly higher on oligonucleotide-coated ePTFE for all time points compared to ePTFE and ePTFE coated with heparin (Figure 10). 2.5 h after adding of cells, nonadherent cells were removed. Values for viability on day one after seeding are an indicator for cell adhesion promoting characteristics. Adhesion of HUVECs was significantly higher on oligonucleotide-coated ePTFE than on ePTFE or ePTFE with heparin. On all materials measured values for viability decreased over time. After 5 days, no viable cells could be detected on ePTFE any more. On ePTFE with heparin viability decreased on day 14 to 13 $\pm$ 10% of the value of day one. On ePTFE with oligonucleotides viability on day 14 was still 43 $\pm$ 5% of viability measured on day one.

3.5. Hemocompatibility. Uncoated ePTFE, diX AM coated suspension cell culture plates and diX AM- and oligonucleotide-coated ePTFE samples were incubated with human blood for 1 h at 37°C on an orbital shaker. As negative control, wells of a suspension cell culture plate were used. The experiment was repeated with six different blood donors. To quantify cell adhesion platelets, erythrocytes and leucocytes were counted in blood samples following incubation.

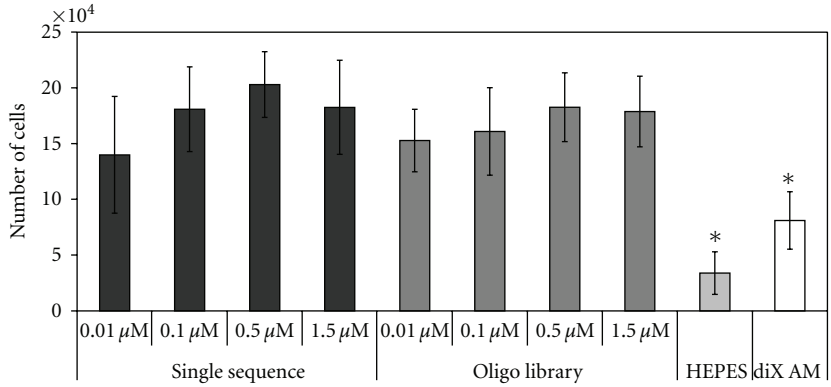

Figure 8: Incubation of eEPC cells on diX AM surfaces with different amounts of oligonucleotides. Amount of oligonucleotides did not significantly influence cell adhesion ($F(7, 16) = 1.598; P = 0,207$). Groups marked with $*$ are significantly different to all oligonucleotide coated samples ($P < 0.05,\ n = 3$).

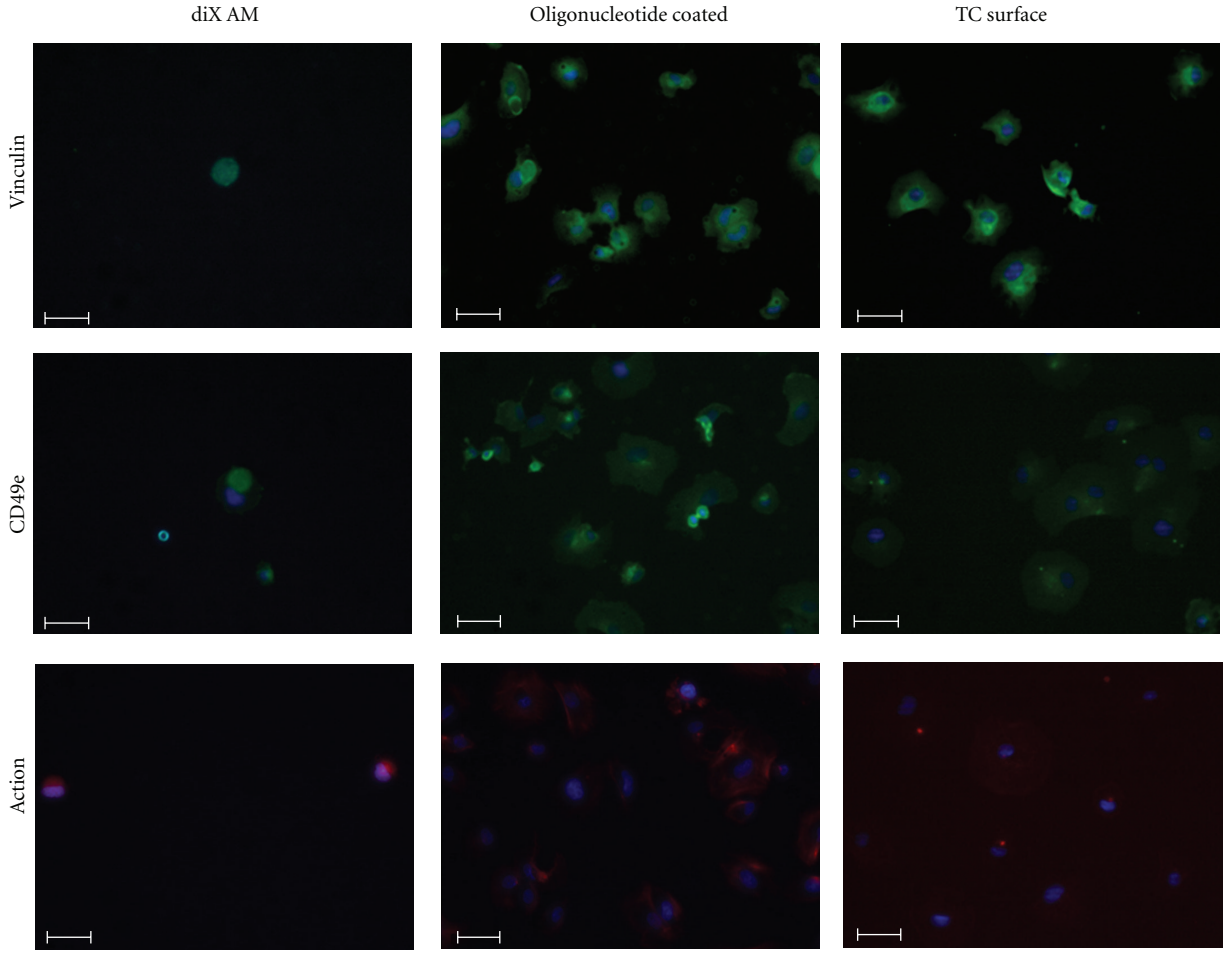

Figure 9: Staining for Vinculin, CD49e and F-Actin of HUVECs after 1 h hour incubation in FCS containing medium under dynamic conditions. Samples were incubated with $0{,}05 * 10^6$ cells in medium containing FCS. Nonadherent cells were removed before staining. Scale bar equals 50 μm. Nuclei are stained with DAPI (blue).

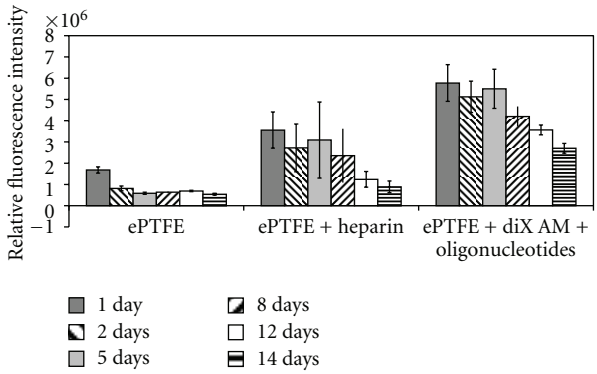

Figure 10: Viability of HUVECs on standard blood vessel graft materials (ePTFE and ePTFE coated with heparin) and on ePTFE coated with diX AM and oligonucleotides over a period of 14 days. Metabolic activity of cells was significantly higher for each time point on oligonucleotide-coated ePTFE compared to ePTFE or ePTFE with heparin ($P < 0.05$).

ANOVA tests revealed no significant decrease in number and therefore no significant adhesion to any of the samples (Figure 11). Surface-dependent activation of platelets and leukocytes was measured by determination of released β-thromboglobuline (β-TG) and PMN-elastase, respectively. β-TG is stored in the α-granules of platelets and released in large amounts after platelet activation. The release of polymorphonuclear- (PMN-)elastase takes place after activation of neutrophile granulocytes or collapse of these cells. It is broadly used to measure granulocyte activity during inflammatory response. Values for β-TG for oligonucleotide coated and uncoated dix AM surfaces did not differ significantly from negative control ($P > 0.05$). PMN-elastase was released to a higher extent by oligonucleotide-coated diX AM surfaces but there was no significant increase compared to the negative control ($P > 0.05$). Surface-dependent activation of the coagulation system was detected by measuring thrombin-antithrombin III (TAT). TAT is an inactive proteinase/inhibitor complex resulting from thrombin and its inhibitor antithrombin III. An increased TAT level is an indicator for thrombotic events. TAT level was not significantly increased for any of the samples ($P > 0.05$).

4. Discussion

Interfaces between implant surfaces and recipient tissue or blood play a crucial role for long-term performance and patency of cardiovascular implants. This study analyzed a novel oligonucleotide-coated diX AM layer in terms of coating stability, EC and EPC adhesion and viability under continuous shear stress application and hemocompatibility. These criteria were chosen as representative key characteristics for cardiovascular implants. Application of the coating concept for other implants is also conceivable.

The oligonucleotide coating showed excellent adhesion properties for human EC and murine EPC under continuous shear stress application as well as good viability properties over a period of 14 days for HUVECs. Cell morphology of HUVECs after adhesion on oligonucleotide-coated surfaces was similar to cell morphology of cells adhered to tissue culture surfaces. This qualifies the material for *in vivo* endothelialization either by EC migration from adjacent native tissue or by EPC capture and adhesion from the blood stream. Stability of the oligonucleotides coated on the diX AM layer was excellent. The applied oligonucleotides withstand shear stress in the amount of shear stress occurring in blood vessels *in vivo*. Additionally, the oligonucleotides were not degraded by human blood serum during prolonged exposure of 96 hours. Maintained hemocompatibility was confirmed by testing for thrombocyte, granulocyte, and coagulation system activation.

A combination of two parylenes, with an intermediate layer of Parylene C and the outer layer of diX AM, an amino-modified parylene derivate, was chosen as a protection film between synthetic material and tissue or blood, as polymers of the parylene family are known to offer good elasticity, biostability and biocompatibility and can be coated easily to different substrate materials even of irregular shape. Parylene C coatings are currently used as protection films for biomedical devices, for example, metal stents, implantable electrode probes, and electronic circuitries [25, 26, 38]. The limitations of Parylene C for cardiovascular and other tissue engineering approaches are the low cell adhesion characteristics [27, 39]. Other parylene derivates such as diX AM offer better growth capacities [39]. Even so we observed low adhesion rates of cells to diX AM-coated areas. Additional coating of diX AM with oligonucleotides enhanced cell adhesion significantly and allowed stable and confluent growth of the cells.

These oligonucleotides were robustly immobilized on the diX AM surface. Shear stress up to 9,5 N/m^2 was applied to the samples, which exceeded the maximum shear stresses observed in blood vessels and heart valves [34, 35, 40]. Xanthan gum was used in the shear stress test fluid to simulate rheological properties of blood [36, 37]. Shear stress stability is crucial as denuded implants exhibit highly thrombotic surface characteristics. Also, DNA molecules may be easily degraded and their solubility in aqueous solutions is high [19]. This was not observed in the present study. After immobilization on diX AM, the oligonucleotides were retained in both the aqueous solutions used in the shear experiments and during incubation with human blood serum.

Interestingly, it did not matter whether a single sequence or an entire oligonucleotide library was used, both enhanced cell adhesion equally. The mechanism of enhanced attachment, therefore, is more likely to be dependent on the overall characteristics of DNA-oligonucleotides than on a specific sequence. As cells were only able to adhere, when they were added to the oligonucleotide-coated surface in FCS supplied medium or when the coated samples were preincubated in medium containing FCS, the mechanism of enhanced cell attachment maybe mediated through attachment-facilitating serum proteins deposited on the surface from FCS. It has been reported in the literature that deposition of serum

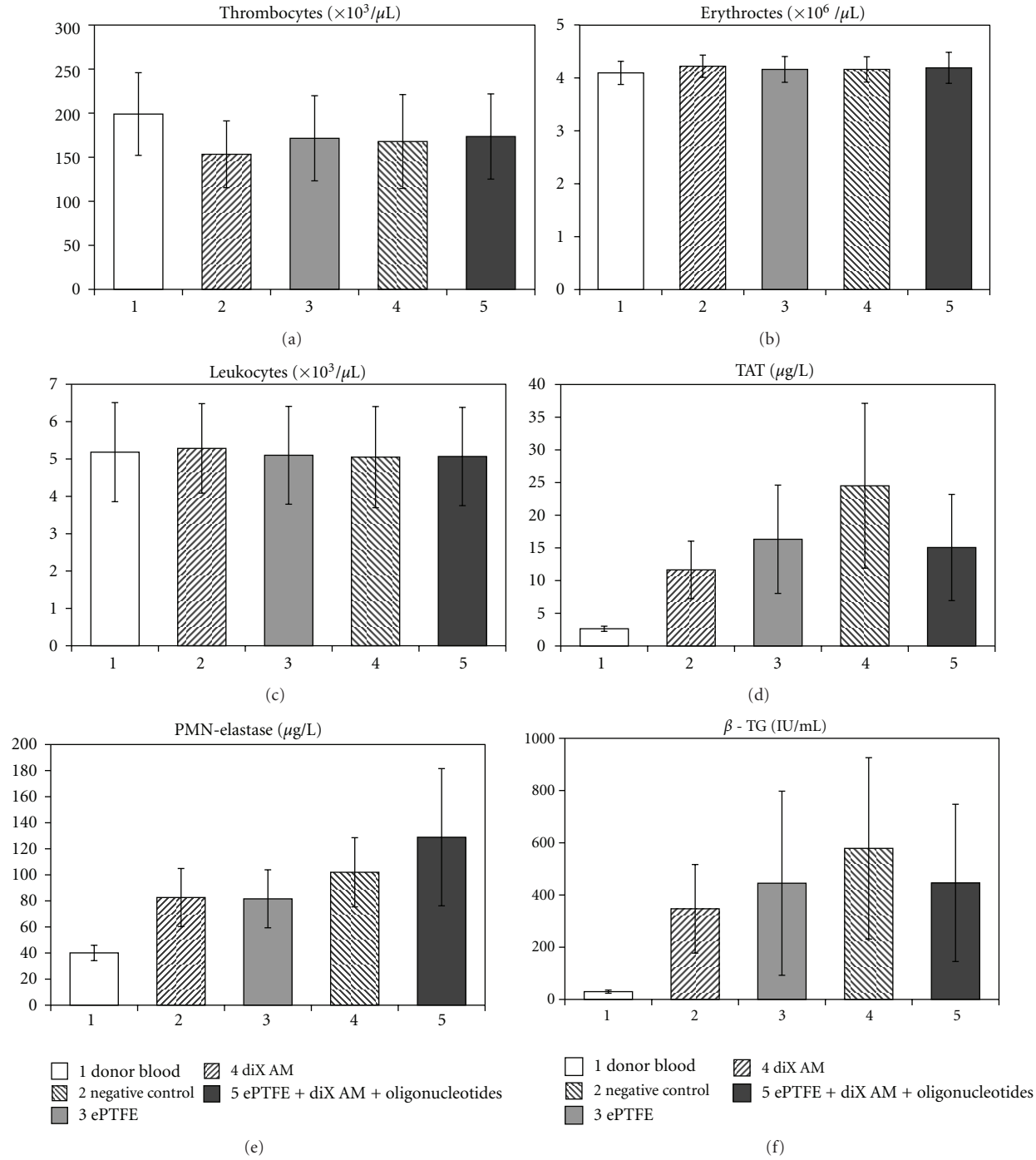

Figure 11: Hemocompatibility testing of oligonucleotide coated diX AM surfaces. Samples were incubated with human whole blood for 1 h at 37°C under continuous shaking. Cell number and different factors, which give information about the activation of thrombocytes (β-TG), granulocytes (PMN-Elastase) and the coagulation system (TAT) were measured in the supernatant. ANOVA tests revealed no significant difference between the groups ($P > 0.05$, $n = 6$).

proteins like fibronectin and vitronectin contained in serum-supplemented culture medium on cell culture material surfaces mediates initial cell attachment, spreading, and behavior [41, 42]. No enhanced cell adhesion could be detected for serum-free medium or PBS. Even supplementation of PBS with calcium, which plays a major role in adhesion via cadherins [43, 44] did not favor cell adhesion. Oligonucleotide coating obviously changes surface properties in a way that facilitates adsorption of functional proteins. A factor that was shown to affect protein adsorption is surface wettability. Protein adsorption is usually higher on hydrophobic surfaces [45, 46], but protein function is presumably maintained better after adhesion to hydrophilic substrates [47–51]. The oligonucleotide coating changes surface wettability to a more

hydrophilic condition compared to the diX AM coating as shown by contact angle measurements. This corresponds to the observed enhanced cell adhesion. Therefore, the more hydrophilic oligonucleotide surface may be involved in this phenomenon, but other determinants such as surface charge might also play a role in cell attachment and hemocompatibility. The ability of materials to adsorb proteins (in an active state) from serum determines their ability to support cell adhesion and spreading [52] and, hence, is an important aspect of their biocompatibility. It will be very interesting to further characterize this adsorption in a future work.

Viability of the adhered cells was measured over a time period of 14 days. As a high number of cells were used for seeding, samples were assumed to be confluent on day one. Viability on oligonucleotide-coated samples decreased to 43 ± 5% on day 14. As the alamarBlue assays measure metabolic turnover, this might be due to less metabolic activity as further cell proliferation might not have been possible. Measured viability on ePTFE and ePTFE with heparin decreased more dramatically. In these cases, cell loss is probable. ePTFE coated with diX AM and oligonucleotides, therefore, showed considerably improved properties for cell growth. Additionally, the similar cell morphology of HUVECs adhered on oligonucleotide-coated surfaces like on tissue culture surfaces as shown by staining for Vinculin, CD49e, and F-Actin confirms the good properties for endothelial cell growth of oligonucleotide-coated surfaces.

For blood contacting material, hemocompatibility is a further important point. Many surface modifications used for engineering of material interfaces for EC adhesion that bind EC also will bind platelets and initiate thrombosis. Here, we provide data, demonstrating that the adhesion of erythrocytes, thrombocytes, and leucocytes was low to the oligonucleotide-coated ePTFE. This is an indication that oligonucleotide-coated diX AM surfaces do not activate inflammatory or thrombogenic responses. The measured values confirmed this result by not showing any activation of thrombocytes (β-TG), granulocytes (PMN-elastase) or the coagulation system (TAT) by oligonucleotide-coated ePTFE. Values for all examined variables were in the same range as the values for clinically routinely used standard ePTFE material (Gore-Tex Cardiovascular Patch, W.L. Gore & Associates, Inc., Flagstaff, Arizona, USA). Furthermore, the determined values were in a similar range as known values for materials with excellent hemocompatibility previously published: β-TG ranges around 500 IU/mL for biopassive or active coated membrane oxygenators (Jostra Quadrox, Maquet Cardiopulmonary, Hirrlingen, Germany) [53], glutaraldehyde-fixed pericardium [54] or star-PEG-modified substrates [55]. Values for PMN-elastase in literature range between 300–400 μg/L for coated membrane oxygenators [53, 56]. Data for TAT revealed levels of 6–8 μg/L for star-PEG-coated surfaces [55] and nitinol stents [57]. Positive controls are known to range between 2300–6000 IU/mL for β-TG [53–55], 450–1000 μg/L for PMN-elastase [53, 56], and 500–6000 μg/L for TAT [55, 57]. Other studies have reported nonimmunogenic characteristics of oligonucleotides [15, 17, 18]. This might be due to their small size and their natural occurrence in the human body thus being no foreign body material [15, 16]. Advantages of oligonucleotides as coating material are easy synthetization and many functional groups for coupling of additional molecules, such as growth factors. The amino groups of the diX AM surface can also be utilized for molecule coupling. We determined an amount of free amino groups on diX AM polymer coating of about 1 million per μm^2. To confirm the applicability of the presented DNA coating for *in vivo* endothelialization of cardiovascular implants, further experiments to clarify the adhesion properties of EC and EPC in human blood vessel environment conditions are required. As diX AM can be coated to substrates of various shapes and material, the coating process can be easily transferred to currently used vessel graft materials. In this work, we developed the successful coating of ePTFE with diX AM and oligonucleotides by surface activation using microwave plasma processing and subsequent chemical vapour deposition of diX AM and oligonucleotide adsorption.

This study revealed DNA-oligonucleotides coated to diX AM surfaces as attractive coating materials for cardiovascular implants. They are shear resistant, nondegradable by human blood serum, offer excellent adhesion properties for EC, and are hemocompatible. Furthermore, they might support adhesion of circulating EPC or transanastomotic ingrowth of EC. This opens new opportunities for the manufacturing of "off-the-shelf" cardiovascular implants to achieve *in vivo* endothelialization after implantation. Additionally, immobilization of oligonucleotides on other types of implants, for example, orthopedic tissues might enhance their incorporation into surrounding tissues.

Acknowledgments

The authors would like to thank Ilka Degenkolbe, Henrike Peuker, Michaela Braun and Doris Armbruster for their excellent technical assistance. This work was supported by contract research "Biomaterialien/Biokompatibilität" of the Baden-Württemberg Stiftung. All authors declare that they have no direct financial relation to the Baden-Württemberg Stiftung and no other competing financial interests.

References

[1] R. Y. Kannan, H. J. Salacinski, P. E. Butler, G. Hamilton, and A. M. Seifalian, "Current status of prosthetic bypass grafts: a review," *Journal of Biomedical Materials Research Part B*, vol. 74, no. 1, pp. 570–581, 2005.

[2] J. G. Meinhart, M. Deutsch, T. Fischlein, N. Howanietz, A. Fröschl, and P. Zilla, "Clinical autologous in vitro endothelialization of 153 infrainguinal ePTFE grafts," *Annals of Thoracic Surgery*, vol. 71, no. 5, pp. S327–S331, 2001.

[3] A. C. Thomas, G. R. Campbell, and J. H. Campbell, "Advances in vascular tissue engineering," *Cardiovascular Pathology*, vol. 12, no. 5, pp. 271–276, 2003.

[4] M. T. Kasimir, G. Weigel, J. Sharma et al., "The decellularized porcine heart valve matrix in tissue engineering: platelet adhesion and activation," *Thrombosis and Haemostasis*, vol. 94, no. 3, pp. 562–567, 2005.

[5] M. Grabenwoger, M. Grimm, E. Eybl et al., "Endothelial cell lining of bioprosthetic heart valve material," *Journal of Cardiac Surgery*, vol. 7, no. 1, pp. 79–84, 1992.

[6] M. Deutsch, J. Meinhart, P. Zilla et al., "Long-term experience in autologous in vitro endothelialization of infrainguinal ePTFE grafts," *Journal of Vascular Surgery*, vol. 49, no. 2, pp. 352–362, 2009.

[7] A. de Mel, G. Jell, M. M. Stevens, and A. M. Seifalian, "Biofunctionalization of biomaterials for accelerated in situ endothelialization: a review," *Biomacromolecules*, vol. 9, no. 11, pp. 2969–2979, 2008.

[8] K. R. Kidd, V. B. Patula, and S. K. Williams, "Accelerated endothelialization of interpositional 1-mm vascular grafts," *Journal of Surgical Research*, vol. 113, no. 2, pp. 234–242, 2003.

[9] J. I. Rotmans, J. M. M. Heyligers, H. J. M. Verhagen et al., "In vivo cell seeding with anti-CD34 antibodies successfully accelerates endothelialization but stimulates intimal hyperplasia in porcine arteriovenous expanded polytetrafluoroethylene grafts," *Circulation*, vol. 112, no. 1, pp. 12–18, 2005.

[10] C. Li, A. Hill, and M. Imran, "In vitro and in vivo studies of ePTFE vascular grafts treated with P15 peptide," *Journal of Biomaterials Science*, vol. 16, no. 7, pp. 875–891, 2005.

[11] R. Blindt, F. Vogt, I. Astafieva et al., "A novel drug-eluting stent coated with an integrin-binding cyclic Arg-Gly-Asp peptide inhibits neointimal hyperplasia by recruiting endothelial progenitor cells," *Journal of the American College of Cardiology*, vol. 47, no. 9, pp. 1786–1795, 2006.

[12] K. J. Pratt, B. E. Jarrell, S. K. Williams, R. A. Carabasi, M. A. Rupnick, and F. A. Hubbard, "Kinetics of endothelial cell-surface attachment forces," *Journal of Vascular Surgery*, vol. 7, no. 4, pp. 591–599, 1988.

[13] S. K. Williams, B. E. Jarrell, and L. Friend, "Adult human endothelial cell compatibility with prosthetic graft material," *Journal of Surgical Research*, vol. 38, no. 6, pp. 618–629, 1985.

[14] P. Zilla, D. Bezuidenhout, and P. Human, "Prosthetic vascular grafts: wrong models, wrong questions and no healing," *Biomaterials*, vol. 28, no. 34, pp. 5009–5027, 2007.

[15] A. M. Krieg, "Immune effects and mechanisms of action of CpG motifs," *Vaccine*, vol. 19, no. 6, pp. 618–622, 2000.

[16] J. M. Berg, J. L. Tymoczko, and L. Stryer, *Biochemistry*, Palgrave Macmillan, 6th edition, 2006.

[17] A. M. Krieg, A. K. Yi, S. Matson et al., "CpG motifs in bacterial DNA trigger direct B-cell activation," *Nature*, vol. 374, no. 6522, pp. 546–549, 1995.

[18] S. Yamamoto, T. Yamamoto, S. Shimada et al., "DNA from bacteria, but not from vertebrates, induces interferons, activates natural killer cells and inhibits tumor growth," *Microbiology and Immunology*, vol. 36, no. 9, pp. 983–997, 1992.

[19] T. Fukushima, Y. Inoue, T. Hayakawa, K. Taniguchi, K. Miyazaki, and Y. Okahata, "Preparation of and tissue response to DNA-lipid films," *Journal of Dental Research*, vol. 80, no. 8, pp. 1772–1776, 2001.

[20] T. Fukushima, J. Ohno, T. Hayakawa et al., "Mold fabrication and biological assessment of porous DNA-chitosan complexes," *Journal of Biomedical Materials Research Part B*, vol. 91, no. 2, pp. 746–754, 2009.

[21] J. J. J. P. Van Den Beucken, M. R. J. Vos, P. C. Thüne et al., "Fabrication, characterization, and biological assessment of multilayered DNA-coatings for biomaterial purposes," *Biomaterials*, vol. 27, no. 5, pp. 691–701, 2006.

[22] M. H. Werner, A. M. Gronenborn, and G. M. Clore, "Intercalation, DNA kinking, and the control of transcription," *Science*, vol. 271, no. 5250, pp. 778–784, 1996.

[23] T. Fukushima, M. Kawaguchi, T. Hayakawa et al., "Drug binding and releasing characteristics of DNA/lipid/PLGA film," *Dental Materials Journal*, vol. 26, no. 6, pp. 854–860, 2007.

[24] J. M. Hsu, L. Rieth, R. A. Normann, P. Tathireddy, and F. Solzbacher, "Encapsulation of an integrated neural interface device with parylene C," *IEEE Transactions on Biomedical Engineering*, vol. 56, no. 1, pp. 23–29, 2009.

[25] E. M. Schmidt, J. S. McIntosh, and M. J. Bak, "Long-term implants of Parylene-C coated microelectrodes," *Medical and Biological Engineering and Computing*, vol. 26, no. 1, pp. 96–101, 1988.

[26] A. B. Fontaine, K. Koelling, S. Dos Passos, J. Cearlock, R. Hoffman, and D. G. Spigos, "Polymeric surface modifications of tantalum stents," *Journal of Endovascular Surgery*, vol. 3, no. 3, pp. 276–283, 1996.

[27] T. Y. Chang, V. G. Yadav, S. De Leo et al., "Cell and protein compatibility of parylene-C surfaces," *Langmuir*, vol. 23, no. 23, pp. 11718–11725, 2007.

[28] A. K. Hatzopoulos, J. Folkman, E. Vasile, G. K. Eiselen, and R. D. Rosenberg, "Isolation and characterization of endothelial progenitor cells from mouse embryos," *Development*, vol. 125, no. 8, pp. 1457–1468, 1998.

[29] J. Lahann, "Vapor-based polymer coatings for potential biomedical applications," *Polymer International*, vol. 55, no. 12, pp. 1361–1370, 2006.

[30] R. K. Samal, H. Iwata, and Y. Ikada, "Introduction of reactive groups onto polymer surfaces," in *Physicochemical Aspects of Polymer Surfaces*, K. L. Mittal, Ed., pp. 810–815, Plenum, New York, NY, USA, 1983.

[31] S. R. Wickramasinghe, C. M. Kahr, and B. Han, "Mass transfer in blood oxygenators using blood analogue fluids," *Biotechnology Progress*, vol. 18, no. 4, pp. 867–873, 2002.

[32] E. J. Hinch, Lecture 3: Simple Flows, 2009, http://www.whoi.edu/fileserver.do?id=28327&pt=10&p=17274.

[33] A. St-Georges-Robillard, J. C. Ruiz, A. Petit, F. Mwale, B. Elkin, and C. Oehr, "Adhesion of U-937 monocytes on amine-functionalised parylene and plasma polymer surfaces," *Macromolecular Bioscience*, 2011.

[34] M. W. Weston, D. V. LaBorde, and A. P. Yoganathan, "Estimation of the shear stress on the surface of an aortic valve leaflet," *Annals of Biomedical Engineering*, vol. 27, no. 4, pp. 572–579, 1999.

[35] C. Cheng, F. Helderman, D. Tempel et al., "Large variations in absolute wall shear stress levels within one species and between species," *Atherosclerosis*, vol. 195, no. 2, pp. 225–235, 2007.

[36] M. Pohl, M. O. Wendt, B. Koch, R. Kühnel, O. Samba, and G. Vlastos, "Model fluids of blood for in-vitro testing of artificial heart valves," *Zeitschrift fur Medizinische Physik*, vol. 11, no. 3, pp. 187–194, 2001.

[37] M. Pohl, M. O. Wendt, S. Werner, B. Koch, and D. Lerche, "In vitro testing of artificial heart valves: comparison between Newtonian and Non-Newtonian fluids," *Artificial Organs*, vol. 20, no. 1, pp. 37–46, 1996.

[38] P. Hanefeld, U. Westedt, R. Wombacher et al., "Coating of poly(p-xylylene) by PLA-PEO-PLA triblock copolymers with excellent polymer - Polymer adhesion for stent applications," *Biomacromolecules*, vol. 7, no. 7, pp. 2086–2090, 2006.

[39] Y. X. Kato, I. Saito, H. Takano, K. Mabuchi, and T. Hoshino, "Comparison of neuronal cell adhesiveness of materials in the diX (Parylene) family," *Neuroscience Letters*, vol. 464, no. 1, pp. 26–28, 2009.

[40] M. S. Sacks and A. P. Yoganathan, "Heart valve function: a biomechanical perspective," *Philosophical Transactions of the Royal Society B*, vol. 362, no. 1484, pp. 1369–1391, 2007.

[41] C. R. Jenney and J. M. Anderson, "Adsorbed serum proteins responsible for surface dependent human macrophage behavior," *Journal of Biomedical Materials Research*, vol. 49, no. 4, pp. 435–447, 2000.

[42] C. J. Wilson, R. E. Clegg, D. I. Leavesley, and M. J. Pearcy, "Mediation of biomaterial-cell interactions by adsorbed proteins: a review," *Tissue Engineering*, vol. 11, no. 1-2, pp. 1–18, 2005.

[43] M. Takeichi, "Cadherins: a molecular family important in selective cell-cell adhesion," *Annual Review of Biochemistry*, vol. 59, pp. 237–252, 1990.

[44] M. Overduin, T. S. Harvey, S. Bagby et al., "Solution structure of the epithelial cadherin domain responsible for selective cell adhesion," *Science*, vol. 267, no. 5196, pp. 386–389, 1995.

[45] J. H. Lee and H. B. Lee, "A wettability gradient as a tool to study protein adsorption and cell adhesion on polymer surfaces," *Journal of Biomaterials Science*, vol. 4, no. 5, pp. 467–481, 1993.

[46] M. Mrksich and G. M. Whitesides, "Using self-assembled monolayers to understand the interactions of man-made surfaces with proteins and cells," *Annual Review of Biophysics and Biomolecular Structure*, vol. 25, pp. 55–78, 1996.

[47] G. K. Toworfe, R. J. Composto, C. S. Adams, I. M. Shapiro, and P. Ducheyne, "Fibronectin adsorption on surface-activated poly(dimethylsiloxane) and its effect on cellular function," *Journal of Biomedical Materials Research Part A*, vol. 71, no. 3, pp. 449–461, 2004.

[48] M. Bergkvist, J. Carlsson, and S. Oscarsson, "Surface-dependent conformations of human plasma fibronectin adsorbed to silica, mica, and hydrophobic surfaces, studied with use of Atomic Force Microscopy," *Journal of Biomedical Materials Research Part A*, vol. 64, no. 2, pp. 349–356, 2003.

[49] S. S. Cheng, K. K. Chittur, C. N. Sukenik, L. A. Culp, and K. Lewandowska, "The conformation of fibronectin on self-assembled monolayers with different surface composition: an FTIR/ATR study," *Journal of Colloid And Interface Science*, vol. 162, no. 1, pp. 135–143, 1994.

[50] R. L. Williams, J. A. Hunt, and P. Tengvall, "Fibroblast adhesion onto methyl-silica gradients with and without preadsorbed protein," *Journal of Biomedical Materials Research*, vol. 29, no. 12, pp. 1545–1555, 1995.

[51] P. A. Underwood, J. G. Steele, and B. A. Dalton, "Effects of polystyrene surface chemistry on the biological activity of solid phase fibronectin and vitronectin, analysed with monoclonal antibodies," *Journal of Cell Science*, vol. 104, no. 3, pp. 793–803, 1993.

[52] J. G. Steele, B. A. Dalton, G. Johnson, and P. A. Underwood, "Adsorption of fibronectin and vitronectin onto Primaria ® and tissue culture polystyrene and relationship to the mechanism of initial attachment of human vein endothelial cells and BHK-21 fibroblasts," *Biomaterials*, vol. 16, no. 14, pp. 1057–1067, 1995.

[53] A. K. Zimmermann, N. Weber, H. Aebert, G. Ziemer, and H. P. Wendel, "Effect of and biopassive and bioactive surface-coatings on the hemocompatibility of membrane oxygenators," *Journal of Biomedical Materials Research Part B*, vol. 80, no. 2, pp. 433–439, 2007.

[54] J. Zhou, O. Fritze, M. Schleicher et al., "Impact of heart valve decellularization on 3-D ultrastructure, immunogenicity and thrombogenicity," *Biomaterials*, vol. 31, no. 9, pp. 2549–2554, 2010.

[55] J. Hoffmann, J. Groll, J. Heuts et al., "Blood cell and plasma protein repellent properties of Star-PEG-modified surfaces," *Journal of Biomaterials Science*, vol. 17, no. 9, pp. 985–996, 2006.

[56] A. Straub, H. P. Wendel, R. Azevedo, and G. Ziemer, "The GP IIb/IIIa inhibitor abciximab (ReoPro®) decreases activation and interaction of platelets and leukocytes during in vitro cardiopulmonary bypass simulation," *European Journal of Cardio-Thoracic Surgery*, vol. 27, no. 4, pp. 617–621, 2005.

[57] G. Tepe, H. P. Wendel, S. Khorchidi et al., "Thrombogenicity of various endovascular stent types: an in vitro evaluation," *Journal of Vascular and Interventional Radiology*, vol. 13, no. 10, pp. 1029–1035, 2002.

Hindawi Publishing Corporation
International Journal of Biomaterials
Volume 2012, Article ID 212417, 5 pages
doi:10.1155/2012/212417

Research Article

Modulation of C1-Inhibitor and Plasma Kallikrein Activities by Type IV Collagen

Sriram Ravindran,[1,2] Marc Schapira,[3] and Philip A. Patston[1]

[1] *Department of Oral Medicine and Diagnostic Sciences, College of Dentistry, University of Illinois at Chicago, 801 S. Paulina Street, Chicago, IL 60612, USA*
[2] *Department of Oral Biology, College of Dentistry, University of Illinois at Chicago, Chicago, IL 60612, USA*
[3] *Department of Hematology, CHUV, University of Lausanne, 1011, Switzerland*

Correspondence should be addressed to Philip A. Patston, patston@uic.edu

Received 11 April 2011; Accepted 10 November 2011

Academic Editor: Narayana Garimella

The contact system of coagulation can be activated when in contact with biomaterials. As collagen is being tested in novel biomaterials in this study, we have investigated how type IV collagen affects plasma kallikrein and C1-inhibitor. Firstly, we showed C1-inhibitor binds to type IV collagen with a Kd of 0.86 μM. The effects of type IV collagen on plasma kallikrein, factor XIIa, and β-factor XIIa activity and on C1-inhibitor function were determined. Factor XIIa rapidly lost activity in the presence of type IV collagen, whereas plasma kallikrein and β-factor XIIa were more stable. The rate of inhibition of plasma kallikrein by C1-inhibitor was decreased by type IV collagen in a dose-dependent manner. These studies could be relevant to the properties of biomaterials, which contain collagen, and should be considered in the testing for biocompatibility.

1. Introduction

Surface-dependent activation of factor XII and plasma prekallikrein is not believed to be a major component of the normal *in vivo* blood coagulation activation process [1]. However, contact activation readily occurs *in vitro*, as a result of contact with surfaces such as glass, kaolin, and other materials and during procedures such as cardiopulmonary bypass [2–5]. Under conditions such as these, factor XIIa could convert factor XI to factor XIa and result in unwanted thrombin generation. Therefore, it remains critical to understand the mechanisms of contact activation, as this has important implications for the thrombogenic properties and biocompatibility of many materials. For example, novel biomaterials are being developed for wound healing and drug delivery. Notably, many of these materials contain collagen [6–9]. Although collagens are naturally occurring molecules, if they are present in nonphysiological situations or at elevated concentrations, they might have unwanted properties, such as being thrombogenic [10].

C1-inhibitor is a proteinase inhibitor in the serpin family which is an important physiological inhibitor of plasma kallikrein and factor XIIa [11]. Previously we have shown that C1-inhibitor can bind to type IV collagen and that this can modulate the reaction with the complement proteinase C1s [12]. As C1-inhibitor is the main inhibitor of plasma kallikrein, we considered it to be important to investigate the effect of type IV collagen on the inhibition of plasma kallikrein by C1-inhibitor. In this study we have investigated binding of C1-inhibitor to type IV collagen in more detail and studied the effects of type IV collagen on plasma kallikrein and factor XIIa activities and on the inhibition of plasma kallikrein by C1-inhibitor.

2. Materials and Methods

2.1. Proteins and Reagents. Human plasma kallikrein, factor XIIa, and C1s were from Enzyme Research Labs (South Bend, IN). β-factor XIIa was from Calbiochem (San Diego, CA,

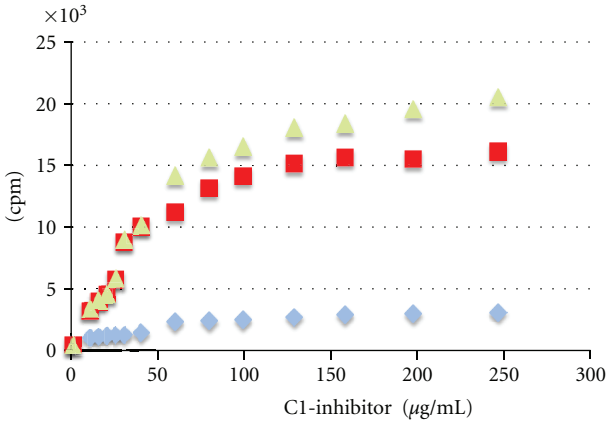

Figure 1: Binding of C1-inhibitor to type IV collagen. The figure shows the binding curve for biotinylated C1-inhibitor to type IV collagen (×), BSA (■), and the collagen binding with the subtraction of the BSA blank (▲). On the y-axis is counts per minute (cpm).

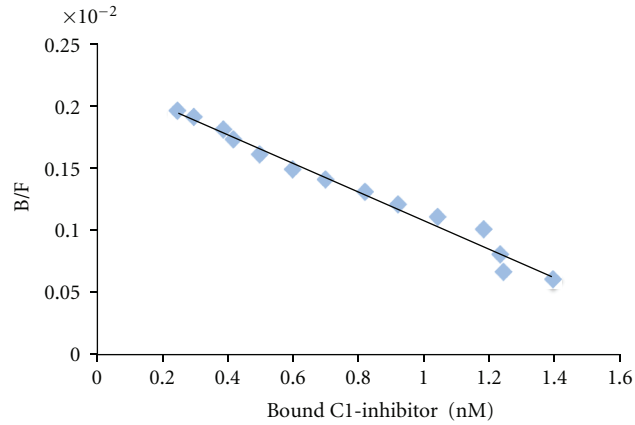

Figure 2: Scatchard plot of C1-inhibitor binding to type IV collagen. Analysis of the data from Figure 1. B/F is the ratio of bound/free biotinylated C1-inhibitor.

USA). Human C1-inhibitor was from the Behringwerke (Marburg, Germany). Inactive C1-inhibitor polymers were removed by chromatography on Phenyl-Sepharose as described previously [13]. Human types I, IV, and V collagen and mouse type IV collagen were from Research Diagnostics (Flanders, NJ, USA). The chromogenic substrates S-2302 (for kallikrein, factor XIIa and β-factor XIIa) and Spectrozyme C1-E (for C1s) were from DiaPharma (Westchester, OH) and American Diagnostica, (Greenwich, CT), respectively.

2.2. Binding of C1-Inhibitor to Type IV Collagen. Biotinylation of C1-inhibitor was carried out by incubating 0.5 mL of C1-inhibitor in PBS (1 mg/mL) and 0.04 mL of freshly prepared biotinylation reagent (2.2 mg NHS-LC-biotin (Pierce, Rockford, IL) in 0.08 mL water) on ice for 2.5 h. Thereafter, excess reagent was removed using a desalting PD10 column (Pharmacia, Piscataway, NJ, USA), with protein detection at 280 nm. To measure the binding affinity, Immulon 2 ividastrip 96-well plates were coated with 100 μL mouse type IV collagen or bovine serum albumin at 10 μg/mL in carbonate/bicarbonate buffer at pH 7.5, for 18 hrs at 4°C. Wells were blocked with 1% bovine serum albumin, 0.1% Tween 20, in Tris-buffered saline, followed by washing with 0.1% Tween 20 in Tris-buffered saline. Biotinylated C1-inhibitor was added to the wells at 1.9–125 ng/mL. Binding was measured by subsequent incubation with 125-I streptavidin, washing and counting the individual wells in a gamma counter. Affinity was determined by Scatchard plot. To confirm that binding of C1-inhibitor to the type IV collagen was specific, the biotinylated C1-inhibitor was displaced by use of an increasing concentration of unlabelled C1-inhibitor.

Tryptophan fluorescence was also used to analyze the interaction between C1-inhibitor and type IV collagen, using a Photon Technology International fluorimeter. Excitation was at 280 nm, and emission was measured between 290 nm and 400 nm. Samples contained 1 mg/mL C1-inhibitor, 6 μg/mL type IV collagen, or a mixture of both, all in 3 mL of 50 mM Tris-HCl, pH 7.4, 20 mM NaCl.

2.3. Effect of Collagen on Proteinase Activity. Plasma kallikrein, factor XIIa, and β-factor XIIa were assayed using S-2302, and C1s was assayed using Spectrozyme C1-E, as described previously [14]. To determine the effect of collagen on activity of the proteinases, kallikrein (30 nM), factor XIIa (0.649 μM), β-factor XIIa (0.185 μM), and C1s (0.46 μM) were incubated in 20 mM Tris-HCl, pH 7.4, 150 mM NaCl, 0.1% polyethylene glycol 8000 (with kallikrein, factor XIIa, and β-factor XIIa) or 1 mg/mL BSA (with C1s), at 37°C in the absence of collagen, or with collagen at 20, 40, 60, 80, or 100 μg/mL. Aliquots were removed at various times for assay of residual proteinase activity.

2.4. Effect of Type IV Collagen on Inhibition of Plasma Kallikrein by C1-Inhibitor. The inhibition of plasma kallikrein by C1-inhibitor was measured under pseudo-first-order conditions using a discontinuous assay as described previously [14]. Kallikrein (30 nM) was incubated with a 10-fold excess of C1-inhibitor in 20 mM Tris-HCl, pH 7.4, 150 mM NaCl, 0.1% polyethylene glycol 8000 at 37°C in the absence of collagen, or with collagen at 20, 40, 60, 80, or 100 μg/mL. Aliquots were removed at various times (from 30 seconds to 150 seconds) for assay of residual proteinase activity with S-2302.

3. Results

3.1. Binding of C1-Inhibitor to Type IV Collagen. We have shown previously in a qualitative assay that C1-inhibitor will bind to type IV collagen [12]. To determine the affinity for this interaction, the binding of biotinylated C1-inhibitor to immobilized type IV collagen was measured (Figure 1). The affinity was determined to be 0.86 μM from the Scatchard plot of this data (Figure 2). Confirmation of the specificity of binding of labeled C1-inhibitor was shown by displacement

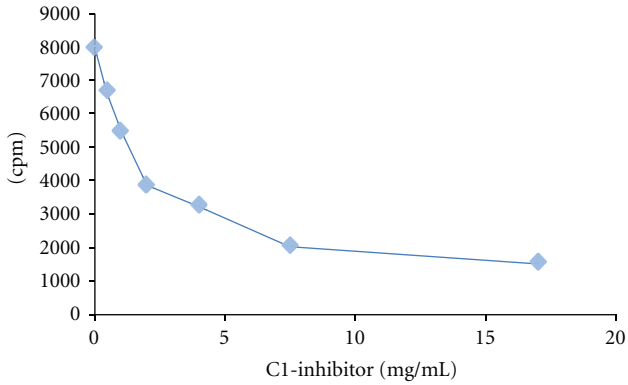

Figure 3: Displacement of biotinylated C1-inhibitor from type IV collagen. To confirm specificity of binding of the biotinylated C1-inhibitor to the immobilized collagen, the labeled protein was displaced with unlabeled C1-inhibitor. On the *y*-axis is counts per minute (cpm).

of the labeled protein by unlabeled protein (Figure 3). Further evidence for the interaction is shown in Figure 4, which shows the fluorescence emission spectra of C1-inhibitor alone, collagen alone, and a mixture of the two. Collagen had very little fluorescence due to the low tryptophan content. The mixture of type IV collagen and C1-inhibitor showed less fluorescence than the C1-inhibitor alone, and less fluorescence than when the individual spectra of type IV collagen and C1-inhibitor were added together. Although no red or blue shift occurred, this small quench is indicative of an interaction between the two proteins. In addition, the magnitude of quench was dependent on the amount of collagen used (not shown). However, as this quench was small, it could not be reliably used to quantify binding affinity.

3.2. Effect of Type IV Collagen on Proteinase Activity. The effect of type IV collagen on the activity of kallikrein, factor XIIa, or β-factor XIIa activity was determined. The proteinases were incubated with increasing amounts of collagen, and the residual activity was measured. Figure 5 shows a time course of loss of enzyme activity in the presence of 20 or 100 μg/mL of type IV collagen. There was a rapid loss of factor XIIa activity, with 50% of the activity lost after 14.5 minutes in the presence of 20 μg/mL of collagen and 50% of the activity lost after 3 minutes in the presence of 100 μg/mL of collagen. This loss of activity is attributed to factor XIIa adsorbing to the collagen [15]. In the absence of collagen, only 10% of the activity was lost after 30 minutes of incubation. With β-factor XIIa, the loss of activity was less, consistent with β-factor XIIa not containing the surface binding heavy chain. In the case of kallikrein, 20 μg/mL of collagen caused only a slight loss of activity even after 5 hours, whereas with 100 μg/mL of collagen, there was an initial rapid decrease of activity to about 40%. A similar loss of kallikrein activity by adsorption to surfaces has been observed previously [16, 17], and so these results are entirely consistent with published data. As a control, the complement proteinase C1s showed no loss of activity even after 6 hours with 100 μg/mL of type IV collagen indicating that the effects of collagen were specific for the different proteinases (data not shown).

Table 1: Effect of type IV collagen on the inhibition of plasma kallikrein by C1-inhibitor.

Amount of type IV collagen (μg/mL)	Second-order rate constant for inhibition of kallikrein ($M^{-1}s^{-1}$)
0	16580
10	14370
20	13905
30	11650
40	10510
50	8450

3.3. Effect of Type IV Collagen on the Inhibition of Plasma Kallikrein by C1-Inhibitor. The rate constant for the inhibition of kallikrein by C1-inhibitor in the presence of type IV collagen was determined. Table 1 shows that there was dose-dependent effect on inhibition. As these assays were performed over a short time frame (under 3 minutes), there was no loss of kallikrein activity during this time (compared to the longer times involved for loss of kallikrein activity seen in Figure 5). The second-order rate constant for inhibition decreased by 50% with 100 μg/mL of collagen. In other studies we have shown that kallikrein inhibition by C1-inhibitor is also reduced when the inhibition reaction is carried out in type IV collagen-coated microtiter plates [18].

4. Discussion

In this study we provide evidence that C1-inhibitor can bind tightly to type IV collagen (Figures 1, 2, 3, and 4). We also show that type IV collagen caused a concentration-and time-dependent loss of kallikrein and factor XIIa activities (Figure 5). However, by measuring the inhibition of kallikrein by C1-inhibitor at early time points, we show that type IV collagen can dramatically reduce the rate of inhibition. The most likely explanation for these data is that the binding of C1-inhibitor to collagen reduces the concentration of C1-inhibitor available to react with kallikrein and so the rate of inhibition drops. Given that the plasma C1-inhibitor concentration is $\sim$2 μM, this is an interaction which potentially could occur *in vivo*. However, whether this has any regulatory significance for the contact system *in vivo* remains to be determined, particularly as high concentrations of collagen were used. Perhaps a more important consideration is that the effects of collagen on the activities of the proteins tested indicate that studies with biomaterials should consider such reactions as part of their screening for biocompatibility, especially as high local concentrations of collagen would likely be present in such materials. Thus we would suggest that all materials that use collagen (especially type IV) should be evaluated not only for their thrombogenic potential, but also for more specific actions on the contact system proteinases and C1-inhibitor, such as have been carried out with other biomaterials [5, 6, 19–21].

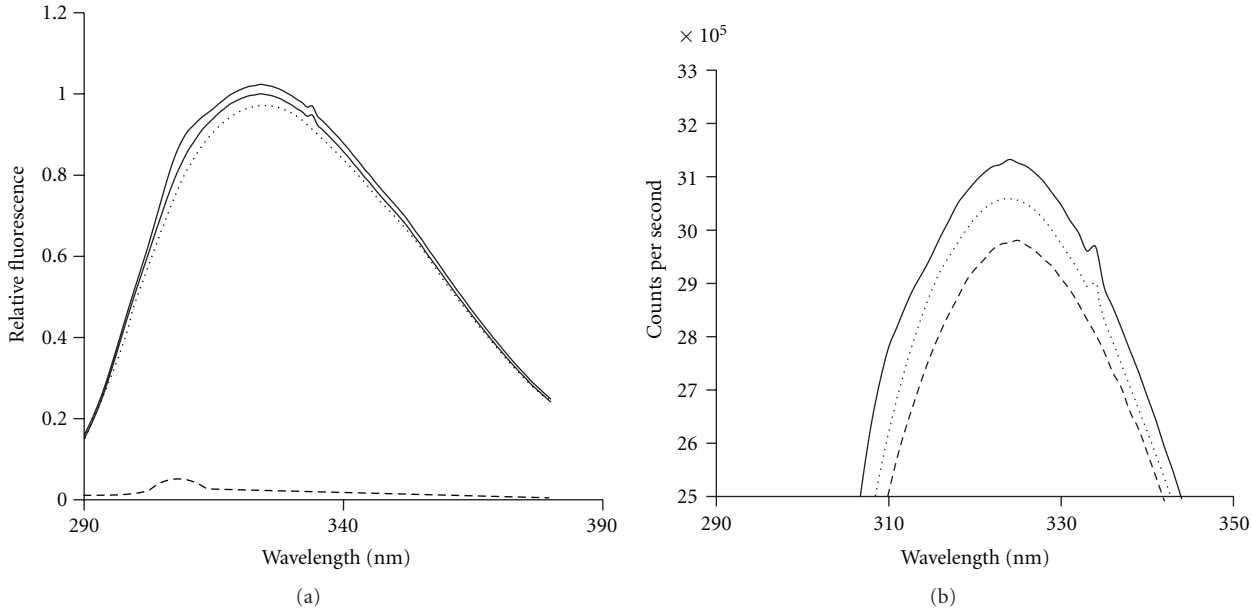

Figure 4: The interaction of type IV collagen and C1-inhibitor assessed by fluorescence spectroscopy. (a) The fluorescence spectra of C1-inhibitor alone (2nd line from top), type IV collagen alone (4th line, at bottom of figure), a mixture of type IV collagen and C1-inhibitor (3rd line from top), and the individual spectra of C1-inhibitor alone and type IV collagen alone added together (1st line at top of figure). (b) An amplified view of the same data at the apex of the peaks (between 295 nm and 355 nm).

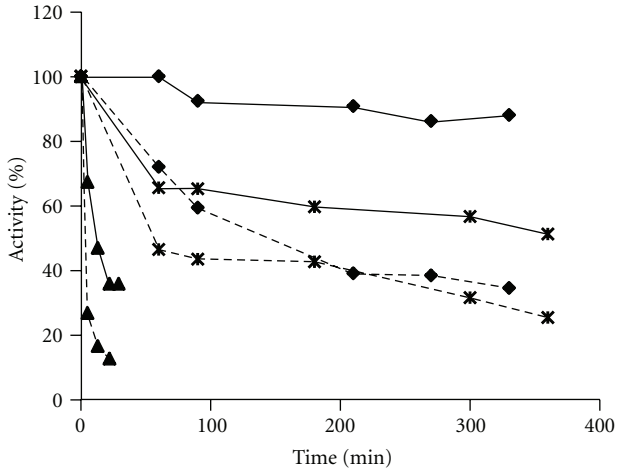

Figure 5: The time course of inactivation of kallikrein, factor XIIa, and β-factor XIIa by type IV collagen. Kallikrein was incubated with 20 μg/mL collagen (♦) or 100 μg/mL collagen (■), factor XIIa was incubated with 20 μg/mL collagen (▲) or 100 μg/collagen (×), and β-factor XIIa was incubated with 20 μg/mL collagen (∗) or 5 μg/mL collagen (•). At the indicated times, a sample was assayed for residual activity with S-2302. The activity is presented as the percentage of the original activity prior to incubation. In the absence of collagen, there was no loss of activity during the same time course.

Acknowledgments

This work was supported by the National Institutes of Health Grant HL-49242 (to PAP) and by the Swiss National Science Foundation Grant 31-36080.92 (to M. Schapira).

References

[1] A. H. Schmaier, "Assembly, activation, and physiologic influence of the plasma kallikrein/kinin system," *International Immunopharmacology*, vol. 8, no. 2, pp. 161–165, 2008.

[2] Y. T. Wachtfogel, P. C. Harpel, L. H. Edmunds, and R. W. Colman, "Colman RW: formation of C1s-C1-inhibitor, kallikrein-C1-inhibitor, and plasmin-alpha 2-plasmin-inhibitor complexes during cardiopulmonary bypass," *Blood*, vol. 73, no. 2, pp. 468–471, 1989.

[3] D. J. Campbell, B. Dixon, A. Kladis, M. Kemme, and J. D. Santamaria, "Activation of the kallikrein-kinin system by cardiopulmonary bypass in humans," *American Journal of Physiology*, vol. 281, no. 4, pp. R1059–R1070, 2001.

[4] K. W. H. J. Van der Kamp and W. Van Oeveren, "Factor XII fragment and kallikrein generation in plasma during incubation with biomaterials," *Journal of Biomedical Materials Research*, vol. 28, no. 3, pp. 349–352, 1994.

[5] J. Hong, A. Larsson, K. N. Ekdahl, G. Elgue, R. Larsson, and B. Nilsson, "Contact between a polymer and whole blood: sequence of events leading to thrombin generation," *Journal of Laboratory and Clinical Medicine*, vol. 138, no. 2, pp. 139–145, 2001.

[6] C. H. Lee, A. Singla, and Y. Lee, "Biomedical applications of collagen," *International Journal of Pharmaceutics*, vol. 221, no. 1-2, pp. 1–22, 2001.

[7] C. Yang, P. J. Hillas, J. A. Báez et al., "The application of recombinant human collagen in tissue engineering," *BioDrugs*, vol. 18, no. 2, pp. 103–119, 2004.

[8] D. Olsen, C. Yang, M. Bodo et al., "Recombinant collagen and gelatin for drug delivery," *Advanced Drug Delivery Reviews*, vol. 55, no. 12, pp. 1547–1567, 2003.

[9] Z. Ruszczak and W. Friess, "Collagen as a carrier for on-site delivery of antibacterial drugs," *Advanced Drug Delivery Reviews*, vol. 55, no. 12, pp. 1679–1698, 2003.

[10] J. F. W. Keuren, S. J. H. Wielders, A. Driessen, M. Verhoeven, M. Hendriks, and T. Lindhout, "Covalently-bound heparin makes collagen thromboresistant," *Arteriosclerosis, Thrombosis, and Vascular Biology*, vol. 24, no. 3, pp. 613–617, 2004.

[11] P. A. Patston and A. E. Davis, "C1 Inhibitor: structure, function biologic activity and angioedema," in *Molecular and Cellular Aspects of the Serpinopathies and Disorders in Serpin Activity*, G. A. Silverman and D. A. Lomas, Eds., pp. 555–592, 2007.

[12] P. A. Patston and M. Schapira, "Regulation of C1-inhibitor activity by binding to type IV collagen and heparin," *Biochemical and Biophysical Research Communications*, vol. 230, pp. 597–601, 1997.

[13] E. W. Brown, S. Ravindran, and P. A. Patston, "The reaction between plasmin and C1-inhibitor results in plasmin inhibition by the serpin mechanism," *Blood Coagulation and Fibrinolysis*, vol. 13, no. 8, pp. 711–714, 2002.

[14] P. A. Patston, N. Roodi, J. A. Schifferli, R. Bischoff, M. Courtney, and M. Schapira, "Reactivity of α1-antitrypsin mutants against proteolytic enzymes of the kallikrein-kinin, complement, and fibrinolytic systems," *Journal of Biological Chemistry*, vol. 265, no. 18, pp. 10786–10791, 1990.

[15] S. Niewiarowski, E. Bańkowski, and T. Fiedoruk, "Adsorption of hageman factor (factor XII) on collagen," *Experientia*, vol. 20, no. 7, pp. 367–368, 1964.

[16] P. C. Harpel, "Studies on the interaction between collagen and a plasma kallikrein-like activity. Evidence for a surface-active enzyme system," *Journal of Clinical Investigation*, vol. 51, no. 7, pp. 1813–1822, 1972.

[17] C. F. Scott, E. P. Kirby, P. K. Schick, and R. W. Colman, "Effect of surfaces on fluid-phase prekallikrein activation," *Blood*, vol. 57, no. 3, pp. 553–560, 1981.

[18] S. Ravindran, T. E. Grys, R. A. Welch, M. Schapira, and P. A. Patston, "Inhibition of plasma kallikrein by CI-inhibitor: role of endothelial cells and the amino-terminal domain of CI-inhibitor," *Thrombosis and Haemostasis*, vol. 92, no. 6, pp. 1277–1283, 2004.

[19] B. M. Matata, J. M. Courtney, S. Sundaram et al., "Determination of contact phase activation by the measurement of the activity of supernatant and membrane surface-adsorbed factor XII (FXII): its relevance as a useful parameter for the in vitro assessment of haemodialysis membranes," *Journal of Biomedical Materials Research*, vol. 31, no. 1, pp. 63–70, 1996.

[20] J. Sánchez, P. B. Lundquist, G. Elgue, R. Larsson, and P. Olsson, "Measuring the degree of plasma contact activation induced by artificial materials," *Thrombosis Research*, vol. 105, no. 5, pp. 407–412, 2002.

[21] A. Golas, P. Parhi, Z. O. Dimachkie, C. A. Siedlecki, and E. A. Vogler, "Surface-energy dependent contact activation of blood factor XII," *Biomaterials*, vol. 31, no. 6, pp. 1068–1079, 2010.

Hindawi Publishing Corporation
International Journal of Biomaterials
Volume 2012, Article ID 345029, 10 pages
doi:10.1155/2012/345029

Research Article

Evaluation of Antithrombogenicity and Hydrophilicity on Zein-SWCNT Electrospun Fibrous Nanocomposite Scaffolds

Brahatheeswaran Dhandayuthapani, Saino Hanna Varghese, Ravindran Girija Aswathy, Yasuhiko Yoshida, Toru Maekawa, and D. Sakthikumar

Bio-Nano Electronics Research Center, Graduate School of Interdisciplinary New Science, Toyo University, 2100 Kujirai, Saitama, Kawagoe, 350-8585, Japan

Correspondence should be addressed to D. Sakthikumar, sakthi@toyo.jp

Received 12 May 2011; Accepted 4 November 2011

Academic Editor: Narayana Garimella

Design of blood compatible surfaces is required to minimize platelet surface interactions and increase the thromboresistance of foreign surfaces when they are used as biomaterials especially for artificial blood prostheses. In this study, single wall carbon nanotubes (SWCNTs) and Zein fibrous nanocomposite scaffolds were fabricated by electrospinning and evaluated its antithrombogenicity and hydrophilicity. The uniform and highly smooth nanofibers of Zein composited with different SWCNTs content (ranging from 0.2 wt% to 1 wt%) were successfully prepared by electrospinning method without the occurrence of bead defects. The resulting fiber diameters were in the range of 100–300 nm without any beads. Composite nanofibers with and without SWCNT were characterized through a variety of methods including scanning electron microscopy, transmission electron microscopy, thermogravimetric analysis, and tensile mechanical testing. The water uptake and retention ability of composite scaffolds decreased whereas thermal stability increased with an addition of SWCNTs. Hemolytic property and platelet adhesion ability of the nanocomposite (Zein-SWCNTs) were explored. These observations suggest that the novel Zein-SWCNTs composite scaffolds may possibly hold great promises as useful antithrombotic material and promising biomaterials for tissue engineering application.

1. Introduction

Implantation always involves penetration to the skin and damage of smaller or larger blood vessels through the surgical procedure and the implanted scaffold material will have direct contact with human blood. Scaffolds as medical implants require assessment of hemocompatibility to predict potential procoagulation or immune system activity [1, 2]. Antithrombogenic biomaterial is being extensively studied in order to fabricate artificial organs and biomaterials in contact with blood. A significant goal for the application of antithrombogenic biomaterial is to prevent thrombus formation on the material surface. In general, the factors, which influence the hemocompatibility of a material, include the chemical structure of the surface, the hydrophobicity/hydrophilicity, surface charge, surface roughness and the thrombus formation when the surface is in contact with blood [3]. The design of a suitable biomaterial that offers improved blood biocompatibility is highly desirable for blood-contacting devices.

The fabrication and design of submicron to nanoscale structural architectures, which geometrically or topologically mimic the native state of extra cellular matrix, have received much attention in regenerative medical applications [4]. Electrospinning has recently emerged as a leading technique for the formation of nanofibers because it can produce fibers with diameters ranging from several microns to tens of nanometer depending upon the solution and process parameters [5]. Nanofibrous scaffolds have attracted lot of attention as scaffolds for tissue engineering applications due to their structural similarity to extra cellular matrix, having very large surface area to volume ratio, flexibility in surface functionality, superior mechanical properties, and its high porosity [5, 6].

Zein is a protein present in corn in the seeds of maize in large amounts. Due to its biodegradability and biocompatibility [7], researchers have provided proofs that Zein was also used as a biomaterial in various biomedical applications. The proposed uses of Zein in biomedical applications are as carriers for drug delivery [8–10], food packaging [11], and scaffolding materials for cell/tissue culture [7, 12]. However the mechanical strength of the electrospun Zein scaffold was found to be very low. In an effort to improve the tensile properties of zein nanofiber, we have incorporated zein with the SWCNT.

Due to the unique properties of CNTs such as mechanical, electrical, thermal, optical, and structural properties, currently researchers have been being explored its applications in biomedical engineering and medical chemistry [13, 14]. Researchers have focused on utilizing these remarkable characteristics for engineering applications such as polymeric composites, materials for energy storage [15], electronics [16], catalysis [17], and vaccine delivery [18]. A recent report on safety issues and toxic effects of CNTs argued that exposure to pristine CNTs causes minimal cytotoxicity at higher concentrations, while chemically functionalized CNTs did not show any toxicity for drug delivery applications [19]. Furthermore, the cell growth on CNTs-based materials has been shown to change cell behavior, such as migration and viability due to the influence of electric fields [20]. CNTs have been claimed to suffer the demerit of not being biodegradable [21]. However, it has been shown that CNTs can be discharged from the body without any side effect or mortality [22].

In recent years, considerable attention has been focused on preparing nanocomposites wherein CNTs are dispersed in different polymeric matrices [23–25]. The dispersion of nanometer-sized materials in the polymer medium was suggested as an effective method to increase the mechanical and electrical properties of the system [26–28]. One promising candidate as the nanocomposite component is the SWCNTs. These composites may consist of synthetic polymers [29, 30], naturally derived biopolymers [31] or a combination of both [32]. The reinforcement of naturally derived polymers with CNTs is another promising area that is just beginning to be explored. Up to date, the nanoscale fillers and polymer composite reinforced with electrospun nanofibers have been developed mainly for providing some outstanding physical (e.g., optical and electrical) and chemical properties and provides superior structural properties such as high modulus and strength to weight ratios. The rigidity and cylindrical shape of CNTs make their surfaces good supports for protein crystallization [33] which can improve the mechanical properties of the electrospun nanofibers. Supronowicz and Webster et al., have observed that the potential use of composites of synthetic polymers and CNT in neural and orthopedic tissue engineering applications [34, 35]. The inert nature and biocompatible chemical surfaces to cells and tissues, multiwalled carbon nanotubes—polyurethane composite [36] and poly(carbonate urethane) [37] have been demonstrated to have excellent antiadhesion to platelets.

Inspired by these promising results, we aim to develop a novel nanofibrous blood-compatible scaffold incorporating CNTs for its reduced thrombogenicity effect and with improved mechanical strength. In addition, electrospinning method offers the synthesis polymer/carbon nanotubes (CNTs) nanocomposite fibers without compromising the structural integrity of the individual CNTs [38, 39].

In this study, we have attempted the coelectrospinning method to prepare SWCNTs-Zein nanofiber with different SWCNTs content (ranging from 0.2 wt% to 1 wt%) through a solution-based method, which has the potential of providing much better dispersion of SWCNTs on the polymer matrix yielding a composite with uniform structure. We are reporting here the effect of SWCNTs content on the morphology, mechanical properties thermal stability, and its excellent antiadhesion to platelets of Zein-SWCNT nanocomposite scaffolds. We found that Zein-SWCNT composite containing 22 wt% zein and 0.8 wt% SWCNT is very good candidate for biomaterial applications.

2. Materials and Methods

2.1. Materials. Zein (Wako pure chemicals Industries LTD., Japan), SWCNT was obtained from Sigma-Aldrich. The solvent used Trifluoro ethanol (TFE) was purchased from Kanto Chemical Co. (Tokyo, Japan) used as such without further purification.

2.2. Preparation of Spinning Dope Solutions. The spinning solutions were prepared from single-solvent system. Zein was dissolved in TFE (100%) to form a homogeneous solution and maintained under constant stirring for 24 hrs. The spinning dope was prepared by sonicating 0.2–1 wt% SWCNTs in TFE for 2 hrs. Zein (22 wt%) was added to the SWCNT-TFE mixture and further sonicated for an hour and then stirred for another hour.

2.3. Electrospinning Process. To fabricate the ultrafine composite nanofibrous scaffold we have used NANON electrospinning setup (NANON-01A, MECC Co., Ltd., Fukuoka, Japan). For electrospinning, 10 mL of each kind of Zein-SWCNTs solution was loaded into a 10 mL glass syringe and injected through an 18 G stainless-steel blunt-ended needle. The syringe was then placed in a syringe pump at a flow rate of 0.5 mLh^{-1}. The electric field 2.0 $kVcm^{-1}$ (expressed in terms of voltage/distance) between the collection plate (cathode) and the needle tip (anode) was applied. The collector covered with aluminum foil placed at 10 cm on which fibers were collected. All electrospinning processes were performed at ambient temperature.

2.4. Characterization of Nanocomposite Scaffold. The morphology and diameters of electrospun fibers were determined using scanning electron microscope (JSM-7400F, JEOL, Japan). The sample was sputter coated with a thin platinum layer using an autosputter fine coater (E-1030 Ion sputter, Hitachi, Japan) before imaging. According to the SEM images, the diameter and distributions of ultrafine fibers were measured. Additionally, Zein-SWCNT composite fibers were examined in a TEM (JEM 2100, JEOL, Japan). The samples were prepared by drawing out small fibrils with the aid of

tweezers and placed on carbon-coated copper grids. Samples were stained by exposure to osmium tetroxide vapour for one hour. The accelerating voltage used was 120 kV.

2.5. Thermal Properties of Electrospun Zein-SWCNTs Nanocomposite. To measure the thermal properties of the electrospun nanocomposite fibers, the thermal stability was analyzed in a thermogravimetric analyzer (TGA) (DTG-60H, Shimadzu, Japan). The runs were performed in the temperature range of 30°C to 1000°C and consisted of a ramp at a steady rate of 10°C min^{-1} with continuous nitrogen flow.

2.6. Mechanical Properties of Electrospun Zein-SWCNTs Nanocomposite. The tensile properties of electrospun nanocomposite fibrous scaffolds, approximately $8 \times 0.03 \times 25\ \text{mm}^3$ ($L \times W \times H$), were characterized using a Universal Testing Machine (Instron 3345, UK) equipped with a 500 N load cell. The ends of the rectangular specimens were mounted vertically on two mechanical gripping units of the tensile tester, leaving a 40 mm gauge length for mechanical loading at an extension rate of 1 mm min^{-1}. The reported tensile moduli and maximum tensile strengths represented average results of five tests.

2.7. Evaluation of Hydrophilicity. The water uptake was determined gravimetrically. The weights of the completely dried films were determined directly with an analytical balance (W_{dry}). Strips of Zein-SWCNT-based scaffold (1 cm × 2 cm) were immersed into deionized water at 37°C in an incubator for 24 h. The resultant swollen scaffold was gently blotted with filter paper to remove excess surface water and weighed again (W_{wet}). The water uptake (WT) of the scaffold is expressed as the percentage of weight obtained using (1):

$$\text{WT\%} = \frac{W_{\text{wet}} - W_{\text{dry}}}{W_{\text{dry}}} \times 100. \tag{1}$$

To measure the water retention ability, the wet scaffolds were transferred to centrifuge tubes with filter paper at the bottom, centrifuged at 500 rpm for 3 m and weighed immediately (W_{wet}). The percentage of water retention (WR) of the scaffolds at equilibrium was calculated using following (2):

$$\text{WR\%} = \frac{W_{\text{wet}(R)} - W_{\text{dry}}}{W_{\text{dry}}} \times 100, \tag{2}$$

where $W_{\text{wet}(R)}$ is the wet weight after a predetermined time, W_{dry} is the original weight of the sample.

2.8. Hemolysis Analysis. The nanocomposite scaffolds (Zein nanofiber; Zein-0.2 wt% SWCNT; Zein-0.5 wt% SWCNT; Zein-0.8 wt% SWCNT; Zein-1 wt% SWCNT) were cut into small pieces and the samples were equilibrated in normal saline water for 30 min at room temperature. Rabbit blood obtained from Nihon Seibutsu Zairyo Centre, Japan. 200 μL was added to each scaffold after taking dry weight of each scaffold. After a predetermined time period, 4 mL of saline water added to each sample to stop hemolysis and the samples were kept at constant temperature (35°C) for 1 h. Positive and negative controls were produced by adding 200 μL of rabbit's blood to 4 mL of distilled water and saline water respectively. All the test samples were centrifuged. Optical density (OD) of the supernatant was measured at 545 nm using spectrophotometer (V-650 spectrophotometer, Jasco, Japan). The experiments were run in triplicate and were repeated twice. The percent of hemolysis was calculated using (3):

$$\%\ \text{Hemolysis (HP)} = \frac{\text{OD of test sample} - \text{OD of –ve control}}{\text{OD of +ve control} - \text{OD of –ve control}} \times 100. \tag{3}$$

2.9. Platelet Adhesion Examination. The platelet adhesion study was performed according to International standard 10993-4 [40]. For platelet adhesion studies, nanocomposite scaffolds of 1.5 × 1.5 cm size were used. Experiments were carried out with anticoagulated rabbit blood bought from the Nihon Seibutsu Zairyo Centre, Japan. An anticoagulated blood was centrifuged at 2500 rpm for 5 min to obtain platelet-rich plasma (PRP). To perform the platelet adhesion examination, the Zein-SWCNT fibrous scaffold was placed onto a piece of flat glass. Then, a sample of 20 μL of PRP was carefully dropped on the scaffold center. After incubation for 30 min at room temperature (about 37°C), the scaffold was carefully rinsed several times in phosphate buffer solution (pH-7.4) to remove non-adhering platelets. Adherent platelets on the scaffolds were preserved with 2.5% glutaraldehyde/PBS solution for 30 min, followed by dehydration procedure using a series of ethanol-water mixtures (0, 30, 50, 70, 90, 100 vol % of ethanol) for 30 min, respectively. For electron microscopy, samples were then air dried and coated with platinum and examined in a scanning electron microscope (JSM-7400F, JEOL, Japan).

3. Results and Discussion

3.1. Structural Characterization of Electrospun Zein-SWCNTs Nanofiber Membranes. SWCNT-Zein solutions with varying SWCNT concentrations were prepared under sonication without phase separation and maintained homogenous solution. Due to the methods of dispersion of the SWCNTs by sonication and mechanical stirring, the SWCNT clusters break down. The addition of Zein forms a coating around each individual CNT and keeps them from aggregating or binding together. Solutions with 0 wt%, 0.2 wt%, 0.5 wt%, 0.8 wt%, and 1 wt% SWCNT content are spun according to the spinning conditions. Continuous fibers were obtained using a Zein concentration of 24 wt% and electrospinning at a distance of 10 cm under electric field strength of 2 kVcm^{-1}. As can be seen from Figure 1(a), the absence of beads and the uniform fibers with smooth surface morphology was obtained for all experimental materials (Figures 1(b)–1(e)). Among them, the electrospun pure zein nanofibers Figure 1(a) had an average fiber diameter of 230 nm and diameter distribution for all loadings of SWCNT in the zein fibers (Figures 1(b)–1(e)) are all below the 300 nm range. However, at low concentration of nanotubes, relatively

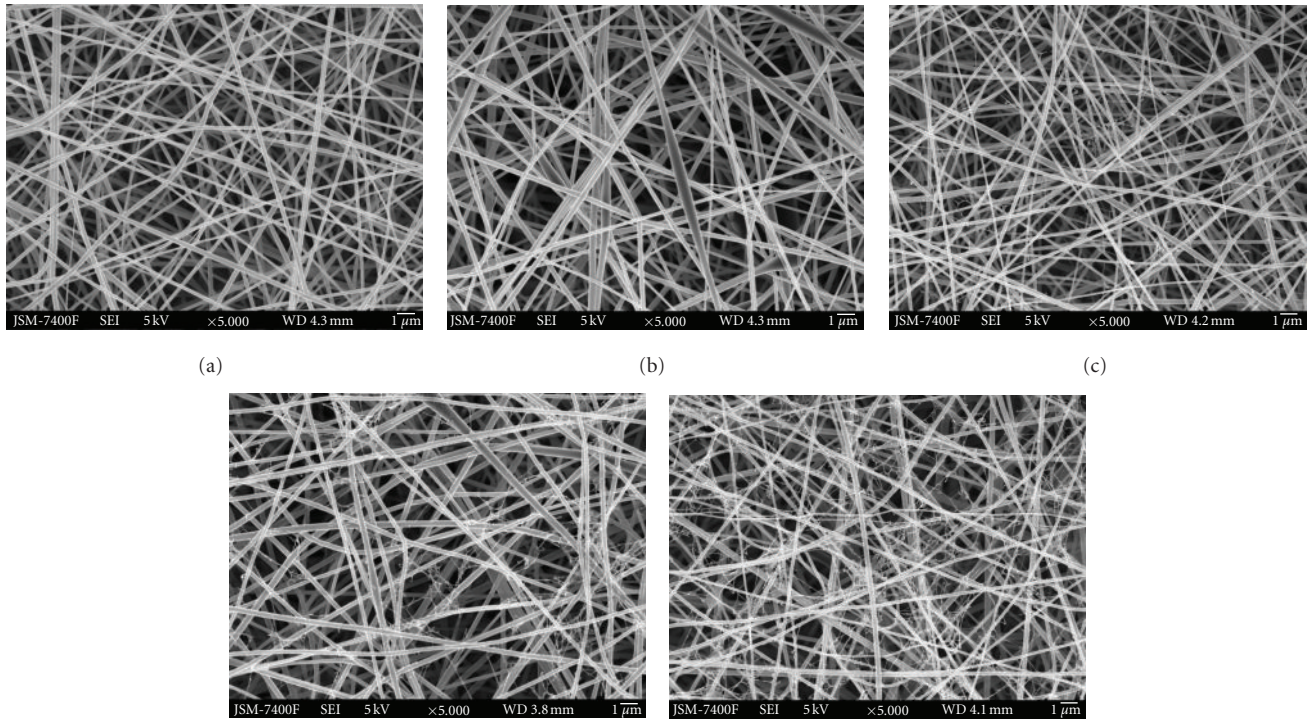

Figure 1: SEM image of electrospun (a) Zein nanofiber, (b) Zein-0.2 wt% SWCNTs, (c) Zein-0.5 wt% SWCNTs, (d) Zein-0.8 wt% SWCNTs, and (e) Zein-1 wt% SWCNTs nanocomposite scaffolds (scale Bar: 1 μ).

good dispersion was achieved, but as the concentration of nanotubes increased from 0.5 wt% to 0.8 wt% and 1 wt% SWCNTs promoted the creation of web-like structures in comparison with the zein nanofibers without SWCNTs. Random nanofiber structures and web-like structures can be obtained (Figures 1(d) and 1(e)), whereas the web-like structures consisted of regularly distributed very fine nanofibers with diameters of just about 20–40 nm, which were strongly embedded in the zein nanofibers. The web formation could be a result of the inclusion of carbon nanotubes into the fibers [41]. During electrospinning the SWCNTs are expelled from the polymer jet under extremely high force and velocity, which causes opening of the cluster to form the web-like structure. The Zein-SWCNT electrospun web like structure is very similar to the structure previously reported with using Bombyx mori silk nanofibers containing SWCNTs [42]. We do believe that these nanowebs were created because of strong secondary electric fields occurring between individual SWCNTs or their agglomerated form during the electrospinning process.

TEM analysis of the Zein-SWCNT nanofibers prepared by the electrospinning process is provided in Figure 2 with the aim of analyzing the creation of the nanoweb fiber. The high resolution TEM micrograph shows the close inspection on electrospun composite fibers which indicates that the SWCNTs are embedded in the nanofibers without any sign of agglomerates. In many regions of the electrospun nanofibers; the embedded nanotubes appeared to be well oriented along the fiber axis. Such alignment is obviously associated with the extreme high longitudinal strain rate of jet during electrospinning process, which may cause disentanglement or pulling out of curved nanotubes under high shear force. SWCNTs were present inside the Zein nanofibers as individual tubes well aligned with nanofibers axes. Similar orientation of CNTs in the electrospun nanofibers has also been observed on other composite systems and it confirms that the original dispersion contains individual CNTs rather than aggregates or bulk [43–45].

3.2. Thermal Analysis for Nanocomposite Scaffold. Thermogravimetric curves of electrospun Zein nanofiber and nanocomposite (Zein-SWCNT; 0.2–1 wt%) are shown in Figure 3. Thermal analysis shows that the improvement in thermal stability in case of Zein-SWCNTs nanocomposite than that of pure Zein nanofiber. The initial weight loss observed for all samples at 80°C is due to loss of moisture. The second weight loss occurs in the range of 230 to 380°C. This can be attributed to the breakdown of the amino acid residues, as well as cleavage of the peptide bonds. The initial degradation temperature is at 230°C and full degradation occurs at 455°C. From their degradation curves, it seems like the degradation of the SWCNT composite fibers occurs in two distinct phases. The electrospun Zein fibers on the other hand, have an initial degradation temperature of 280°C and final degradation temperature of 370°C at which the rate of mass loss is greatest. The 1 wt% SWCNT-Zein composite

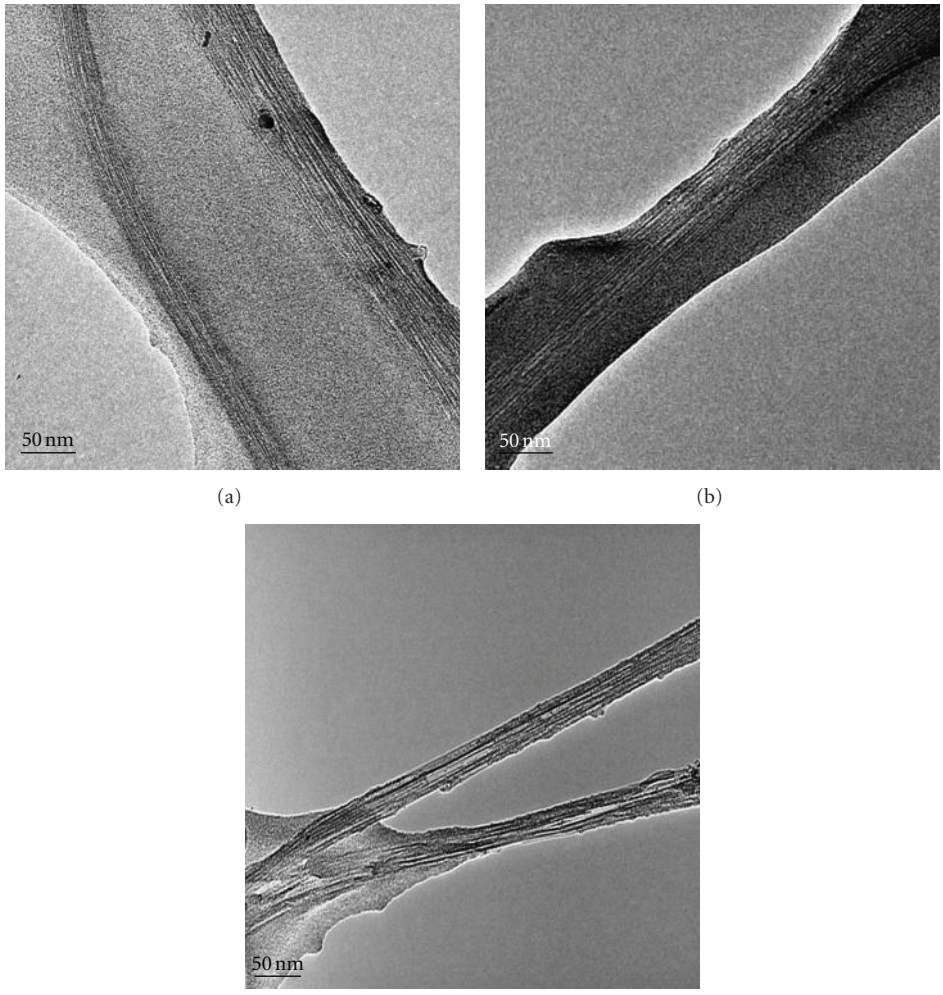

(a) (b)

(c)

Figure 2: TEM micrographs of selected zein-SWNT composite nanofibers (Scale Bar: 50 nm).

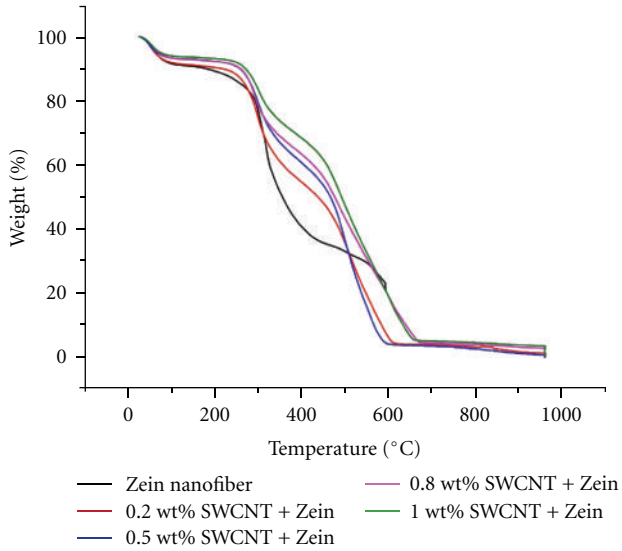

Figure 3: TGA thermograms of the zein nanofiber, zein-SWCNT nanocomposite scaffolds.

fiber has the highest thermal stability, with onset degradation at 250°C and full degradation occurring at 470°C.

3.3. Evaluation of Mechanical Properties of Nanocomposite Scaffold. Studying their mechanical properties can generate an idea about the structure of the nanocomposites. Du et al. [46] reported that the tensile strength, fracture toughness, and hardness tests showed improved properties up to 7 wt% of CNTs. When the CNT content exceeds 7 wt% the mechanical properties of the composites decreases. The composites become very brittle when CNTs get to 10 wt%. The tensile strength of PMMA by the addition of 3 wt% functionalized CNTs increased by 21%, which was low compared to a 90% increase in the modulus of PMMA by the addition of 2 wt% nonfunctionalized SWCNTs.

Figure 4 illustrates the typical stress strain curves of Zein and Zein-SWCNTs composite nanofibrous scaffold. Pure Zein nanofiber shows a tensile strength of 1.4 MPa, while the tensile strength of Zein-SWCNTs nanofiber increased with increasing SWCNTs content (0.2; 0.5 and 0.8 wt%)

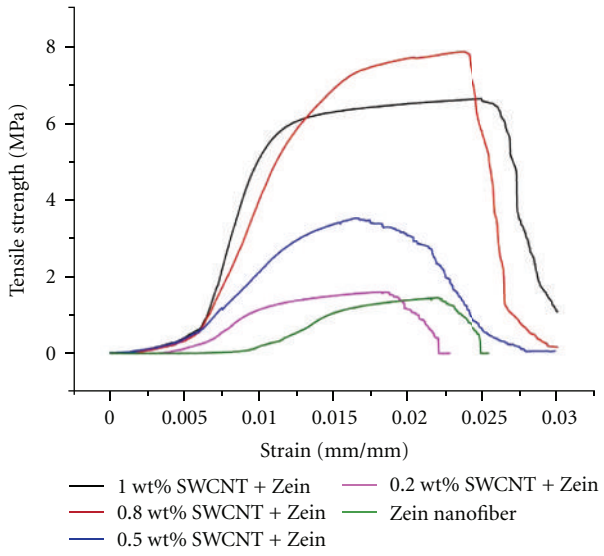

Figure 4: Typical tensile stress-strain curves of Zein nanofiber and Zein-SWCNTs nanocomposite Scaffolds.

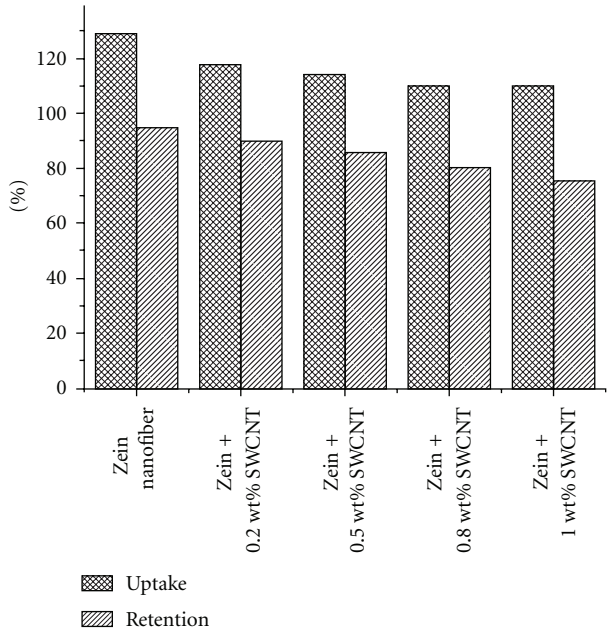

Figure 5: Water uptakes and water retention ability of zein scaffold, and Zein-SWCNT scaffolds after 24 hr. ($n = 5$).

to 3.2 MPa. Moreover, the Zein-0.8 wt% SWCNTs sample exhibited the maximum strength (about 7.7 MPa). Subsequently, further increasing the SWCNTs content (1 wt%) lead to the decrease of tensile strength (6.8 MPa) of Zein-SWCNTs nanofiber scaffold. It was observed that Zein nanofibrous scaffold with SWCNTs content higher than 1 wt% gives poor mechanical properties, which could be explained due to poor dispersions of the CNT within the fiber, result in forming defects of the scaffold. The above results indicate that the mechanical properties of Zein nanofiber can be improved by the addition of SWCNTs. The tensile tests have revealed that the scaffolds containing SWCNTs were able to withstand a higher stress than the corresponding unreinforced scaffolds. This can be explained taking into account the TEM images, which have clearly shown that the SWCNTs are aligned within and along the fiber orientation, thereby improving the mechanical properties. Nanomaterials have high surface energy and are easy to aggregate, which lead to the poor dispersion of nanomaterials in polymer matrix results in poor mechanical properties. Thus, good dispersion of SWCNTs in a polymer matrix the composite exhibited significant mechanical properties increased by incorporating the CNTs [47].

3.4. Water Uptake and Retention Abilities. The composite materials were expected to be used as the scaffolds; hence their water retention ability of the materials to keep water inside the matrix has an important role for the absorption of body fluid and for a transfer of cell nutrients and metabolites through the materials. Scaffolds showing higher degree of water uptake will have a larger surface area/volume ratio thus allowing the scaffold to have the maximum probability of cell growth in 3D scaffold [48]. The increase in water uptake also allows the scaffolds to avail nutrients from culture media more effectively [49]. Hence, controlled water uptake will be ideal for tissue engineering applications [50]. The results in Figure 5 give the water uptake ratios of five groups of scaffolds. The prepared 3D nanocomposite scaffolds based on Zein showed significant water uptake ability; the values were over 100%, and the highest value reached 128 ± 1.09% for Zein nanofiber. The composite nanofiber and native Zein nanofibers show the same general swelling trend. After 24 h of water absorption we have observed only 12% difference in the equilibrium water uptake capacity between native (128 ± 1.09%) and composite nanofiber (109 ± 0.45%) with 1 wt% of SWCNTs. These results demonstrate that the presence of SWCNTs has led to decrease on the water uptake capacity of the scaffold.

The percent water retention values of the nanocomposite scaffolds were measured and showed in Figure 5. It was found that the use of SWCNT resulted in decrease of water retention. Water retention ability of Zein scaffold was higher compared to SWCNT-Zein scaffolds. We found that the values of water retention were still higher than 75% even if SWCNT was used, implying that the scaffolds could retain water whose weight was more than their own. Water retention meant that the scaffolds could absorb water to some extent and the tight aggregation of nanofibers might make the scaffold stable in sizes and shapes.

3.5. Hemolysis Analysis. In this research work, the hemocompatibility of Zein-SWCNTs nanofiber membranes were evaluated by hemolysis. The hemolysis percentage (HP) represents the extent of red blood cells hemolysis when they come in contact with sample. When the polymeric scaffold in contact with blood it must not induce thrombosis, thromboembolisms, antigenic responses, destruction of blood constituents, plasma proteins, and so forth [51]. Thus, biocompatibility, especially blood compatibility, is the most

Table 1: Hemolysis percentage of electrospun zein-SWCNTs electrospun nanocomposite scaffolds.

Sample	Optical density at 545 nm	Hemolysis (%)
Water (positive control)	0.912	—
Saline (Negative control)	0.002	—
Zein	0.025	2.5 ± 0.30
Zein + 0.2 wt% SWCNT	0.028	2.8 ± 0.30
Zein + 0.5 wt% SWCNT	0.030	3.0 ± 0.29
Zein + 0.8 wt% SWCNT	0.033	3.40 ± 0.25
Zein + 1.0 wt% SWCNT	0.039	4.0 ± 0.29

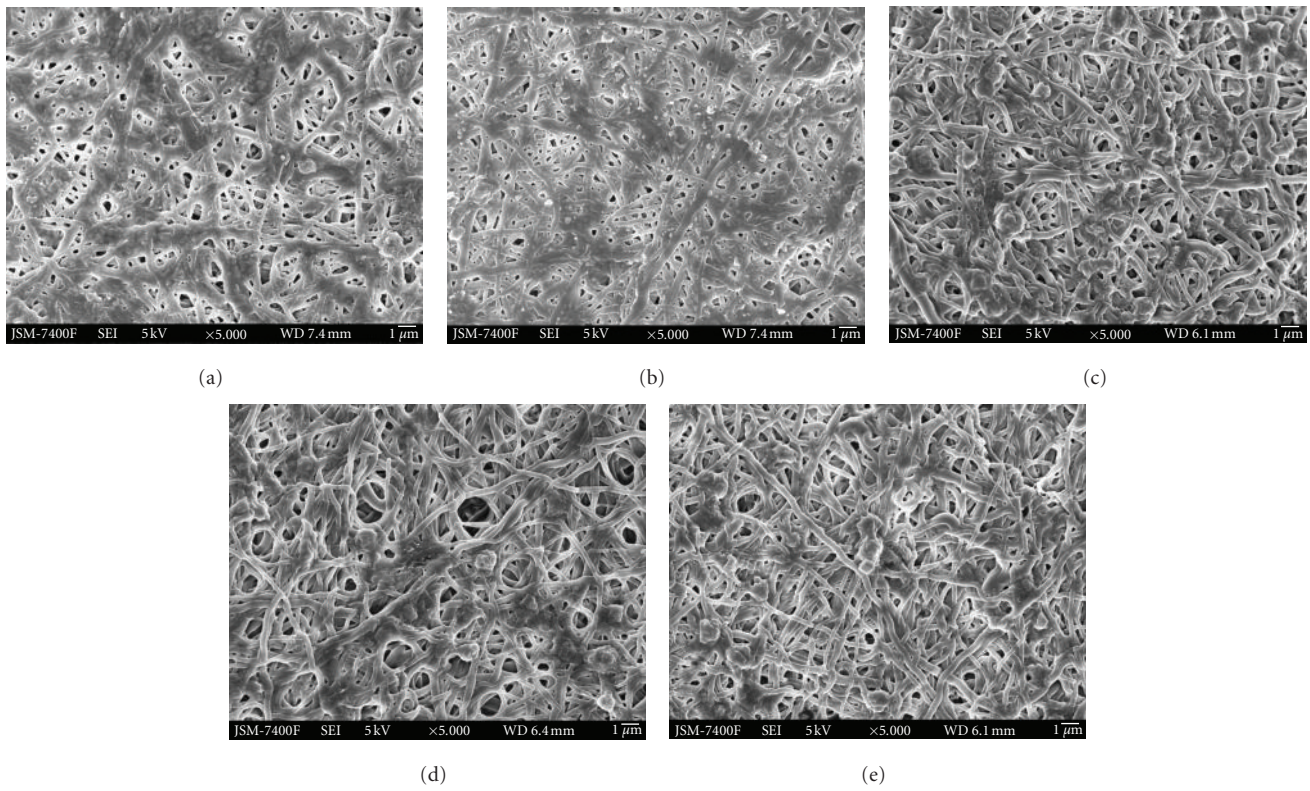

Figure 6: Effects of the composite nanofibers on the adhesion of blood platelets. (a) Zein nanofiber, (b) Zein-0.2 wt% SWCNTs, (c) Zein-0.5 wt% SWCNTs, (d) Zein-0.8 wt% SWCNTs, and (e) Zein-1 wt% SWCNTs nanocomposite Scaffolds (scale Bar: 1 μ).

important property with regard to biomedical materials. Hence we had conducted the blood compatibility test for our nanocomposite scaffolds too. Results obtained for hemolysis of rabbit blood with nanocomposite scaffolds were shown in Table 1. Hemolysis occurs when red blood cells come into contact with water. The positive reference (100% lysis) was blood/water mixture and the negative reference (0% lysis) was a blood/saline mixture. The OD values of positive and negative were 0.9 and 0.02, respectively. Each absorbance data point was obtained by measuring three samples and also the deviations of the three tests were determined. However, Hemolysis was less than 4% for all tested Zein-SWCNTs scaffolds. This results well within the permissible limit set by Autian [52], who reported that a value of up to 5% hemolysis is permissible for biomaterials. The maximum HP value (4.0 ± 0.29%) was obtained for 1 wt% Zein-SWCNTs. When the SWCNTs content of the Zein was altered, no significant difference was observed in the hemolysis assay, indicating good character of antihemolysis among all the Zein-SWCNTs nanofiber Scaffolds (Table 1). It may be conclude from the hemolysis percentage that the Zein-SWCNT composite scaffold may be suitable as biomaterials for specific implant clinical application purpose.

3.6. Platelet Adhesion Examination. To determine the hemocompatibility of the Zein-SWCNT composite nanofiber scaffolds, as is well known, platelet adhesion has generally been applied to evaluate the hemocompatibility of materials. When a foreign material comes into contact with blood, the initial blood response is the adsorption of blood proteins, followed by platelet adhesion and the activation of coagulation pathways, leading to thrombus formation [53].

The morphologies of activated platelets can be divided into 5 categories including dendritic, dendritic spread, spread, fully spread, and nonviable [54]. These criteria were used to assess the activation state of the platelets that adhered to the surface of Zein-SWCNT in the current study. Figure 6 shows the electron micrographs of platelet adhesion on Zein and Zein-SWCNT composite nanofiber scaffolds. As can be seen from the photomicrographs, the both platelet adhesion and activation are observed on the Zein nanofiber (Figure 6(a)). The promotion of activation and adhesion of platelets was obviously due to the presence of nanofibers.

We have observed a trend in the direction of decrease in platelet adhesion and absence of activation while increasing the SWCNTs and found very low in 1 wt% SWCNT-Zein composite (Figure 6(e)), which might be due to a lower water adsorption. However, on Zein nanofiber scaffold with a higher SWCNT content, some of the platelets have extended, but many retain a discoid shape which is similar to the original shape of the platelet and indicates an unactivated state. Changes in surface chemistry or roughness of sample surface will have an effect on the adsorption characteristic. Surfaces with negatively charged groups were reported to be antithrombogenic, whereas positively charged surfaces are thrombogenic [55]. We hypothesize that the decrease in the platelet adhesion on the Zein-SWCNT composite is influenced by the surface chemistry as well the surface morphology, where hydrophilic repulsion occurs and prevented the direct contact between the platelets with the Zein-SWCNT composite surface. These results may suggest that Zein-SWCNT nanofibrous composite containing 22 wt% zein and 0.8 wt% SWCNT could be a potential candidate for anti-thrombogenicity, which would be particularly useful for artificial blood prostheses.

4. Conclusion

We have developed nanofibrous nanocomposite scaffolds which were prepared by electrospinning of Zein and Zein-SWCNTs solutions. This method under sonication effectively dispersed SWCNTs in a continuous polymer scaffold. Microscopy images show good dispersion of SWCNTs and the composite exhibited significant mechanical properties as well as thermal stability of electrospun Zein-SWCNT nanocomposites. We have demonstrated that when the SWCNTs content of the Zein was altered, no significant difference was observed in the hemolysis assay, while it did alter the response in platelet adhesion with the absence of platelet activation on Zein-SWCNT composite. This suggested that platelet activation could be efficiently suppressed on this nanostructured composite with its excellent antiadhesion and subsequently low platelet activation. The developed Zein-SWCNT composite with homogeneous microstructure and improved mechanical properties can be used as a potential biomaterial for implant applications.

Acknowledgments

B. Dhandayuthapani, S. Varghese, and R. G. Aswathy would like to acknowledge the Japanese Government, Ministry of Education, Culture, Sports, Science and Technology (MEXT) for the scholarships provided for the doctoral studies.

References

[1] M. B. Gorbet and M. V. Sefton, "Biomaterial-associated thrombosis: roles of coagulation factors, complement, platelets and leukocytes," *Biomaterials*, vol. 25, no. 26, pp. 5681–5703, 2004.

[2] A. P. McGuigan and M. V. Sefton, "The influence of biomaterials on endothelial cell thrombogenicity," *Biomaterials*, vol. 28, no. 16, pp. 2547–2571, 2007.

[3] J. H. Lee, H. B. Lee, and J. D. Andrade, "Blood compatibility of polyethylene oxide surfaces," *Progress in Polymer Science*, vol. 20, no. 6, pp. 1043–1079, 1995.

[4] R. P. Lanza, R. Langer, and W. L. Chick, *Principles of Tissue Engineering*, Academic Press, New York, NY, USA, 1996.

[5] W. H. Park, L. Jeong, D. I. Yoo, and S. Hudson, "Effect of chitosan on morphology and conformation of electrospun silk fibroin nanofibers," *Polymer*, vol. 45, no. 21, pp. 7151–7157, 2004.

[6] Z. M. Huang, Y. Z. Zhang, M. Kotaki, and S. Ramakrishna, "A review on polymer nanofibers by electrospinning and their applications in nanocomposites," *Composites Science and Technology*, vol. 63, no. 15, pp. 2223–2253, 2003.

[7] J. Dong, Q. Sun, and J. Y. Wang, "Basic study of corn protein, zein, as a biomaterial in tissue engineering, surface morphology and biocompatibility," *Biomaterials*, vol. 25, no. 19, pp. 4691–4697, 2004.

[8] Z. Gao, P. Ding, L. Zhang et al., "Study of a Pingyangmycin delivery system: Zein/Zein-SAIB in situ gels," *International Journal of Pharmaceutics*, vol. 328, no. 1, pp. 57–64, 2007.

[9] H. J. Wang, Z. X. Lin, X. M. Liu, S. Y. Sheng, and J. Y. Wang, "Heparin-loaded zein microsphere film and hemocompatibility," *Journal of Controlled Release*, vol. 105, no. 1-2, pp. 120–131, 2005.

[10] X. Liu, Q. Sun, H. Wang, L. Zhang, and J. Y. Wang, "Microspheres of corn protein, zein, for an ivermectin drug delivery system," *Biomaterials*, vol. 26, no. 1, pp. 109–115, 2005.

[11] C. Mecitoğlu, A. Yemenicioğlu, A. Arslanoğlu, Z. S. Elmaci, F. Korel, and A. E. Çetin, "Incorporation of partially purified hen egg white lysozyme into zein films for antimicrobial food packaging," *Food Research International*, vol. 39, no. 1, pp. 12–21, 2006.

[12] S. Gong, H. Wang, Q. Sun, S. T. Xue, and J. Y. Wang, "Mechanical properties and *in vitro* biocompatibility of porous zein scaffolds," *Biomaterials*, vol. 27, no. 20, pp. 3793–3799, 2006.

[13] E. W. Wong, P. E. Sheehan, and C. M. Lieber, "Nanobeam mechanics: elasticity, strength, and toughness of nanorods and nanotubes," *Science*, vol. 277, no. 5334, pp. 1971–1975, 1997.

[14] A. Bianco and M. Prato, "Can carbon nanotubes be considered useful tools for biological applications?" *Advanced Materials*, vol. 15, no. 20, pp. 1765–1768, 2003.

[15] G. Che, B. B. Lakshmi, E. R. Fisher, and C. R. Martin, "Carbon nanotubule membranes for electrochemical energy storage and production," *Nature*, vol. 393, no. 6683, pp. 346–349, 1998.

[16] S. Frank, P. Poncharal, Z. L. Wang, and W. A. De Heer, "Carbon nanotube quantum resistors," *Science*, vol. 280, no. 5370, pp. 1744–1746, 1998.

[17] J. M. Planeix, N. Coustel, B. Coq et al., "Application of carbon nanotubes as supports in heterogeneous catalysis," *Journal of the American Chemical Society*, vol. 116, pp. 7935–7936, 1994.

[18] M. Panhuis, "Vaccine delivery by carbon nanotubes," *Chemistry and Biology*, vol. 10, no. 10, pp. 897–898, 2003.

[19] S. K. Smart, A. I. Cassady, G. Q. Lu, and D. J. Martin, "The biocompatibility of carbon nanotubes," *Carbon*, vol. 44, no. 6, pp. 1034–1047, 2006.

[20] K. J. Gilmore, S. E. Moulton, and G. G. Wallace, "Incorporation of carbon nanotubes into the biomedical polymer poly(styrene-β-isobutylene-β-styrene)," *Carbon*, vol. 45, no. 2, pp. 402–410, 2007.

[21] B. S. Harrison and A. Atala, "Carbon nanotube applications for tissue engineering," *Biomaterials*, vol. 28, no. 2, pp. 344–353, 2007.

[22] R. Singh, D. Pantarotto, L. Lacerda et al., "Tissue biodistribution and blood clearance rates of intravenously administered carbon nanotube radiotracers," *Proceedings of the National Academy of Sciences of the United States of America*, vol. 103, no. 9, pp. 3357–3362, 2006.

[23] X. L. Xie, Y. W. Mai, and X. P. Zhou, "Dispersion and alignment of carbon nanotubes in polymer matrix: a review," *Materials Science and Engineering R*, vol. 49, no. 4, pp. 89–112, 2005.

[24] S. Mazinani, A. Ajji, and C. Dubois, "Morphology, structure and properties of conductive PS/CNT nanocomposite electrospun mat," *Polymer*, vol. 50, no. 14, pp. 3329–3342, 2009.

[25] K. K. H. Wong, M. Zinke-Allmang, J. L. Hutter, S. Hrapovic, J. H. T. Luong, and W. Wan, "The effect of carbon nanotube aspect ratio and loading on the elastic modulus of electrospun poly(vinyl alcohol)-carbon nanotube hybrid fibers," *Carbon*, vol. 47, no. 11, pp. 2571–2578, 2009.

[26] J. M. Thomassin, X. Lou, C. Pagnoulle et al., "Multiwalled carbon nanotube/poly(ε-caprolactone) nanocomposites with exceptional electromagnetic interference shielding properties," *Journal of Physical Chemistry C*, vol. 111, no. 30, pp. 11186–11192, 2007.

[27] D. Zhang, M. A. Kandadai, J. Cech, S. Roth, and S. A. Curran, "Poly(L-lactide) (PLLA)/multiwalled carbon nanotube (MWCNT) composite: characterization and biocompatibility evaluation," *Journal of Physical Chemistry B*, vol. 110, no. 26, pp. 12910–12915, 2006.

[28] X. Zhang, J. Zhang, and Z. Liu, "Conducting polymer/carbon nanotube composite films made by in situ electropolymerization using an ionic surfactant as the supporting electrolyte," *Carbon*, vol. 43, no. 10, pp. 2186–2191, 2005.

[29] L. J. Suggs, R. S. Krishnan, C. A. Garcia, S. J. Peter, J. M. Anderson, and A. G. Mikos, "*In vitro* and *in vivo* degradation of poly(propylene fumarate-co-ethylene glycol) hydrogels," *Journal of Biomedical Materials Research*, vol. 42, no. 2, pp. 312–320, 1998.

[30] A. P. Pêgo, B. Siebum, M. J. A. Van Luyn et al., "Preparation of degradable porous structures based on 1,3-trimethylene carbonate and D,L-lactide (Co)polymers for heart tissue engineering," *Tissue Engineering*, vol. 9, no. 5, pp. 981–994, 2003.

[31] C. L. Cummings, D. Gawlitta, R. M. Nerem, and J. P. Stegemann, "Properties of engineered vascular constructs made from collagen, fibrin, and collagen-fibrin mixtures," *Biomaterials*, vol. 25, no. 17, pp. 3699–3706, 2004.

[32] G. Chen, T. Sato, T. Ushida et al., "The use of a novel PLGA fiber/collagen composite web as a scaffold for engineering of articular cartilage tissue with adjustable thickness," *Journal of Biomedical Materials Research*, vol. 67, no. 4, pp. 1170–1180, 2003.

[33] F. Balavoine, P. Schultz, C. Richard, V. Mallouh, T. W. Ebbesen, and C. Mioskowski, "Helical crystallization of proteins on carbon nanotubes: a first step towards the development of new biosensors," *Angewandte Chemie*, vol. 38, no. 13-14, pp. 1912–1915, 1999.

[34] P. R. Supronowicz, P. M. Ajayan, K. R. Ullmann, B. P. Arulanandam, D. W. Metzger, and R. Bizios, "Novel current-conducting composite substrates for exposing osteoblasts to alternating current stimulation," *Journal of Biomedical Materials Research*, vol. 59, no. 3, pp. 499–506, 2002.

[35] T. J. Webster, M. C. Waid, J. L. McKenzie, R. L. Price, and J. U. Ejiofor, "Nano-biotechnology: carbon nanofibres as improved neural and orthopaedic implants," *Nanotechnology*, vol. 15, no. 1, pp. 48–54, 2004.

[36] J. Meng, H. Kong, H. Y. Xu, L. Song, C. Y. Wang, and S. S. Xie, "Improving the blood compatibility of polyurethane using carbon nanotubes as fillers and its implications to cardiovascular surgery," *Journal of Biomedical Materials Research*, vol. 74, no. 2, pp. 208–214, 2005.

[37] T. Sun, H. Tan, D. Han, Q. Fu, and L. Jiang, "No platelet can adhere-largely improved blood compatibility on nanostructured superhydrophobic surfaces," *Small*, vol. 1, no. 10, pp. 959–963, 2005.

[38] G. Wang, Z. Tan, X. Liu et al., "Conducting MWNT/poly(vinyl acetate) composite nanofibres by electrospinning," *Nanotechnology*, vol. 17, no. 23, article 019, pp. 5829–5835, 2006.

[39] K. Saeed, S. Y. Park, H. J. Lee, J. B. Baek, and W. S. Huh, "Preparation of electrospun nanofibers of carbon nanotube/polycaprolactone nanocomposite," *Polymer*, vol. 47, no. 23, pp. 8019–8025, 2006.

[40] *Biological Evaluation of Medical Devices—Part 4: Selection of Tests for Interactions with Blood*, ISO 10993-4, 2nd edition, 2002.

[41] H. Lam, *Electrospinning of single wall carbon nanotube reinforced aligned fibrils and yarns*, Ph.D. thesis, Drexel University, 2004.

[42] J. Ayutsede, M. Gandhi, S. Sukiraga et al., "Carbon nanotube reinforced *Bombyx mori* silk nanofibers by the electrospinning process," *Biomacromolecules*, vol. 7, no. 1, pp. 208–214, 2006.

[43] Y. Dror, W. Salalha, R. L. Khalfin, Y. Cohen, A. L. Yarin, and E. Zussman, "Carbon nanotubes embedded in oriented polymer nanofibers by electrospinning," *Langmuir*, vol. 19, no. 17, pp. 7012–7020, 2003.

[44] M. B. Bazbouz and G. K. Stylios, "Novel mechanism for spinning continuous twisted composite nanofiber yarns," *European Polymer Journal*, vol. 44, no. 1, pp. 1–12, 2008.

[45] M. T. Hunley, P. Pötschke, and T. E. Long, "Melt dispersion and electrospinning of non-functionalized multiwalled carbon nanotubes in thermoplastic polyurethane," *Macromolecular Rapid Communications*, vol. 30, no. 24, pp. 2102–2106, 2009.

[46] F. Du, J. E. Fischer, and K. I. Winey, "Coagulation method for preparing single-walled carbon nanotube/poly(methyl methacrylate) composites and their modulus, electrical conductivity, and thermal stability," *Journal of Polymer Science, Part B*, vol. 41, no. 24, pp. 3333–3338, 2003.

[47] M. Moniruzzaman, J. Chattopadhyay, W. E. Billups, and K. I. Winey, "Tuning the mechanical properties of SWNT/nylon 6,10 composites with flexible spacers at the interface," *Nano Letters*, vol. 7, no. 5, pp. 1178–1185, 2007.

[48] J. P. Vacanti and R. Langer, "Tissue engineering: the design and fabrication of living replacement devices for surgical reconstruction and transplantation," *The Lancet*, vol. 354, no. 1, pp. 32–34, 1999.

[49] M. Peter, P. T. Sudheesh Kumar, N. S. Binulal, S. V. Nair, H. Tamura, and R. Jayakumar, "Development of novel

α-chitin/nanobioactive glass ceramic composite scaffolds for tissue engineering applications," *Carbohydrate Polymers*, vol. 78, no. 4, pp. 926–931, 2009.

[50] A. G. Mikos, G. Sarakinos, M. D. Lyman, D. E. Ingber, J. P. Vacanti, and R. Langer, "Prevascularization of porous biodegradable polymers," *Biotechnology and Bioengineering*, vol. 42, no. 6, pp. 716–723, 1993.

[51] V. I. Sevastianov, "Interrelation of protein adsorption and blood compatibility of biomaterials," in *High Performance Biomaterials: A Comprehensive Guide to Medical and Pharmaceutical Applications*, M. Szycher, Ed., pp. 245–256, Technomic, Lancaster, UK, 1991.

[52] J. Autian, "Polymers in medicine and surgery," in *Polymer Science and Technology*, R. L. Kronenthal, Z. Oser, and E. Martin, Eds., pp. 181–203, Plenum, New York, NY, USA, 1975.

[53] J. H. Lee, Y. M. Ju, W. K. Lee, K. D. Park, and Y. H. Kim, "Platelet adhesion onto segmented polyurethane surfaces modified by PEO- And sulfonated PEO-containing block copolymer additives," *Journal of Biomedical Materials Research*, vol. 40, no. 2, pp. 314–323, 1998.

[54] J. M. Grunkemeier, W. B. Tsai, and T. A. Horbett, "Co-adsorbed fibrinogen and von Willebrand factor augment platelet procoagulant activity and spreading," *Journal of Biomaterials Science, Polymer Edition*, vol. 12, no. 1, pp. 1–20, 2001.

[55] J. H. Lee, H. W. Jung, I. K. Kang, and H. B. Lee, "Cell behaviour on polymer surfaces with different functional groups," *Biomaterials*, vol. 15, no. 9, pp. 705–711, 1994.

Hindawi Publishing Corporation
International Journal of Biomaterials
Volume 2012, Article ID 376321, 9 pages
doi:10.1155/2012/376321

Research Article

Surface Characterization of Asymmetric Bi-Soft Segment Poly(ester urethane urea) Membranes for Blood-Oxygenation Medical Devices

Mónica Faria, Vítor Geraldes, and Maria Norberta de Pinho

ICEMS and Department of Chemical and Biological Engineering, Instituto Superior Tecnico, Technical University of Lisbon, 1049-001 Lisboa, Portugal

Correspondence should be addressed to Mónica Faria, monica.faria@ist.utl.pt

Received 5 July 2011; Accepted 22 August 2011

Academic Editor: Rolf Larsson

Asymmetric bi-soft segment poly(ester urethane urea) (PEUU) membranes containing polycaprolactone (PCL) as a second soft segment are synthesized with PCL-diol ranging from 0% to 15% (w/w). Bulk and surface characteristics of the PEUU membranes were investigated by scanning electron microscopy (SEM), static water contact angles, and surface streaming potentials and were correlated to hemocompatibility properties, namely, hemolysis and thrombosis degrees. SEM analysis reveals PEUU membranes with asymmetric cross-sections and top dense surfaces with distinct morphologies. The increase in PCL-diol content yields PEUU membranes with blood-contacting surfaces that are smoother, more hydrophilic, and with higher maximum zeta potentials. The results obtained in this work give no evidence of a correlation between hydrophilicity/zeta potentials and the hemolysis/thrombosis degree of blood-contacting surfaces of the PEUU membranes. In contrast, other hemocompatibility aspects reveal that the more hydrophilic membranes are associated with lower platelet deposition and inhibition of extreme states of platelet activation.

1. Introduction

Polyurethanes (PUR) are a class of polymers with widespread use in medical devices because of their reasonable bio- and hemocompatible properties, in association with a good flex life, mechanical strength, tear resistance, and versatility in tailoring the final bulk and surface properties [1]. At the nanometer scale PURs are not homogeneous materials: a microphase segregation process leads to the formation of a two-microphase structure with regions enriched in either polyurethane/urea hard or polyether, polyester or polybutadiene soft, amorphous segments. This segregation is thermodynamically driven by unfavorable interactions between polar urethane/urea and relatively nonpolar macroglycol segments. The heterogeneous morphology of polyurethanes is perturbed at an interphase where the chemical composition and morphology ultimately attained is a balance between bulk and interfacial interactions. In bi-soft segment PURs, a second soft segment is used to extend an isocyanate terminated prepolymer that contains the first soft segment. Apart from the possibility of occurrence of different extents of phase separation between soft and hard segments, the two soft segments can also show different extents of phase separation, opening up new possibilities for tuning bulk and surface membrane properties [2–9].

The PUR composition implies a wide diversity of surface characteristics, which in turn are of prime importance when dealing with an eventual use of PURs as blood-contacting materials. The PUR surface layers that are in contact with the blood may differ compositionally from the bulk as polymer chains are mobile and can rearrange in response to interfacial forces [10]. The interaction between a foreign material and blood starts at the material's surface, giving rise to a sequence of events which include protein adsorption, adhesion/activation of platelets, adhesion of leucocytes, blood coagulation, and complement activation; therefore, it is increasingly recognized that the biomedical performance of polymers in blood-contacting devices is a function not only of the bulk properties, but particularly of the nature and the topography of the surface. In this framework of

correlating the structural versatility of bi-soft segment polyurethanes and their surface interaction with blood, there are intense developments in relation to dense films or membranes with symmetric cross-sections [2, 3, 11–16]. In contrast, for bi-soft segment polyurethane membranes with asymmetric cross-sections there is very scarce literature, despite their very different surface properties [17].

In this work, asymmetric bi-soft segment poly(ester urethane urea) (PEUU) membranes were prepared and characterized with view to an application in extracorporeal blood-oxygenation medical devices. For the synthesis of the PEUU membranes we use a triisocyanate terminated prepolymer (PUR) containing poly(propylene oxide) (PPO) as the first soft segment which has been revealing good membrane-forming characteristics in the development of membranes with reasonable hemocompatibility [11, 16]. The second soft segment of poly(ε-caprolactone) diol (PCL diol) was selected as it contributed to the enhancement of hemocompatibility in regard to minimal platelet deposition and inhibition of extreme stages of platelet activation [18]. The PEUU membranes blood-contacting active layers are characterized through scanning electron microscopy (SEM), water contact angles and surface streaming potentials in order to correlate their surface properties with hemocompatibility performance.

2. Materials and Methods

2.1. Materials. Segmented PEUUs were synthesized in bulk by extending a poly(propylene oxide)-(PPO-) based polyurethane prepolymer (PUR) with three isocyanate terminal groups (Companhia Petroquímica do Barreiro, Barreiro, Portugal; MW: 3500; 3.6 wt% of isocyanate groups) with a second prepolymer-poly(ε-caprolactone) diol (PCL diol) (Aldrich; molecular weight 530; 6.4 wt% of hydroxyl groups). Dimethyl formamide (DMF) (p.a. grade, Aldrich) and diethyl ether (DEE) (p.a. grade, Aldrich) were used as solvents and stannous octoate (Aldrich) as a catalyst.

2.2. Membrane Preparation. Four integrally skinned asymmetric membranes, PEUU 100, PEUU 95, PEUU 90 and PEUU 85, were prepared by a modified version of the phase inversion technique. In this process, the PPO-based prepolymer, PUR, with three isocyanate terminal groups and the PCL diol with two terminal hydroxyl are dissolved in a homogeneous phase solvent system of DMF and DEE at a weight ratio DMF/DEE of 3. The polymerization reaction is carried out in an inert (nitrogen) atmosphere at room temperature for 2 h with continuous stirring and was catalyzed by stannous octoate (2 drops). Four casting solutions with PUR/PCL diol weight percentage (wt.%) ratios of 100/0, 95/5, 90/10, and 85/15 and equivalent NCO : OH (wt%) ratios of 100 : 0, 91 : 9, 83 : 17, and 76 : 24 were prepared in a solvent mixture of DMF/DEE, where the weight ratio of total polymer to total solvent was kept constant and equal to 2/3. The solutions were cast onto a glass plate at room temperature with a 250 μm casting knife and after 30 s of solvent evaporation time were quenched into a gelation bath of deionized water at 23 ± 2°C to yield membranes PEUU 100, PEUU 95, PEUU 90, and PEUU 85. After 12 h in the gelation bath the resulting membranes were detached from the glass plate, thoroughly washed with deionized water (conductivity below 0.2 mS/cm) to remove any solvent traces, and finally dried in an oven at 40 ± 3°C for 36 h. Before casting the PEUU membranes, ATR-FTIR spectra were taken for all the solutions to make sure that none showed a peak centered at approximately 2260 cm^{-1} corresponding to the asymmetric isocyanate stretching mode. This was an indication that all isocyanate groups have reacted with the hydroxyl groups of PCL diol, and/or with water in ambient air and, subsequently, with the resulting amine groups, forming urethane and urea linkages.

The PEUU 100 membrane is prepared in the absence of PCL diol and therefore contains only one type of soft segment (PPO); the other three membranes, PEUU 95, PEUU 90, and PEUU 85, contain two soft segments: PPO and PCL. Figure 1 shows the reaction scheme for the synthesis of bi-soft segmented integrally skinned asymmetric PEUU membranes.

2.3. Scanning Electron Microscopy (SEM). Scanning electron microscopy (SEM) was carried out with a JSM-7001F (JEOL, Japan). The bottom porous, top dense blood-contacting surfaces and cross-sections of the PEUU membranes were gold coated before the imaging, and the images of the membrane surfaces with scanned areas of 32 μm × 24 μm and magnification of 3500 were obtained at a scanning voltage of 10 kV. Quantitative analysis of the surface area occupied by the polymer matrix as well as the range of diameters of the pores was calculated using the software ImageJ version 1.4.3.67 (NIH Image, USA) [19].

2.4. Blood-Contacting Surface Hydrophilicity—Static Water Contact Angles. The water contact angle measurements were carried out by the pendant drop method using a video camera (jAi CV-A50) mounted on a Wild M3Z microscope to record the drop image. The video signal was transmitted to a frame grabber (Data Translation model DT3155), with the image acquisition and analysis performed on a computer running the ADSA-P software (Axisymmetric Drop Shape Analysis, Applied Surface Thermodynamics Research Associates, Toronto, Canada). Mean static contact angle values were obtained with distilled water by 10 measurements on different positions of the top dense blood-contacting surface of randomly chosen samples of the PEUU 100, PEUU 95, PEUU90, and PEUU 85 membranes.

2.5. Blood-Contacting Surface Charge—Surface Streaming Potential. The streaming potential on the blood-contacting surface of the PEUU membranes was measured by an Electrokinetic Analyzer (Electrokinetic Analyzer EKA, A. Paar GmbH). Two samples of each membrane were placed on the membrane holder with their active layers or blood-contacting surfaces facing each other separated by a spacer at a distance of approximately 1 mm. Using the Clamping Cell a pressure ramp from 0 to 600 mbar was employed

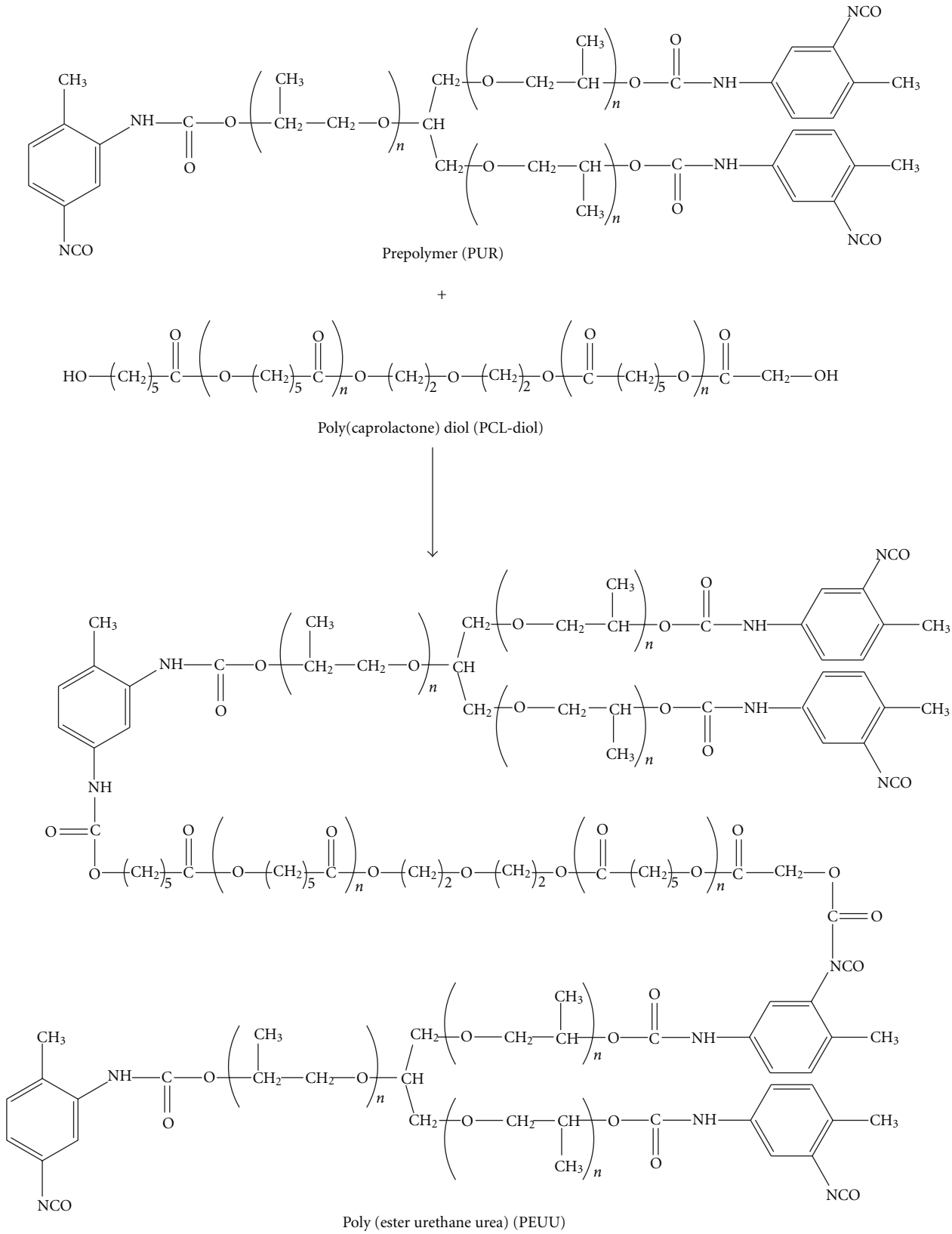

Figure 1: Preparation of segmented integrally skinned asymmetric PEUU membranes.

to force the electrolyte solution through the cell. The pH dependence of the zeta potential for the blood-contacting surfaces of the PEUU membranes was determined from streaming potential measurements in an electrolyte solution of 1×10^{-3} mol/L KCl with pH adjusting solutions 0.1 M HCl and 0.1 M NaOH. The three aqueous solutions were prepared from deionized water, and the streaming potentials were converted to zeta potentials using the Helmholtz-Smoluchowski equation [20]. Each value of the zeta potential at a given pH value represents an average value over at least five individual measurements. The evaluation and interpretation of the zeta potential versus pH plots is based on the following general findings and concepts: polymers without dissociating surface functions can be highly charged in diluted KCl solutions due to preferential adsorption of OH^- ions. The isoelectric point (IEP) for these polymer surfaces obtained when decreasing the solution pH by addition of HCl is found at pH 4.0 ± 0.1 [21, 22]. It is independent of any properties of the polymer beyond the absence of Bronsted functions and almost independent of the KCl solution concentration. The occurrence of the IEP in the acidic pH range is attributed to the preferential OH^- adsorption; that is, it reflects the ratio of the OH^-/H^+ adsorption [23–25]. Another conclusion can be drawn from the extreme zeta potential value obtained for its dependence on the solution concentration of surface charge-determining ions if the polymer surface is smooth and nonporous and does not contain dissociating surface functions Since the adsorption of the charge-determining ions onto indifferent surface sites occurs in competition with the adsorption of water, the maximum zeta potential correlates with the hydrophobicity of the surface [26].

2.6. Hemocompatibility Evaluation. The hemocompatibility evaluation was carried out *in vitro* according to the ISO 10993-4:2002 standard [27]. All tests used pooled rabbit blood anticoagulated with acid citrate dextrose (ACD) solution, at a blood/ACD ratio of 9 : 1. Blood was collected by standard venipuncture (18G needles) from normal, healthy rabbits.

2.6.1. Hemolysis. Hemolysis was assessed according to the ISO 10993-4:2002 standard [27] following a method detailed by us before [11] which is based on the ASTM F 756-00 standard recommended in the ISO 10993-4 : 2002 standard [28]. Briefly, triplicate samples of each membrane were studied before and after extraction with phosphate-buffered saline (PBS, 0.01 M, pH 7.4) for 48 h at 37°C, under static conditions (titled unextracted membranes and PBS-extracted membranes, resp.). After 4 h of contact with static blood at 37°C, the hemoglobin (Hb) released was quantified (cyanmethemoglobin method) [29]. From the Hb concentration released, the hemolysis index was calculated and expressed as a percentage in relation to the Hb concentration in the positive control (blood plus water), after subtracting a blank (blood plus PBS) from each Hb concentration. The membranes are classified according to the hemolysis index (HI) as nonhemolytic (HI 0–2%), slightly hemolytic (HI 2–5%), or hemolytic (HI >5%) [28].

Table 1: Molecular composition and water static contact angles of the PEUU membranes.

Membrane	PUR/PCL diol (wt.%)	Water contact angle (°)
PEUU 100	100/0	70.9 ± 0,6
PEUU 95	95/5	65.8 ± 0,8
PEUU 90	90/10	63.0 ± 0,6
PEUU 85	85/15	59.4 ± 1,0

2.6.2. Thrombosis. Thrombosis was evaluated through an assay described by us in previous studies [11] which is based on a version of the method proposed by Imai and Imai and Nose [30] and Allmer et al. [31]. In brief, the thrombus mass formed on the top dense blood-contacting surface of the PBS-extracted membranes was determined gravimetrically after different contact times (one membrane sample, in triplicate, for each contact time) with recalcified, static blood. For each contact time of 15 mins, 25 mins, 35 mins, 45 mins, and 55 mins, a filter paper disk (in triplicate), which followed this procedure in parallel but in the absence of a membrane sample and of blood, was used as a blank. From the thrombus mass formed on each sample, a thrombosis degree was calculated as a percentage of the thrombus mass formed on the positive control (glass, evaluated in triplicate for each contact time) after subtracting the blank from each thrombus mass. A thrombosis degree of 100% was assigned to the positive control (glass).

3. Results and Discussion

Four different PEUU membranes prepared with PUR/PCL-diol in wt% ratios of 100/0, 95/5, 90/10, and 85/15 were designated by PEUU 100, PEUU 95, PEUU 90, and PEUU 85. They were white in color, very flexible, and with thicknesses ranging from 40–65 μm (measured and averaged on 6 sampling points for each membrane). Table 1 shows the chemical compositions of the PEUU membranes in terms of PUR/PCL-diol (wt.%) and the water static contact angles measured on the top dense blood-contacting surface of the PEUU membranes.

Figure 2 shows the SEM images (scan area 32 μm × 24 μm) of the surfaces of the top dense and bottom porous layers and of the cross-section of PEUU 100, PEUU 95, PEUU 90, and PEUU 85 membranes casted from solutions with varying concentrations of PUR and PCL-diol. The left and center columns of Figure 2 refer to the top dense blood-contacting surfaces and the bottom porous gas contacting surfaces of the PEUU membranes, respectively. Figure 2(a) shows the SEM image of the dense layer of the PEUU 100 membrane as a very nonuniform surface. Figure 2(b) shows the bottom porous layer of the same membrane (PEUU 100) where depressions with diameters ranging from 1.0 μm to 3.5 μm are dispersed in a nonuniform manner throughout the polymer matrix that covers approximately 70% of the total surface area. In Figure 2(d), the SEM image of the dense layer of the PEUU 95 membrane shows round/oval depression areas with diameters ranging from approximately

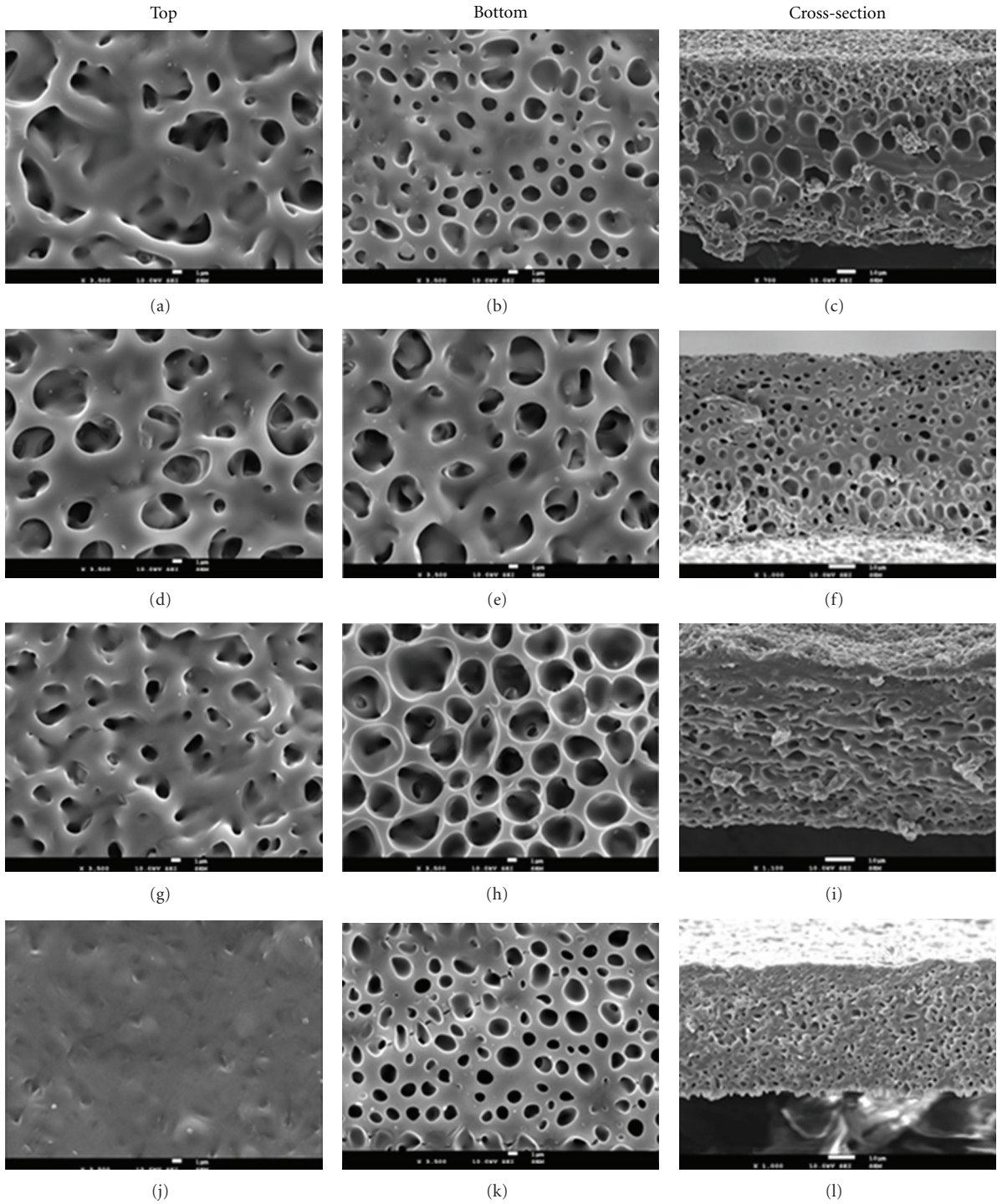

Figure 2: SEM images of PEUU 100 (a, b, and c), where, (a) active layer, (b) bottom surface, (c) cross-section, PEUU 95 (d, e, and f) where, (d) active layer, (e) bottom surface, (f) cross-section, PEUU 90 (g, h, and i) where, (g) active layer, (h) bottom surface, (i) cross-section, PEUU 85 (j, k, and l) where, (j) active layer, (k) bottom surface, (l) cross-section of the membranes.

1.5 to 5.5 μm and dispersed in a polymer matrix with approximately 50% of the total surface area. The porous surface of this PEUU 95 membrane (Figure 2(e)) shows depression areas with roughly the same shape and sizes ranging from 3.0 μm to 5.5 μm in diameter and dispersed throughout the polymer matrix in a similar manner as the top dense surface. In Figure 2(g), the top dense layer of the PEUU 90 membrane shows very small depressions with an average diameter of 1.5 μm and dispersed in a polymer matrix occupying approximately 66% of the total surface area. Figure 2(h) shows the bottom porous surface of membrane PEUU 90. There are large and very irregular depressions with

diameters ranging from 3.5 μm to 5.5 μm that lead to a very small polymer matrix surface area of approximately 35% of the total surface area. There is a very big difference in the surface morphology of the top dense and bottom porous layer of this membrane containing 90 wt% of PCL-diol. In Figure 2(j), the SEM image of the dense layer of the PEUU 85 membrane shows a very homogeneous surface. Figure 2(k) shows the porous surface of the PEUU 85 membrane with pores of round shape with diameters ranging approximately from 0.5 μm to 2.0 μm which are dispersed throughout the polymer matrix and with this polymer matrix covering a surface area of 70%. For the PEUU 100, PEUU 90, and PEUU 85 membranes, the difference in the surface morphology of the top layer and of the porous sub layer is very clear with top layers that are much denser and have higher polymer concentration than the bottom surface. For the membrane with the smallest content of PCL diol, 5 wt.%, the differences in morphology between the two surfaces are less evident. The column on the right of Figure 2: Figures 2(c), 2(f), 2(i), and 2(l) show the cross-sections of the PEUU 100, PEUU 95, PEUU 90, and PEUU 85 membranes, respectively. Figure 2(c) depicts a structure with large round-like pores in the center which appear to become smaller towards the surfaces of the PEUU 100 membrane. In Figure 2(f), we can see for the PEUU 95 membrane the round-like pores of bigger dimensions near the bottom porous surface which seem to become smaller towards the top active layer. For the PEUU 100 and PEUU 95 membranes the pores seen in the cross-sections have a round-like structure and seem to be somewhat smaller for the PEUU 95 membrane than for the PEUU 100 membrane. Figure 2(i) shows the cross-section image for the PEUU 90 membrane, and unlike the PEUU 100 and PEUU 95 membranes, the pores do not seem to have a round-like shape and are instead characterized by an anisotropic shape. In the near active layer surface region there seem to be less pores than in the center and the near bottom porous surface of the PEUU 90 membrane. Figure 2(l) shows the cross-section of the PEUU 85 membrane, and like for the PEUU 90 membrane the pores are of different shapes unlike the round-like pores in the PEUU 100 and PEUU 95 membranes. Although similar in shape to the ones present in the PEUU 90 membrane, the pores in the PEUU 85 membrane seem to be smaller.

The hydrophilicity of the blood-contacting dense surface of the bi-soft poly(ester urethane urea) membranes was characterized by static water contact angles. Table 1 shows the contact angles on the top dense blood-contacting surfaces decreasing from approximately 71° to 66° to 63° and finally to 59° with the increasing content of the second soft segment, PCL-diol, from 0 wt.% to 5 wt.% to 10 wt.%, and finally to 15 wt.%, respectively. The smallest contact angle, approximately 59°, indicating the most hydrophilic surface, was measured for the PEUU 85 membrane which contains the highest PCL-diol content, 15 wt.%, while the most hydrophobic blood-contacting surface was verified for the PEUU 100 membrane with no PCL-diol content, and that contains only one type of soft segment—PPO.

The pH dependence of the zeta potential was determined from the streaming potential measurements for the four

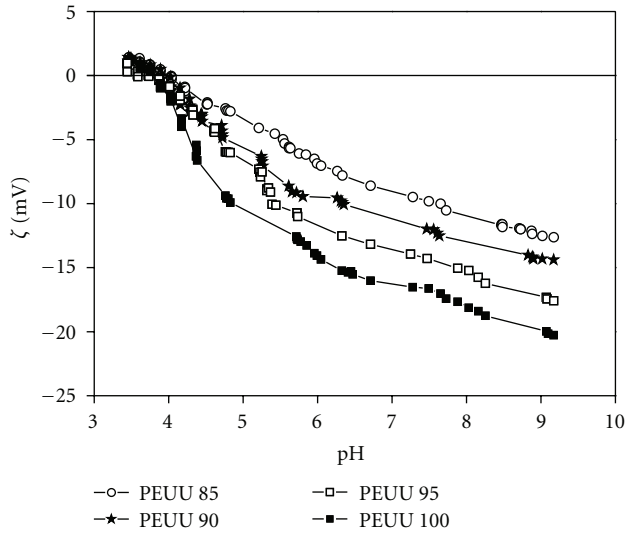

Figure 3: Zeta potential versus pH plot for the blood-contacting surface of the PEUU membranes.

blood-contacting dense surface of the bi-soft poly(ester urethane urea) membranes. Figure 3 shows the zeta potential versus pH plot for the blood contacting dense surface of the PEUU membranes. The isoelectric point (IEP) for all the PEUU membranes was found at a pH of approximately 3.9 and the maximum zeta potentials observed were approximately of −20 mV, −17 mV, −14 mV, and −12 mV for the PEUU 100, PEUU 95, PEUU 90, and PEUU 85 membranes, respectively. For all PEUU membranes, both the IEP at approximately a pH of 3.9 and the absence of a plateau range in the zeta potential versus pH plot are typical characteristics of polymers bearing no dissociating groups. Due to the hydrophobic character of the poly(ester urethane urea) membranes, preferred absorption of the chloride anions is observed which gives a negative zeta potential in the range of pH = 4–10. Further, a maximum of the zeta potential is observed with increasing solution pH caused by NaOH addition. This extreme value is attributed to the superposition of increasing interfacial charge due to preferential OH^- ion adsorption and double-layer compression with increased NaOH solution concentration [32]. In the past, studies have shown for smooth, nonporous polymer membranes, the existence of a linear correlation between the water contact angle and the maximum zeta potential; this is explained by the fact that the charge formation at the interface by ion adsorption occurs in competition with the adsorption of water molecules [22, 33]. Figure 4 shows the correlation between water contact angles (Table 1) and maximum zeta potential observed in zeta potential versus pH plots at alkaline pH values (NaOH addition, 10^{-3} M KCl background electrolyte) for the blood-contacting surface of the PEUU membranes. As expected, a correlation between decreasing water contact angle and decreasing maximum zeta potential was confirmed for the PEUU membranes. The most hydrophilic membrane, PEUU 85, which has the lowest contact angle, approximately 59°, exhibits the highest value

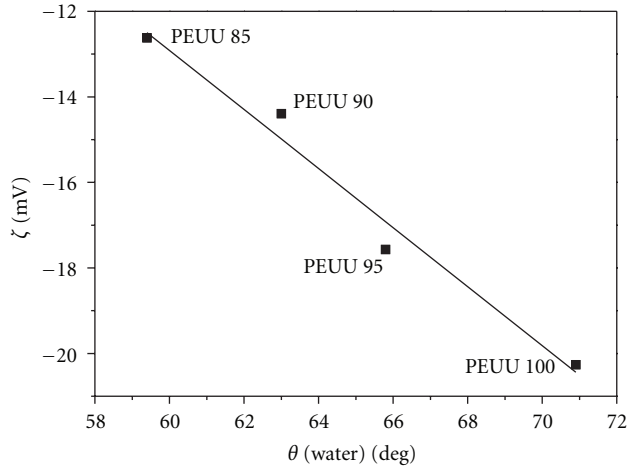

Figure 4: Correlation between water contact angle and maximum zeta potential observed in zeta potential versus pH plots at alkaline pH values (NaOH addition, 10^{-3} M KCl background electrolyte) for the blood-contacting surface of the PEUU membranes.

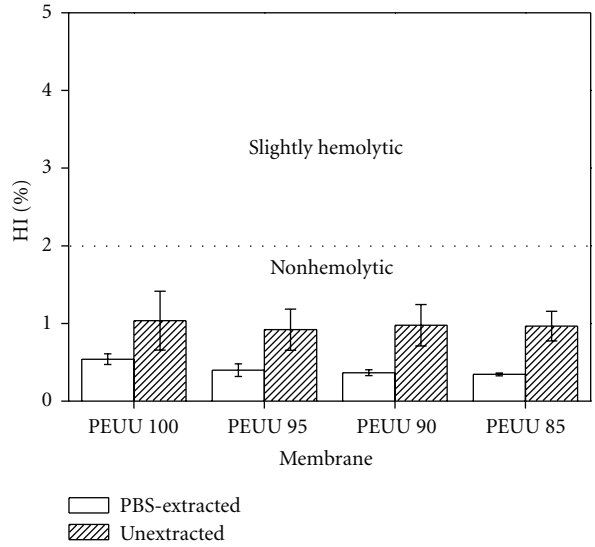

Figure 5: Hemolysis index (HI) of PEUU membranes before and after extraction with PBS. HI between 0 and 2% indicate non hemolytic membranes. The mean hemolysis degrees of the PBS-extracted samples were not significantly different from each other (one-way ANOVA, $P > 0.05$).

of extreme zeta potential, approximately −12 mV, while the most hydrophobic membrane, PEUU 100, for which the highest contact angle was observed, approximately 71°, has the lowest extreme zeta potential value, approximately −20 mV. Such a linear correlation enables us to predict the hydrophobicity/hydrophilicity nature of the PEUU membranes by analyzing the zeta potential values and vice versa. Furthermore, it opens the possibility of estimating the values of extreme zeta potential and of water contact degrees of PEUU membranes containing different PUR/PCL compositions.

Figure 5 shows the results of the hemolysis essay for the PEUU membranes. Damage to the membrane of red cells, as a result of blood exposure to foreign materials, can be evaluated by the hemolysis test. According to ASTM F-756 [28], materials can be labeled nonhemolytic when the Hemolytic Index (HI) is between 0–2, slightly hemolytic when HI is between 2–5, and hemolytic when HI > 5. All of the PEUU membranes were nonhemolytic both before and after PBS extraction for a contact time with blood of 3 h. The differences between the PEUU membranes containing only one type of soft segment (PEUU 100) and the membranes containing two types of soft segments (PEUU 95, PEUU 90, and PEUU 85) were not statistically significant (ANOVA, $P = 0.05$). The hemolysis degree did not vary regularly with PCL content, and the extraction with PBS decreased considerably the hemolysis degree. Since this hemolysis assay was performed with static blood, which excludes the occurrence of hemolysis due to mechanical damage to the erythrocyte's membrane, this difference pointed to the possibility that a fraction of the hemolysis degree detected could be due to foreign substances extracted with PBS (residuals of catalyst, solvent, and oligomers). However, when these extracts were assayed, no hemolysis could be detected, probably due to lack of sensitivity of the method. All subsequent hemocompatibility tests were then carried out with PBS-extracted membranes.

Figure 6 shows the percentage of thrombus formation on the top dense blood-contacting surface of the PEUU membranes for different contact times, admitting that the thrombosis degree on a glass surface is of 100% (positive control). For each and every one of the blood contact times evaluated 15 s, 25 s, 35 s, 45 s, and 55 s, there was no statistical difference in the extent of clot formation on the blood-contacting surface of all PEUU membranes, PEUU 100, PEUU 95, PEUU 90, and PEUU 85. For the shortest contact times with blood (15 min, the earliest time at which it was possible to quantify the thrombus formed), the whole set of membranes showed thrombosis degrees of 48–54%. The thrombosis degree of all the PEUU membranes was highest for a contact time of 55 min (73–76%) but has still not reached that of the positive control (glass surface with thrombosis degree of 100%). For contact times with blood between 45 min and 55 min, the thrombosis degree for all the PEUU membranes was approximately between 71% and 76%, and statistical analysis (one-way ANOVA, $P > 0.05$) did not show significant differences. This may reveal that the highest thrombosis degree is reached after a contact of 45 minutes between blood and the blood-contacting surface of the PEUU membranes, and that at least for the following 10 minutes (blood contacting time of 55 mins) remains approximately constant.

In a previous investigation, Besteiro et al. [16] casted PEUU membranes with the same chemical composition as the ones addressed in this work by the solvent evaporation method of polymeric solutions with PUR/PCL ratios of 100/0, 95/5, 90/10, and 75/25 and a single solvent (toluene). These membranes had symmetric dense cross-sections and the blood-contacting surfaces were characterized by contact angles and by hemocompatibility essays of hemolysis,

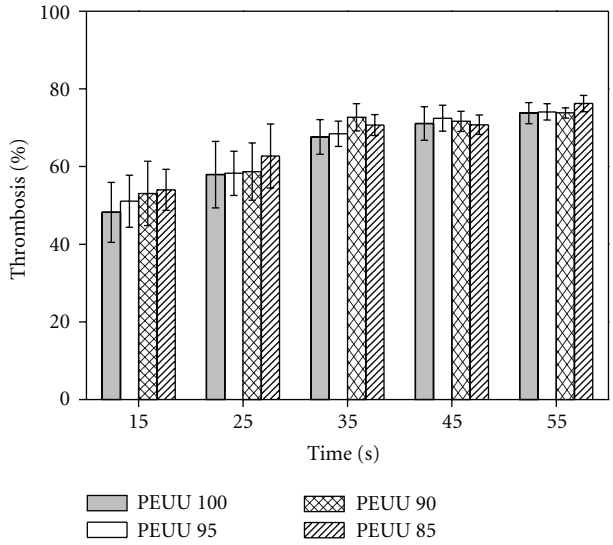

Figure 6: Percentage of thrombosis on the blood-contacting surface of the PBS-extracted PEUU membranes for different contact times with blood (glass: 100%, top line of the graph).

thrombosis, and platelet adhesion. No firm correlation was obtained between the contact angles and the hemocompatibility properties. In contrast with that, membranes casted as reported in this work, by the phase inversion technique, with the same DMF/DEE solvent system and PUR/PCL ratios, described in Table 1, yielded asymmetric cross-sections and dense top layers (blood-contacting surface) that upon characterization by Atomic Force Microscopy revealed a strong correlation between surface properties and platelet deposition. In fact, the top dense layers became smoother, and their submicron average roughness decreases monotonically by a factor of five to approximately 1 nm as the PCL-diol content increases from 0 wt.% to 15 wt.%. In the same work, the platelet/membrane surface interactions that are quantified by the global parameters of platelet deposition and platelet coverage and are correlated to the submicron average roughness parameter that in turn is controlled through the PCL-diol content of the membrane casting solutions. Furthermore, progressive stages of platelet activation depend on the membrane surface morphologies associated with different PCL contents as extreme states of platelet activation, spread, and fully spread, are inhibited in membranes casted from solutions with 15 wt.% of PCL-diol and the fully spread stage is already inhibited for intermediate PCL-diol contents of 5 wt.% and 10 wt.% [18].

4. Conclusions

The poly (ester urethane urea) membranes prepared by the modified phase inversion technique under the same casting conditions displayed asymmetric integrally skinned cross-sectional structures that were tailored upon the variation of the PCL-diol content. The characterization of the PEUU membranes through SEM analysis gives evidence that the top dense blood-contacting surfaces become smoother and more dense with increasing concentrations of PCL-diol while static water contact angles and surface streaming potential measurements reveal that the increase in PCL-diol content yields more hydrophilic PEUU membranes with higher maximum zeta potentials. Despite the nonsignificant differences in the hemolysis index and thrombosis percentage between the PEUU membranes containing different PCL content, the more hydrophilic membranes are associated with lower platelet deposition and inhibition of extreme states of platelet activation. Further investigation of local charge distribution and surface energies should be carried out to elucidate the correlation between the streaming potential and the eventual liaison with PCL content.

Acknowledgments

The authors are grateful to "Fundação para a Ciência e Tecnologia (FCT)", Portugal, for the financial help through contract Programs POCTI/FCB/47661/2002 and REEQ1764/EQU/2005. Mónica Faria is grateful to INL—International Iberian Nanotechnology Laboratory for a Ph.D. grant.

References

[1] S. Gogolewski, "Selected topics in biomedical polyurethanes. A review," *Colloid & Polymer Science*, vol. 267, no. 9, pp. 757–785, 1989.

[2] S. C. Yoon, B. D. Ratner, B. Iván, and J. P. Kennedy, "Surface and bulk structure of segmented poly(ether urethanes) with perfluoro chain extenders. 5. Incorporation of poly(dimethylsiloxane) and polyisobutylene macroglycols," *Macromolecules*, vol. 27, no. 6, pp. 1548–1554, 1994.

[3] Y. Deslandes, G. Pleizier, D. Alexander, and P. Santerre, "XPS and SIMS characterisation of segmented polyether polyurethanes containing two different soft segments," *Polymer*, vol. 39, no. 11, pp. 2361–2366, 1998.

[4] C. T. Zhao and M. Norberta De Pinho, "Design of polypropylene oxide/polybutadiene bi-soft segment urethane/urea polymer for pervaporation membranes," *Polymer*, vol. 40, no. 22, pp. 6089–6097, 1999.

[5] D. P. Queiroz and M. N. Pinho, "Gas permeability of polypropylene oxide/polybutadiene bi-soft segment urethane/urea membranes," *Desalination*, vol. 145, no. 1–3, pp. 379–383, 2002.

[6] D. P. Queiroz, M. N. De Pinho, and C. Dias, "ATR-FTIR studies of poly(propylene oxide)/polybutadiene bi-soft segment urethane/urea membranes," *Macromolecules*, vol. 36, no. 11, pp. 4195–4200, 2003.

[7] D. P. Queiroz and M. N. De Pinho, "Structural characteristics and gas permeation properties of polydimethylsiloxane/poly(propylene oxide) urethane/urea bi-soft segment membranes," *Polymer*, vol. 46, no. 7, pp. 2346–2353, 2005.

[8] D. P. Queiroz, A. M. Botelho do Rego, and M. N. de Pinho, "Bi-soft segment polyurethane membranes: surface studies by X-ray photoelectron spectroscopy," *Journal of Membrane Science*, vol. 281, no. 1-2, pp. 239–244, 2006.

[9] D. P. Queiroz, M. C. Gonçalves, and M. N. De Pinho, "Tailoring of phase-segregation structures in two-soft-segment urethane/urea polymer membranes," *Journal of Applied Polymer Science*, vol. 103, no. 1, pp. 315–320, 2007.

[10] H. J. Griesser, "Degradation of polyurethanes in biomedical applications-A review," *Polymer Degradation and Stability*, vol. 33, no. 3, pp. 329–354, 1991.

[11] D. P. Queiroz, I. M. Pinto, M. C. F. Besteiro et al., "Surface and hemocompatibility studies of bi-soft segment polyurethane membranes," *International Journal of Artificial Organs*, vol. 29, no. 9, pp. 866–872, 2006.

[12] A. Takahara, J. I. Tashita, T. Kajiyama, M. Takayanagi, and W. J. MacKnight, "Microphase separated structure, surface composition and blood compatibility of segmented poly(urethaneureas) with various soft segment components," *Polymer*, vol. 26, no. 7, pp. 987–996, 1985.

[13] T. G. Grasel and S. L. Cooper, "Surface properties and blood compatibility of polyurethaneureas," *Biomaterials*, vol. 7, no. 5, pp. 315–328, 1986.

[14] K. Nojima, K. Sanui, N. Ogata, N. Yui, K. Kataoka, and Y. Sakurai, "Material characterization of segmented polyether poly(urethane-urea-amide)s and its implication in blood compatibility," *Polymer*, vol. 28, no. 6, pp. 1017–1024, 1987.

[15] T. Kajiyama and A. Takahara, "Surface properties and platelet reactivity of segmented poly(etherurethanes) and poly(etherurethaneureas)," *Journal of Biomaterials Applications*, vol. 6, no. 1, pp. 42–71, 1991.

[16] M. C. Besteiro, A. J. Guiomar, C. A. Gonçalves, V. A. Bairos, M. N. De Pinho, and M. H. Gil, "Characterization and in vitro hemocompatibility of bi-soft segment, polycaprolactone-based poly(ester urethane urea) membranes," *Journal of Biomedical Materials Research A*, vol. 93, no. 3, pp. 954–964, 2010.

[17] "Process of synthesis of asymmetric polyurethane based membranes with hemocompatibility characteristic and membranes by said processes," PCT/IB2007/003340.

[18] M. Faria, P. Brogueira, and M. N. de Pinho, "Sub-micron tailoring of bi-soft segment asymmetric polyurethane membrane surfaces with enhanced hemocompatibility properties," *Colloids and Surfaces B*, vol. 86, no. 1, pp. 21–27, 2011.

[19] W. S. Rasband, "ImageJ," U.S. National Institutes of Health, Bethesda, Md, USA, 1997–2005, http://rsb.info.nih.gov/ij/.

[20] M. Smoluchowski, *Handbook of Electricity and Magnetism*, vol. 2, Barth, Leipzig, Germany, 1921.

[21] M. Kosmulski, "The pH-dependent surface charging and points of zero charge. V. Update," *Journal of Colloid and Interface Science*, vol. 353, no. 1, pp. 1–15, 2011.

[22] C. Werner, U. König, A. Augsburg et al., "Electrokinetic surface characterization of biomedical polymers—A survey," *Colloids and Surfaces A*, vol. 159, no. 2-3, pp. 519–529, 1999.

[23] J. C. Vickerman and N. M. Reed, *Surface Analysis-Techniques and Applications*, John Wiley & Sons, Chichester, UK, 1996.

[24] P. Weidenhammer, C. Werner, and H.-J. Jacobasch, "Electrical double layer forces and adhesion on non-polar polymer surfaces," *Polymer*, vol. 37, no. 2, pp. 614–615, 1996.

[25] H.-J. Jacobasch, *Oberflachenchemie Faserbildender Polymere*, Akademie, Berlin, Germany, 1984.

[26] N. Kuehn, H. J. Jacobasch, and K. Lunkenheimer, "Zum Zusammenhang zwischen dem Kontaktwinkel zwischen Wasser und festen Polymeren und ihrem Zeta-Potential gegenüber wäßrigen Lösungen," *Acta Polymerica*, vol. 37, p. 394, 1986.

[27] International Standards Organization (ISO), *ISO 10993-4:2002—Biological Evaluation of Medical Devices. Part 4: Selection of Tests for Interactions with Blood*, International Standards Organization, Geneva, Switzerland, 2nd edition, 2002.

[28] American Society for Testing of Materials (ASTM), *ASTM F 756-00—Standard Practice for Assessment of Hemolytic Properties of Materials*, American Society for Testing of Materials, West Conshohocken, Pa, USA, 2000.

[29] A. Zwart, O. W. Van Assendelft, B. S. Bull, J. M. England, S. M. Lewis, and W. G. Zijlstra, "Recommendations for reference method for haemoglobinometry in human blood (ICSH standard 1995) and specifications for international haemiglobincyanide standard (4th edition)," *Journal of Clinical Pathology*, vol. 49, no. 4, pp. 271–274, 1996.

[30] Y. Imai and Y. Nose, "New method for evaluation of antithrombogenicity of materials," *Journal of Biomedical Materials Research*, vol. 6, pp. 165–172, 1972.

[31] K. Allmer, J. Hilborn, P. H. Larsson, A. Hult, and B. Ranby, "Surface modification of polymers. V. Biomaterial applications," *Journal of Polymer Science A*, vol. 28, no. 1, pp. 173–183, 1990.

[32] H. O. Stern, "Über das Gleichgewicht zwischen Materie und Strahlung," *Zeitschrift für Elektrochemie und angewandte physikalische Chemie*, vol. 31, p. 448, 1924.

[33] R. Hunter, *Zeta Potential in Colloid Science*, Academic Press, London, UK, 1981.